71-0225-01-00

STUDY OF AUTOMATIC AND MANUAL TERMINAL GUIDANCE AND CONTROL SYSTEMS FOR SPACE SHUTTLE VEHICLES

VOLUME I - SECTIONS I THROUGH III

FINAL REPORT
(MARCH 1970 THROUGH MARCH 1971)

AUGUST 1971

BY

STEPHEN OSDER
ROGER KELLER

SPERRY FLIGHT SYSTEMS DIVISION
SPERRY RAND CORPORATION
PHOENIX, ARIZONA

PREPARED FOR

NATIONAL AERONAUTICS AND SPACE ADMINISTRATION
AMES RESEARCH CENTER
MOFFETT FIELD, CALIFORNIA
PER CONTRACT NAS 2-5804

PREPARED BY

SPERRY FLIGHT SYSTEMS DIVISION
SPERRY RAND CORPORATION
PHOENIX, ARIZONA

FOREWORD

This report was prepared by the Advanced Systems and Avionics Department, Sperry Flight Systems Division of the Sperry Rand Corporation under NASA Contract NAS2-5804, "Study of Automatic and Manual Terminal Guidance and Control Systems for Horizontal Landing of Space Shuttle Vehicles". The work was administered under the direction of the Guidance and Navigation Branch of the NASA Ames Research Center's Full Scale and Systems Research Division, with Mr. Donald W. Smith as Technical Monitor. Contributions of the following individuals at the Sperry Flight Systems Division are acknowledged:

Dr. John Dunfield	High Altitude Energy Management and Flareout Simulator Studies
Mr. Randall Gaylor	Manual/Flight Director Modes, Energy Management Techniques and Direction of the NASA ARC Simulator Evaluations
Mr. George Yeh	Design of the EADI/NASA Simulation Interface
Mr. Robert Eslinger	Study of Candidate Flight Test Aircraft for Simulating SSV Landings
Mr. Robert Jacobson	Study of Candidate Navigation Sensors for SSV Landing

Also acknowledged are the contributions of NASA's Guidance and Navigation Branch and the Simulator Computer Systems Branch in operating the NASA visual scene simulator for the final performance verifications and evaluations.

TABLE OF CONTENTS

VOLUME I

TABLE OF CONTENTS (cont)

TABLE OF CONTENTS (cont)

TABLE OF CONTENTS (cont)

LIST OF ILLUSTRATIONS

LIST OF ILLUSTRATIONS (cont)

LIST OF ILLUSTRATIONS (cont)

LIST OF ILLUSTRATIONS (cont)

LIST OF ILLUSTRATIONS (cont)

LIST OF ILLUSTRATIONS (cont)

LIST OF ILLUSTRATIONS (cont)

LIST OF ILLUSTRATIONS (cont)

SECTION I

SUMMARY

SECTION I

SUMMARY

This report presents the results of a study to analyze, design, and evaluate guidance and control systems that start at an altitude of about 100,000 feet and bring the unpowered space shuttle orbiters to a precision horizontal landing. The systems under consideration included fully automatic versions which involve no pilot participation as well as various manual configurations that provide combinations of displays and control augmentation which permit the pilot to control the vehicle to a successful landing.

Two classes of vehicles wery studied: the Low Cross-Range (LCR) or straight-wing orbiter and the High Cross-Range (HCR) or delta-wing (delta body) orbiter. Designs and simulations were accomplished for two representative LCR vehicles (the preliminary MSC 245 configuration and the McDonnell Douglas design) and three representative HCR vehicles (the Lockheed Space and Missile Company LMSC-8MX, the North American Rockwell NAR SSV-134C and the McDonnell Douglas MDAC-255 BJ0050-B). System designs were evaluated in 6-degree-of-freedom digital simulations which included wind and turbulence models.

The guidance and control system included autopilot and manual control augmentation loops which provided the stability and maneuvering responsiveness required by both the automatic guidance modes and pilot handling quality considerations. All vehicles studied had inherent instabilities at some or all flight regimes, and the recommended control systems were designed to cope with these instabilities. Consistent automatic and augmented manual landings that meet the same performance criteria as those used for conventional transport aircraft were demonstrated for the different unpowered shuttlecraft studied.

High altitude energy management guidance schemes that start at about 100,000 feet and bring the vehicle to a precise capture of the high energy final approach paths were designed and evaluted. Complete terminal area flights using fully automatic, semi-automatic (flight director) and manual (raw data displays plus

voice GCA) were demonstrated in the NASA ARC visual scene simulator. These flights started near 100,000 feet and ended with horizontal landings on the specified runway. Evaluation pilots included astronauts and pilots experienced in unpowered landings of low L/D vehicles.

The recommended navigation, guidance and control system is shown to be compatible with realistic physical constraints that would exist in space shuttlecraft and to be consistent with the 1971 avionics equipment state of the art. Aircraft capable of aerodynamically simulating the various candidate space shuttlecraft in their unpowered, terminal area descent were investigated, and flight test recommendations, including system mechanizations, are made.

SECTION II

INTRODUCTION

SECTION II

INTRODUCTION

This report summarizes the work performed by the Sperry Flight Systems Division of Sperry Rand Corporation on Contract NAS2-5804 for the study of automatic and manual guidance and control systems for space shuttle vehicles. The work reported herein was performed between the period March 1970 through March 1971. An additional short study aimed at verifying the recommended system performance in an updated space shuttle configuration (McDonnell Douglas HCR Orbiter) was performed from March through May 1971. The results of this study extension will be reported in a supplement to the present report.

The scope of this study was defined by the NASA specification A-15698 dated 24 July 1969, which called for the design and evaluation of automatic and manual guidance and control techniques for landing both powered and unpowered space shuttle orbiters and the definition of practical mechanizations for such systems based on state of the art avionics. Although the study concentrated exclusively on the unpowered landing problem, it is noted that the recommended landing technique for a powered orbiter would be identical to that used for the unpowered case; the air breathing engines providing thrust only for a go-around.

The emphasis of this study was in defining practical design solutions to the space shuttle landing problems. For this reason most of the work was done with complete vehicle simulations, which included all of the available non-linear aerodynamic characteristics, known control system constraints and realistic wind and turbulence models. When data pertinent to system design, such as aeroelastic modes, could not be made available because of the preliminary stage of space shuttle development, adequate provision was made to cope with the practical consequences of that data on the guidance and control system. In this regard it is noted that a study of this type tends to become a race against obsolescence if the design studies and analyses are too closely oriented to specific vehicles. During the course of the work covered by this report, space shuttle vehicle concepts moved through some drastic as well as evolutionary changes. The LCR

straight-wing configuration was a prime contender at the start of this study. It was abandoned by NASA in the winter of 1970-1971. Much of the work done on this study used the straight-wing vehicle as a test bed for the guidance and control system concepts. Those concepts, which relate to the final approach and landing (final 20,000 feet of altitude), were not restricted to vehicle type but the high altitude phase of the straight-wing vehicle's guidance and control system was unique to that vehicle. Although no longer pertinent to the space shuttle program, the results relating to those unique problems of the straight-wing vehicle are nevertheless presented in this report, perhaps in anticipation of some future time when that vehicle's interesting potential is rediscovered.

Even the HCR configurations went through some significant evolutionary changes during the course of this study. It soon became apparent that if we attempted to keep the simulation models current with the progress of the NASA Phase B Shuttle Design Program, this study would have been reduced to a simulator programming exercise. For this reason the HCR test vehicle for simulator evaluation was fixed at about September 1970 to the North American Rockwell (NAR) vehicle as it was defined in the summer of 1970. The HCR vehicle used previously in this study was a Lockheed design that pre-dated the NASA Phase B Shuttle Design Program. Although the NAR vehicle was representative of the more recent NASA space shuttle requirements, the continuous updating of the NAR design during the latter part of 1970 was not incorporated into the simulation model. The guidance and control system concept is independent of specific vehicle characteristics and the design studies were performed in a manner that identified how a few different parameters should be changed to accommodate changing vehicle aerodynamics. Finally, to verify that this objective of guidance and control system universality was met, this study was extended to demonstrate performance in a 1971 HCR configuration, the McDonnell Douglas (MDAC) final Phase B configuration. Although the specific results of that study extension are not included in this report, it is noted that the identical system that flew the NAR vehicle provided excellent performance with the MDAC vehicle when only a few control system parameters were re-optimized.

Section III of this report describes the theory of operation of the terminal guidance and control system. It provides a historical perspective of the recommended techniques and discusses the rationale for the guidance and control laws used for different phases of the vehicle's terminal area trajectory. In Section IV the specific design studies and performance trade-offs for the MDAC LCR vehicle and the Lockheed and NAR HCR vehicles are described. In Section V, the results of the final simulator verification tests including pilot evaluation tests are summarized. Finally, in Section VI, a summary of system mechanization recommendations is presented. This includes the analyses to determine a suitable aircraft that can simulate the aerodynamic characteristics of unpowered shuttlecraft in their terminal area descents. The mechanization study and flight test aircraft selection study were previously documented in a separate report. That report is summarized and updated in Section VI. The study conclusions and recommendations are itemized in Section VII. These conclusions confirm that the guidance and control technology exists to provide consistent automatic and augmented manual landings of unpowered space shuttle vehicles. These landings can be made to the same level of performance that is attained today in the landing of conventionally-powered transport aircraft.

SECTION III

DISCUSSION OF SYSTEM CONCEPTS

SECTION III

DISCUSSION OF SYSTEM CONCEPTS

A. VEHICLE MISSION AND PERFORMANCE REQUIREMENTS

1. Classes of Vehicles

Space shuttle concepts and vehicle configurations as related to reusable transportation system requirements have been evolving for about a decade. In this study the vehicle concepts were bounded by the two classes of vehicles that were in contention for the space shuttle during 1970. These were the low cross-range or straight wing orbiter and the high cross-range or delta orbiter. The recent history of space shuttle requirements and configuration trends is documented in References 1 through 9 as well as in a large part of the aerospace technology literature in 1970 and 1971. Although a significant part of this study concentrated on guidance and control techniques for the low cross-range, straight wing vehicle, that configuration was abandoned about January 1971. Despite its apparant elimination as a space shuttle candidate, the low cross-range vehicle had many interesting problems from the guidance/navigation/control viewpoint and the study results obtained with this class of vehicle are included in this report.

Five different vehicles, (three high cross-range and two low cross-range) were used in the evaluation of the guidance, control and energy management techniques for landing unpowered space shuttle orbiters. The vehicles were:

North American Rockwell (NAR) - High Cross-Range (HCR)
Lockheed Missile and Space Company (LMSC) - High Cross-Range (HCR)
McDonnell Douglas Astronautics Company (MDAC) - High Cross-Range (HCR)
NASA MSC 245 Orbiter - Low Cross-Range (LCR)
McDonnell Douglas Astronautics Company (MDAC) - Low Cross-Range (LCR)

From the standpoint of terminal guidance and control, the essential difference between the LCR and HCR vehicle is the fact that the LCR vehicle "falls" rather than flies through the supersonic and transonic flight regimes until it

has reached low subsonic speeds. The HCR vehicle, on the other hand, has relatively conventional supersonic and subsonic aircraft flight characteristics and can be maneuvered in the terminal area to achieve a large range adjustment; an essential capability for unpowered landings. The LCR vehicle descends (falls at flight path angles that reach as high as 60 degrees) before a transition to conventional, low angle of attack flight is performed. That transition which involves nosing down into a steeper dive in order to arrest the descent, and the prior control at very low dynamic pressures with blended aerodynamic and reaction controls represent unique problems for the guidance and control system designer.

Essential characteristics of the different vehicles that were used as test beds for the landing techniques studied are summarized in Table 3-1. These are the significant characteristics for a guidance and control system design. Of the five vehicles tabulated, only the MDAC HCR vehicle (Figure 3-1) depicts a recent design that is representative of candidate configuration resulting from the NASA Phase B space shuttle studies. Note on Figure 3-1 that the optional cruise engines are shown but these are not used for the unpowered landings of the type covered by this study. The NAR vehicle (Figure 3-2) was revised in late 1970 to a single tail configuration (and with less optimistic L/D capability) but the revisions were not incorporated into the simulations performed in this study. The LMSC vehicle (Figure 3-3) is derived from Lockheed work that predates the NASA Phase B shuttle studies. That vehicle exhibits some of the more troublesome problems to the guidance and control system designer such as relatively low control effectiveness. It is noted that this Lockheed configuration was designed for a cross-range capability of about 1500 NM which exceeds the NASA Phase B shuttle requirement of 1100 NM. The MSC 245 straight wing orbiter is an early design developed at NASA MSC as representative of the low cross-range straight wing concept. This configuration was used in the study for preliminary simulations of landing approach and flareout techniques for LCR vehicles but the final system refinements and evaluations were performed with vehicles that complied with the more recent NASA, space shuttle mission and performance specifications (as identified in the Phase B Program). The vehicle that was used for the development of LCR terminal control and landing techniques was the MDAC straight wing configuration (Figure 3-4). The design of that vehicle was refined by McDonnell Douglas until the winter of 1970-71 when the straight wing orbiter concept was abandoned.

TABLE 3-1

SUMMARY OF PERTINENT VEHICLE CHARACTERISTICS

Characteristics	High Cross Range Orbiters			Low Cross Range Orbiters	
	MDAC 255BJ0050-B	NAR SSV-134C	Lockheed 8MX	MDAC	MSC "245"
	Circa 2/71	Circa 8/70	Circa 1/70	Circa 7/70	Circa 1/70
Weight (landing) - pounds	253,448	207,000	300,000	210,000	155,000
Wing Span (b) - feet	97.5	119.3	164.0	114.94	113.5
MAC ($\bar{c}$) - feet	62.9	68.4	109.0	17.86	17.53
I_{xx} - (slug - foot^2 x 10^6)	2.2	3.35	4.7	1.85	0.778
I_{yy} - (slug - foot^2 x 10^6)	12.74	13.3	12.0	16.4	5.85
I_{zz} - (slug - foot^2 x 10^6)	13.35	14.4	15.0	16.6	5.95
I_{xz} - (slug - foot^2 x 10^6)	-0.087	0.95	0.34	-0.028	--
Ref Area (S) - foot^2	5,330	6,086	5,740	1,900	1,850
Wing Loading (W/S) - pound/foot^2	47.5	34	52.3	110	83.7
Peak L/D at Landing Condition	6.7	9.4	4.7	6.15	6.83
α for L/D_p - (degrees)	7.5	10.5	17.0	6.0	7.5
*Pitch Control Power - M_{δ_e} (1/sec^2)	-2.26	-1.66	-0.745	-1.24	-3.20
*Roll Control Power - L_{δ_A} (1/sec^2)	5.07	3.89	0.258	2.44	3.04
*Yaw Control Power - N_{δ_R} (1/sec^2)	-0.335	-0.756	-0.378	-0.430	-0.289
*For Landing Condition - Q = 150 pounds/foot^2					

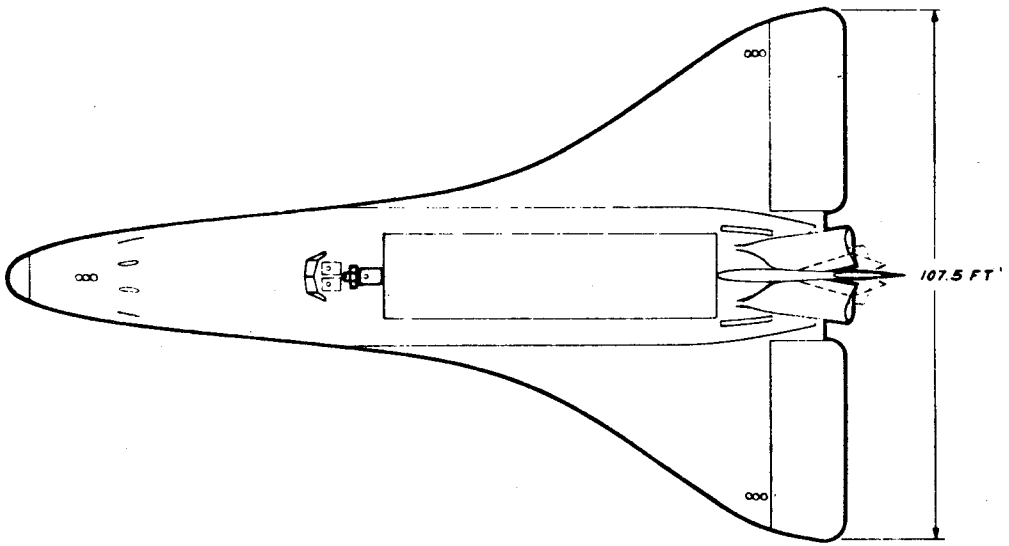

GEOMETRIC DATA

VEHICLE GEOMETRY	
TOTAL PROJECTED PLANFORM AREA	7,527 FT^2
TOTAL VEHICLE WETTED AREA	22,069 FT^2
TOTAL VEHICLE MOLDLINE VOLUME	91,310 FT^3
FUSELAGE GEOMETRY	
FUSELAGE WETTED AREA (INCLUDING BASE)	13,894 FT^2
FUSELAGE MOLDLINE VOLUME	76,095 FT^3
BASE AREA	620 FT^2
WING GEOMETRY	
THEORETICAL AREA	5,543 FT^2
EXPOSED AREA	3,571 FT^2
ASPECT RATIO (THEO.)	2.09
LEADING EDGE SWEEP	55°
TRAILING EDGE SWEEP	0°
DIHEDRAL ANGLE	10°
VERTICAL TAIL GEOMETRY	
THEORETICAL AREA	613 FT^2
ASPECT RATIO	1.71
LEADING EDGE SWEEP	35°
TRAILING EDGE SWEEP	12.5°
TAPER RATIO	0.422
SPAN	32.4FT

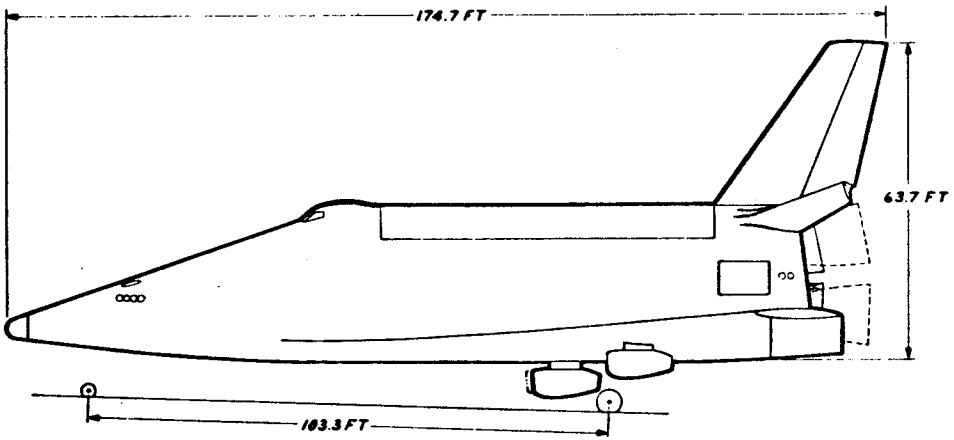

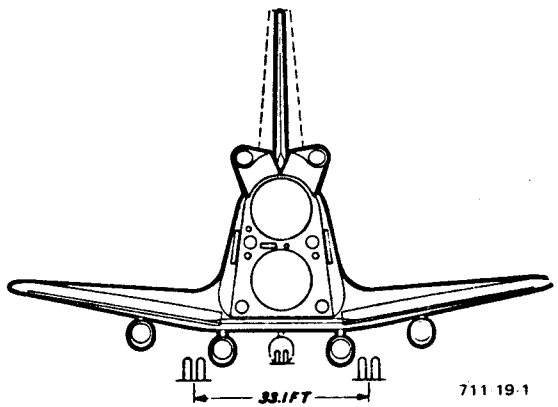

Figure 3-1
McDonnell Douglas HCR Configuration circa June 1971

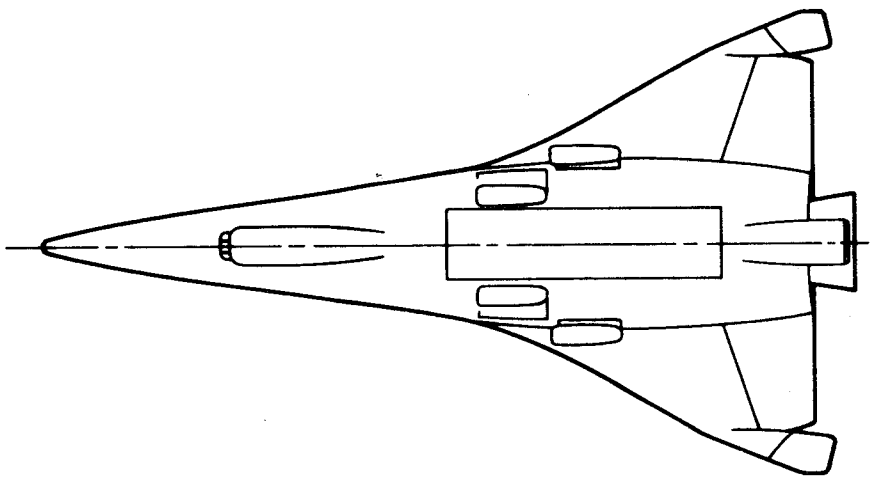

GROSS WT = 650,000 LB	
CONFIGURATION	INTEGRAL LH_2 TANK, FLOATING LO_2 TANK: LOW WEIGHT
AERO/THERMAL	ENTRY L/D: 0.7 – 2.4 SUB L/D: 9.1 W/C_LS: 46 LB/FT^2
STRUCT/TPS	PRIMARY: TITANIUM TANKS: ALUMINUM HEAT SHIELD: RADIATIVE
SYSTEMS	MAIN 2 X 477K LB ENGS: OMS (2 X RL 10) ACPS: SUPERCRITICAL STORAGE, O_2–H_2 ABES: 4 X JTF.22B-IP FUEL
PAYLOAD	26,000 LB

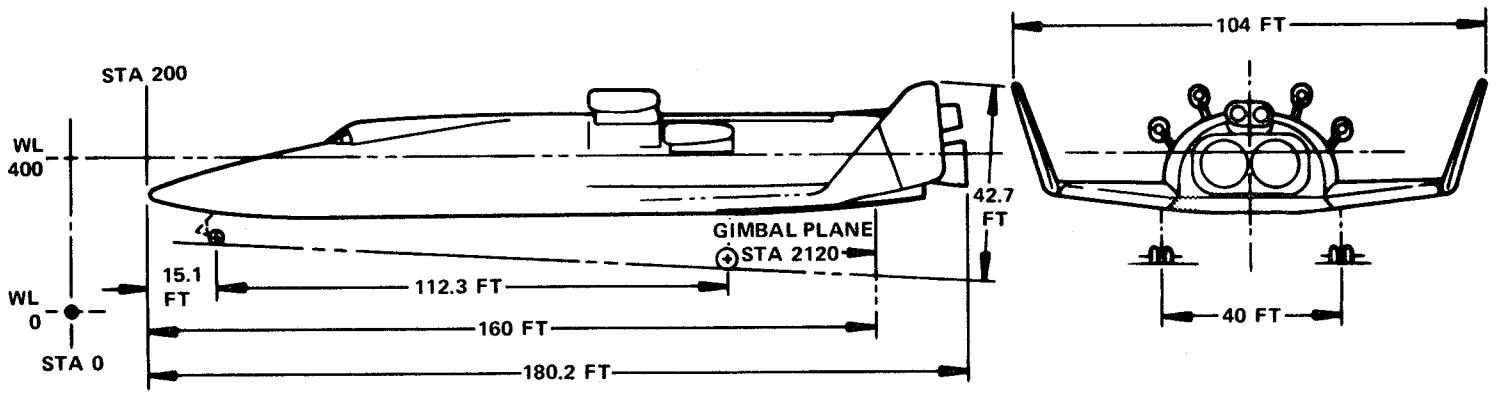

Figure 3-2
NAR Delta Orbiter Configuration SSV 134C circa August 1970

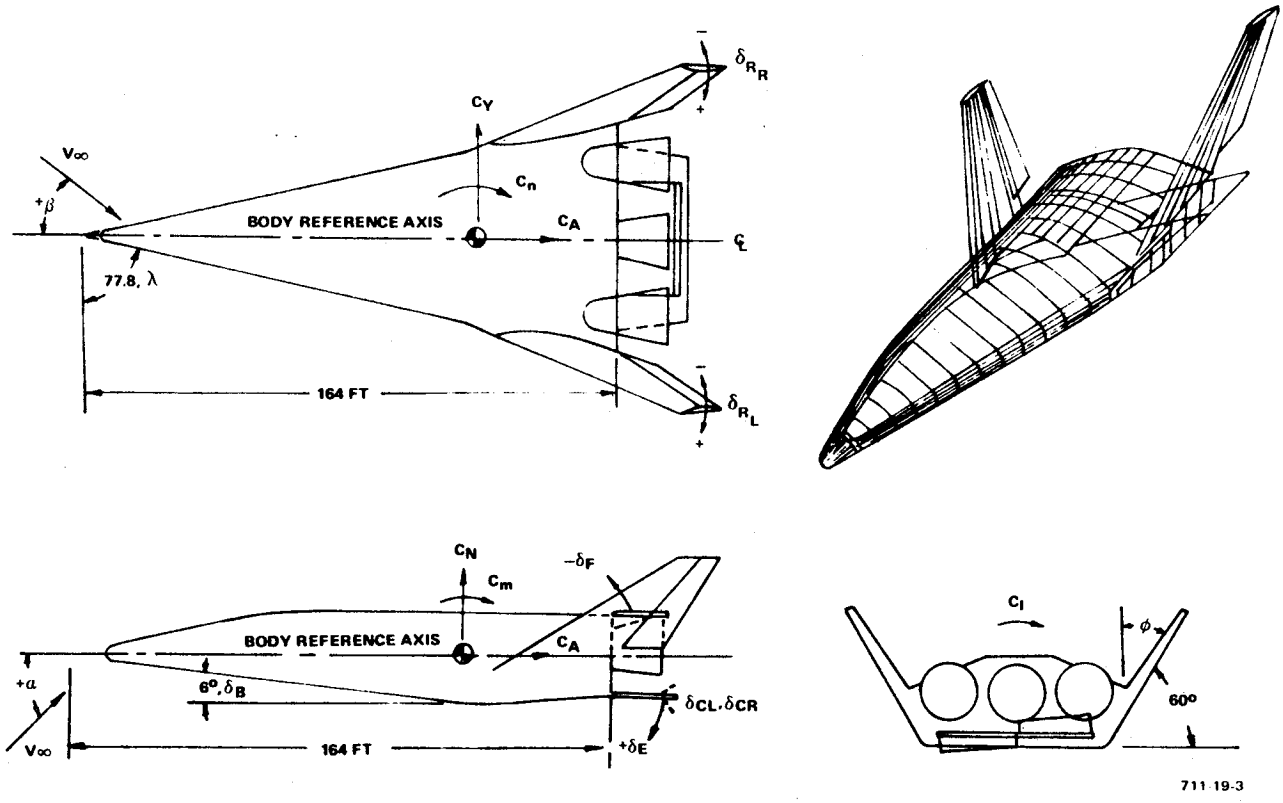

Figure 3-3
LMSC Delta Orbiter Configuration circa January 1970

LOW CROSS RANGE ORBITER ARRANGEMENT

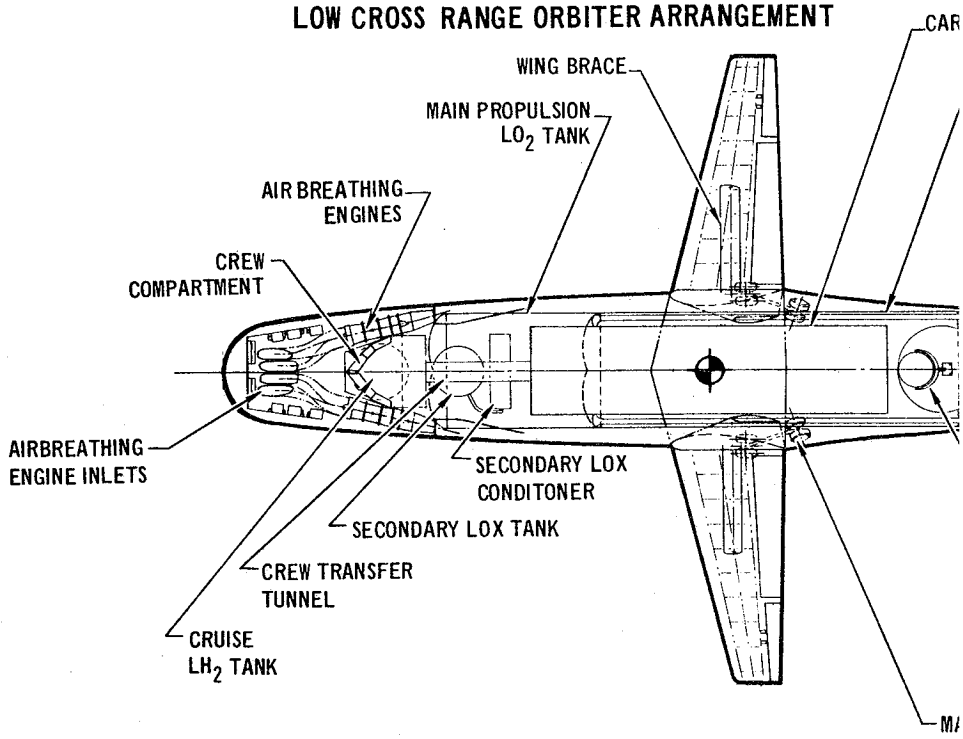

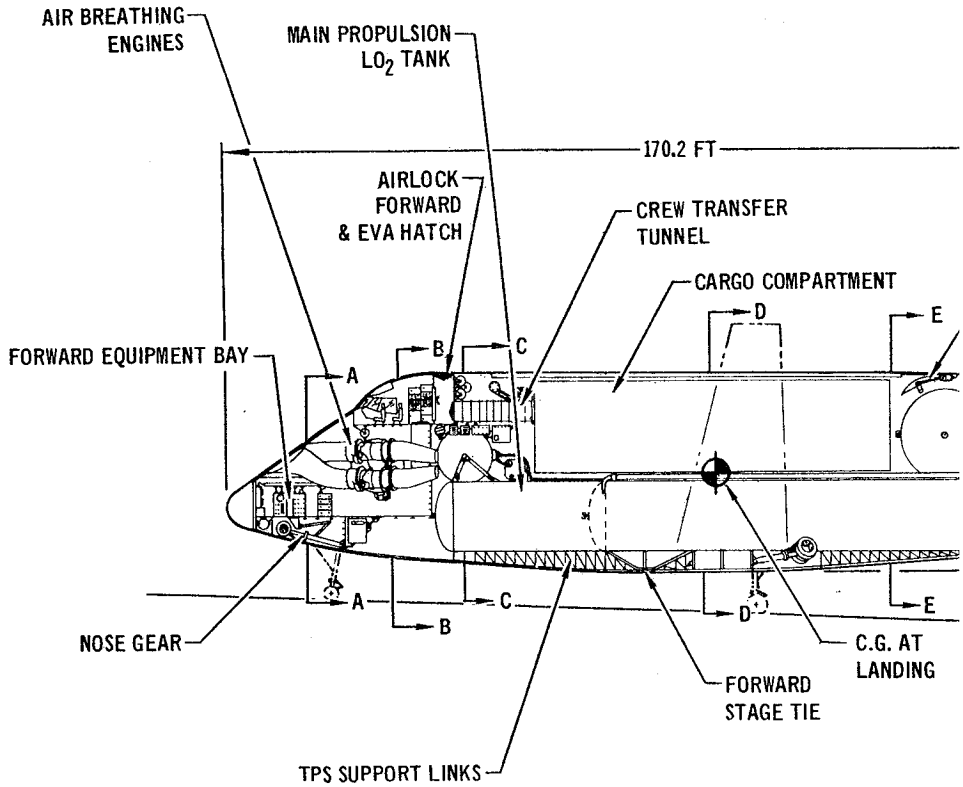

COMPARTMENT

MAIN PROPULSION
LH_2 TANK

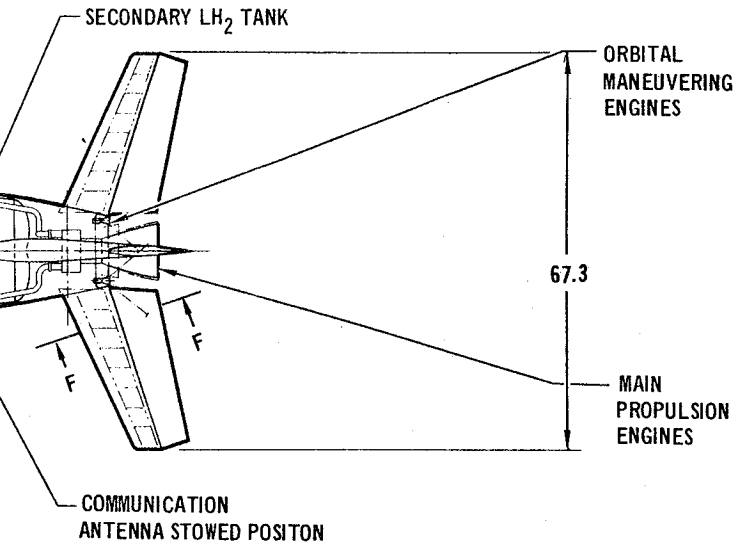

LANDING GEAR

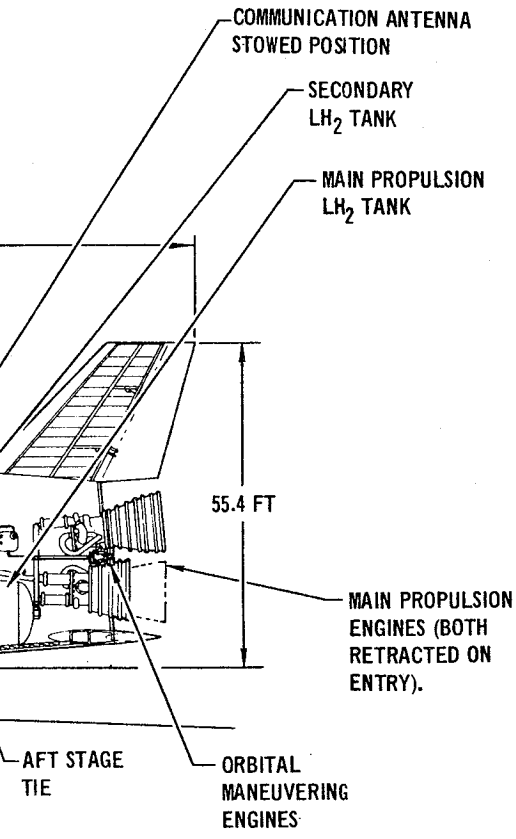

GEOMETRIC CHARACTERISTICS	
VEHICLE GEOMETRY	
TOTAL PROJECTED PLANFORM AREA	5,432 FT^2
BODY GEOMETRY	
WETTED AREA	13,999 FT^2
ML VOLUME	82,962 FT^3
LENGTH	154.8 FT
MAXIMUM HEIGHT	32.1 FT
WING GEOMETRY	
THEORETICAL AREA	1,841 FT^2
EXPOSED AREA	1,228 FT^2
ASPECT RATIO (AR)	7:1
DIHEDRAL ANGLE	7^o
L.E. SWEEP	14^o
TAPER RATIO	0.353:1
VERTICAL TAIL GEOMETRY	
EXPOSED AREA	600 FT^2
HEIGHT	24.5 FT
ASPECT RATIO (AR)	1.0:1
L.E. SWEEP	45^o
TAPER RATIO	0.471:1
HORIZONTAL TAIL GEOMETRY	
EXPOSED AREA	704 FT^2
ASPECT RATIO (AR)	4.18:1
L.E. SWEEP	25^o
TAPER RATIO	0.575:1

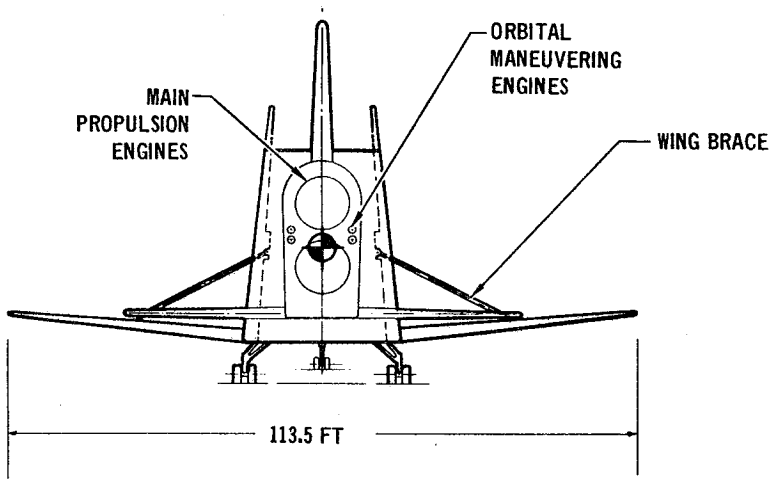

711-19-4

Figure 3-4
McDonnell Douglas LCR Configuration circa March 1970

The source of aerodynamic and mass property data for the five vehicles studied is References 10 through 14.

It is apparent that space shuttle vehicle configurations continue to evolve in several directions. Consequently, a guidance and control concept that is tailored to a specific vehicle configuration should be avoided. The approach taken in this study was to design systems that are applicable to broad classes of vehicles where only a few system parameters need be adjusted from vehicle to vehicle. The systems that were designed met this criterion. (The identical guidance and control system that flew the NAR HCR vehicle was used to fly the MDAC HCR vehicle.) An example of the evolutionary development of one design group's orbiter configuration is illustrated in Figure 3-5. Here the MDAC orbiter is shown changing from a low profile tip fin configuration in June 1970 to the high profile, center tail and higher aspect ratio wing by the spring of 1971. These changes were dictated by payload packaging efficiency (higher profile), L/D requirements for landing maneuvers (wing platform) and weight/cost optimization (elimination of tip fins). Continued changes of this type can be expected so that the guidance and control system design must be insensitive to configuration. As shown subsequently in this report, the only guidance and control parameters affected by such configuration changes are autopilot stabilization loop gains and some of the maneuver command programs associated with the flareout.

2. Nominal Trajectory and Control Phases

The orbiter reentry trajectory defines the initial conditions for the terminal guidance phase of flight. There is no well defined transition between reentry guidance and terminal guidance. In this study it was arbitrarily assumed that terminal guidance begins at an altitude of 100,000 feet. In the subsequent discussions of terminal guidance windows it will be shown that the transition between reentry and terminal guidance is not distinct and that terminal guidance should be initiated on the basis of distance from a target point as well as altitude and velocity. One of the problems with selecting 100,000 feet as an initial point for terminal guidance is that the delta wing orbiter is generally in the middle of a high to low angle of attack attitude transition at that altitude. This angle-of-attack transition maneuver should be related to terminal energy management criteria and therefore should not start before the terminal energy management system is activated.

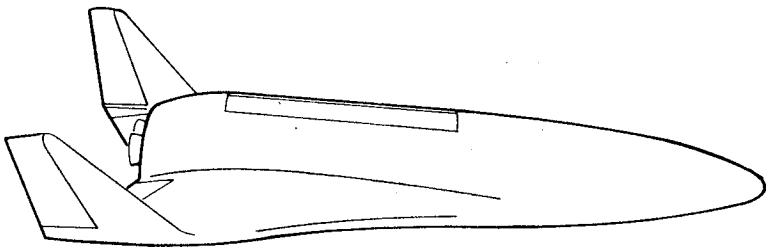

PROPOSAL
MARCH
TO
JUNE 1970

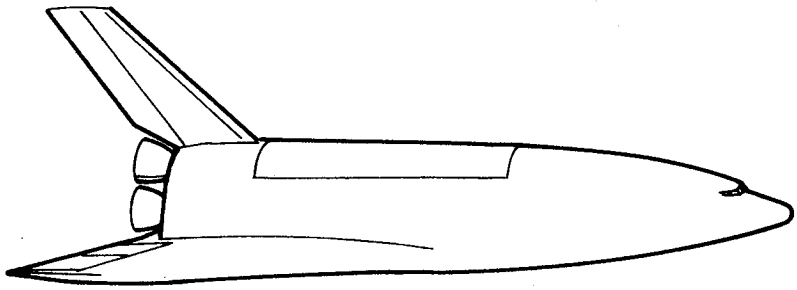

MIDTERM
NOV 1970

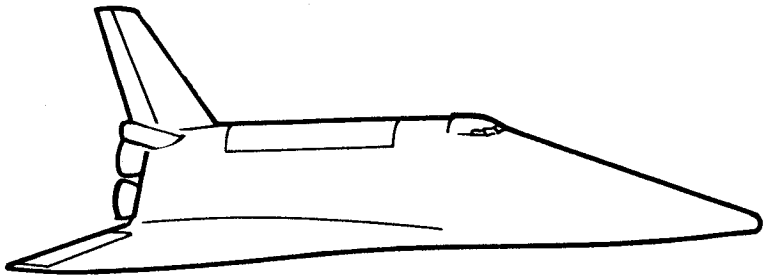

FINAL
SPRING 1971

711-19-5

Figure 3-5
MDAC High Cross-Range Configuration Evolution

The reentry trajectory determines the initial conditions for the terminal phase. Several typical space shuttle orbiter reentry trajectories illustrate this point. Figures 3-6 and 3-7 illustrate the LMSC delta orbiter's reentry for a 1500 NM and a 400 NM cross-range. Note that in the region of terminal control initiation (about 100,000 feet) the dynamic pressures for the two cases are significantly different. Also, for the 400 NM cross-range case, the angle of attack is in its transition phase at 100,000 feet while in the 1500 NM cross-range case the angle of attack had reached its nominal supersonic cruise value at 100,000 feet. Figure 3-8 shows a nominal reentry history for the MDAC delta wing orbiter. It is an 1150 NM cross-range reentry with angle of attack held at 30 degrees. (Bank angle is modulated to maintain the flight path along the thermal boundary.) As transonic speeds are approached, the trim capability of this class of vehicle is decreased sharply so that the 30 degree angle of attack must be reduced as the region of terminal control is reached. This reduction in angle of attack and the concomitant build up in dynamic pressure, Q is not shown on this reentry history but it is the essential first phase of the terminal guidance and control procedure.

The reentry trajectory of the low cross-range, straight wing vehicle is markedly different from the high cross-range vehicles (Figure 3-9) primarily because of the very low dynamic pressures associated with the LCR reentry. The interesting feature of the straight wing LCR vehicle was its ability to lock into a trim angle of attack of 60 degrees by virtue of a deep stall condition. Dynamic pressures must be sufficiently low to permit reasonable sizing of reaction control thrusters and to minimize limit cycle oscillations and reaction control fuel consumption. These oscillations are aggravated by tendencies toward lateral-directional aerodynamic instabilities which must be controlled entirely by the reaction control system. In contrast, the HCR vehicle is designed to use aerodynamic surfaces for stability augmentation (in conjunction with blended reaction controls) during the reentry phase.

A summary of the terminal guidance and control phases (below 100,000 feet) is illustrated with nominal HCR and LCR vehicle altitude-velocity plots on Figure 3-10. Note that the acquisition of the high energy glide path, the tracking of that path, the flare to a shallow glide path and the tracking of that path and finally the flareout and decrab maneuver leading to touchdown are essentially

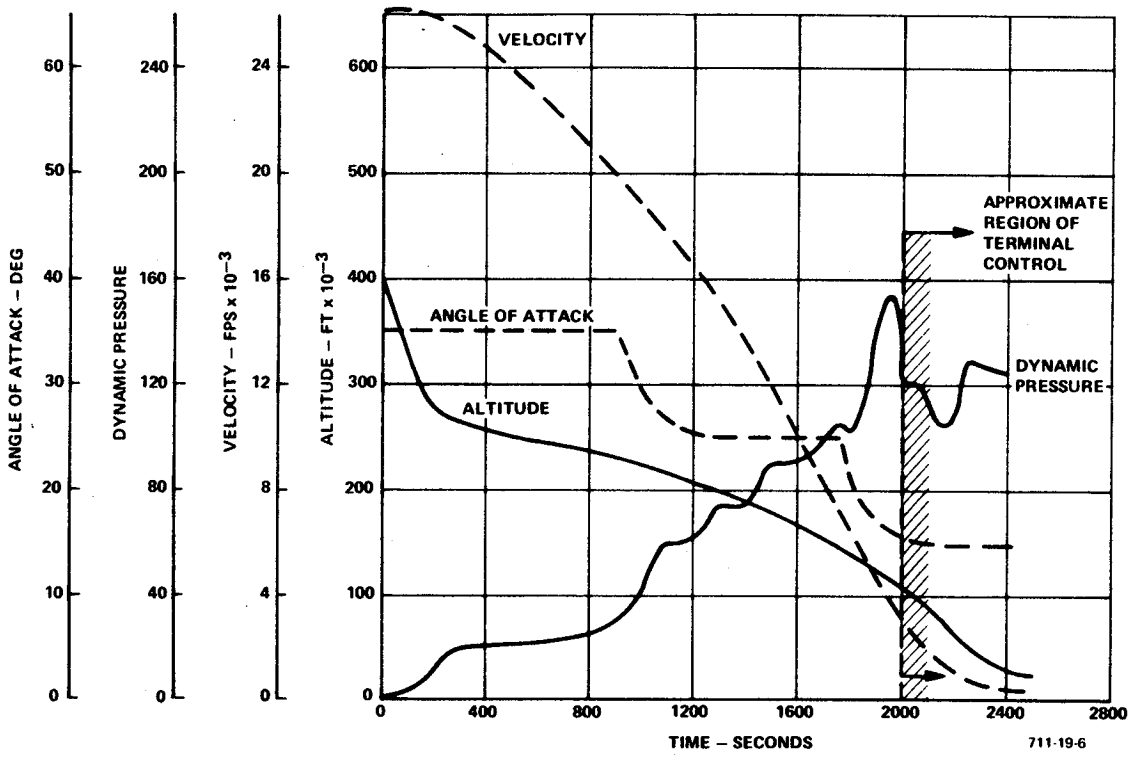

Figure 3-6
Typical HCR Vehicle Reentry Trajectory,
LMSC Vehicle, 1500-nautical mile Cross-Range

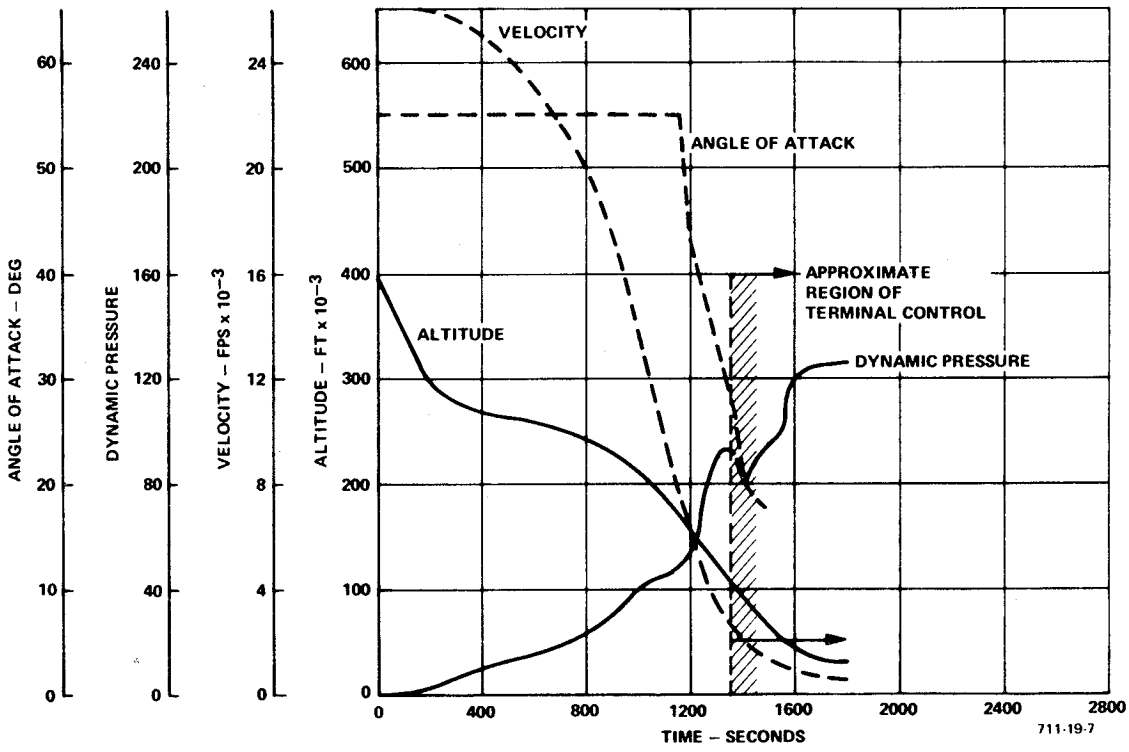

Figure 3-7
Typical HCR Vehicle Reentry Trajectory,
LMSC Vehicle, 400-nautical mile Cross-Range

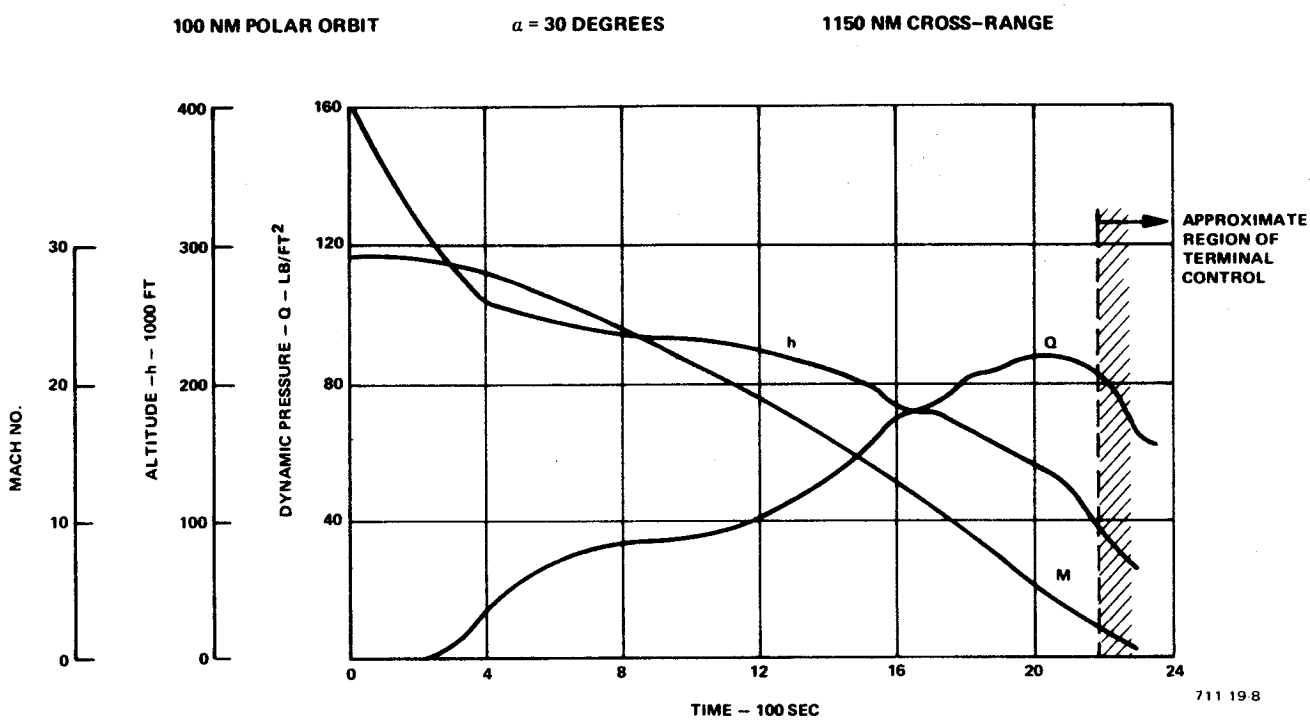

Figure 3-8
McDonnell Douglas Delta Orbiter Entry Time History

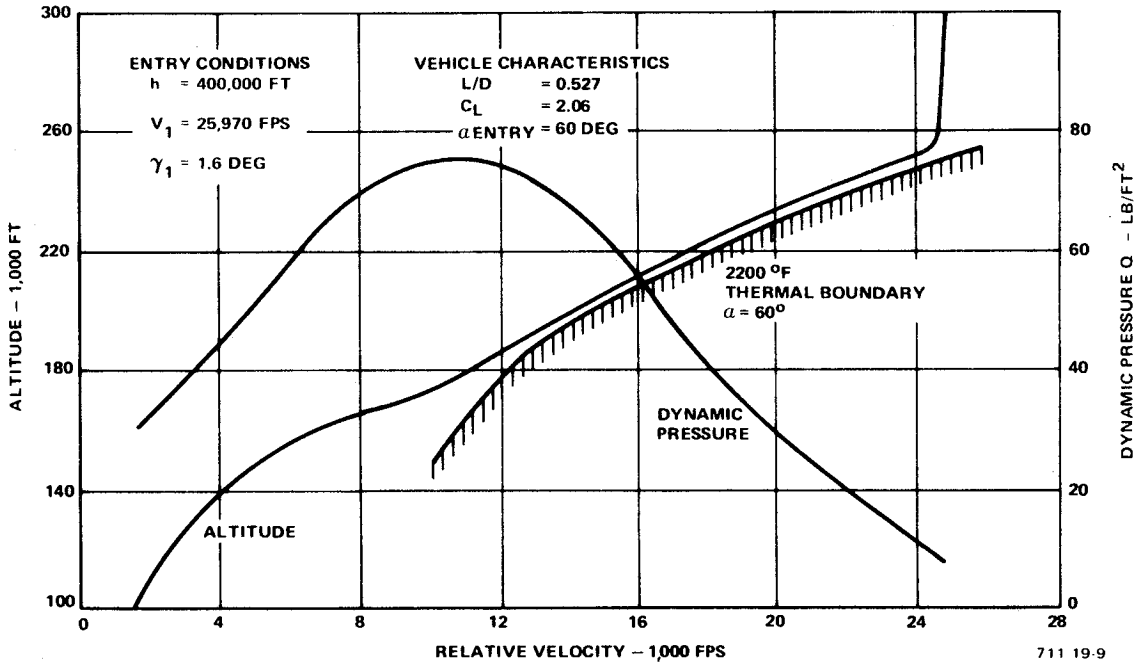

Figure 3-9
Low Cross-Range Orbiter Entry Trajectory

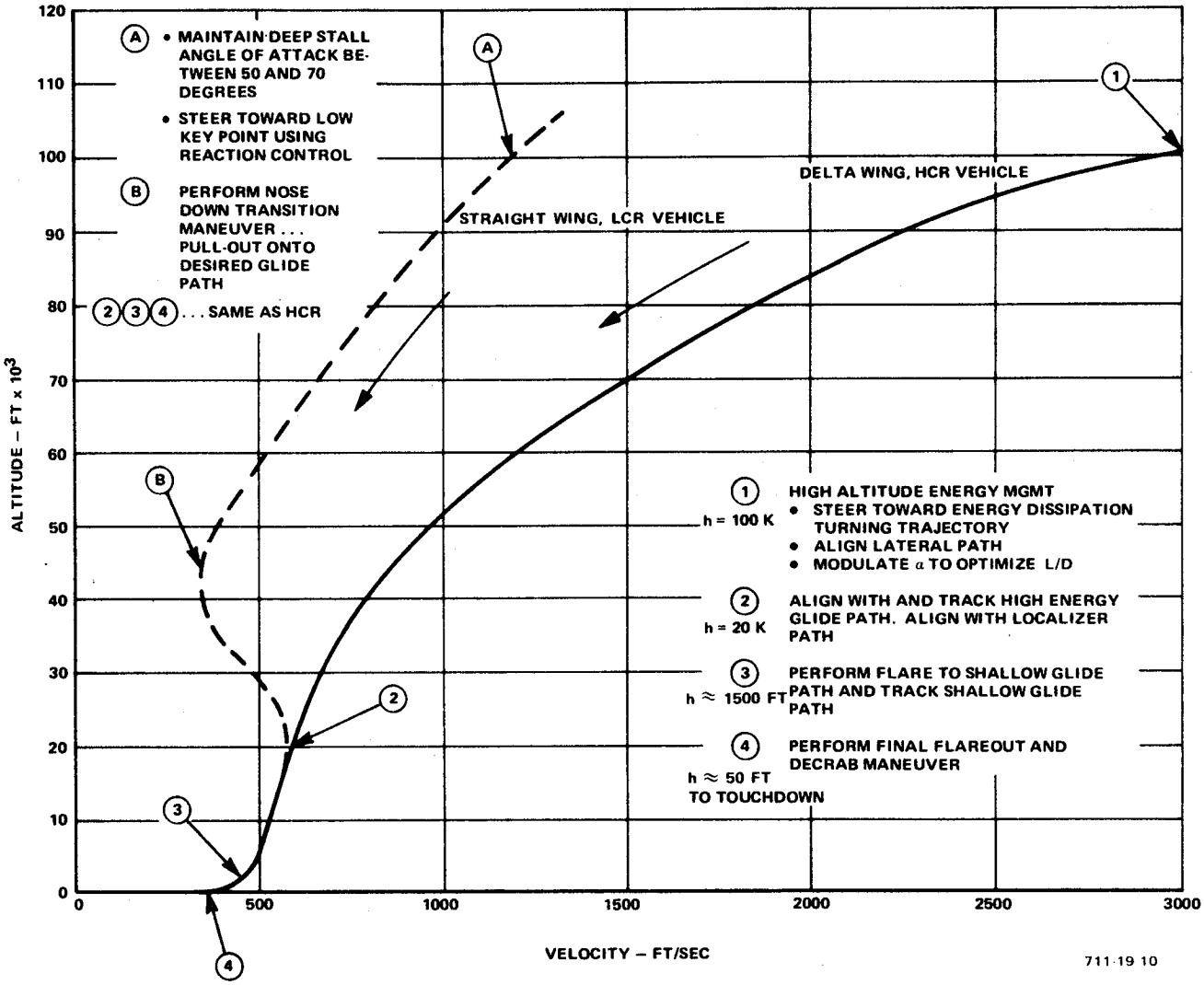

Figure 3-10
Terminal Guidance and Control Phases for HCR and
LCR Vehicles, Typical Altitude-Velocity Trajectories

identical for both classes of vehicles. (Although not shown on Figure 3-10, the final velocities of the LCR vehicle were about 10 percent lower than those of the HCR vehicle.) In the high altitude region the guidance and control activity is significantly different for the two types of vehicles. Lateral-directional control is accomplished with the reaction control system for the LCR vehicle because of the low dynamic pressure (below 30 pounds per ft^2). Pitch control is provided with combined reaction and aerodynamic controls; the elevator or horizontal stabilizer used for achieving steady state trim only. At the transition altitude of about 45,000 feet, the LCR vehicle noses down to conventional angles of attack, picks up speed and pulls out of its dive at a descent angle of about -12 degrees which is the high energy glide path angle. The HCR vehicle, on the other hand, flies as a relatively conventional supersonic aircraft, between (1) and (2) on Figure 3-10, decelerating from Mach 3.0 to about Mach 0.7 before it acquires the high energy approach path. At point (2) and below, both vehicles follow the same control procedures.

3. Operational Considerations

a. The Uses of Air Breathing Engines

Of the illustrations depicting four space shuttle orbiters shown in Figures 3-1 through 3-5, only the MDAC delta wing vehicle suggests the use of air breathing engines. Actually such engines are considered optional on all vehicles and the designs have made provision for their incorporation. They are certainly needed for performing the ferry mission to the launch site. Their use in cruise and landing is still being debated. This study, as well as other work in recent years, has demonstrated that unpowered landings of space shuttle orbiters under IFR conditions are feasible. The payload penalty of landing engines makes the unpowered landing the most desirable appraoch. A configuration that permits their attachment for ferry flights but removal for space missions appears to be favored. Nevertheless the debate continues over the need for a missed appraoch, go-around capability. Even if such a capability is specified, there is no compelling reason to alter the landing approach techniques from those used for the unpowered vehicles. References 15 and 16 present a strong case for using steep angle, high energy approach and landing techniques even for conventionally powered aircraft. If engines must be provided to meet a go-around capability

requirement, then the engines would be started prior to acquisition of the terminal glide path but would be operated at idle thrust for a normal, unpowered landing approach. The thrust would be increased only for an abort situation. Consequently, the use of landing engines need not alter the basic guidance and control system as designed for unpowered landings.

b. Speed Control Techniques

Speed control through proportional deployment of speed brakes provides much of the capability of throttle controls. In the vehicles studied on this program, only the MDAC delta wing configuration specified speed brakes and their aerodynamic characteristics. They were found to be effective in minimizing touchdown dispersions resulting from headwinds and tailwinds. The results obtained with this MDAC vehicle are described in a forthcoming supplement to this report. Those vehicles without speed brakes were studied using the following approach:

- Fly a higher landing speed trajectory to cover worst headwind cases and incur the penalties of higher speed touchdowns.
- Consider such speed control augmentation techniques as variable altitude for flap deployment (when flaps are available).

In every case, the performance obtained without speed brakes may be viewed as worst case performance that will always be improved if speed brakes are used.

c. Role of Pilot in Performance Monitoring and Manual Control Tasks

The role of a pilot in a guidance and control task that is dependent upon computers has always been questionable. His participation in an abort situation such as a manual takeover to avoid a collision has never been controversial. Likewise, his aborting a mission and returning the vehicle in a purely manual back-up mode is readily accepted. The controversy lies in the question of why and how should the pilot participate in the guidance and control task when sensors and computers are the only means of determining the required vehicle maneuver and control action. The problem is aggravated further in a fly-by-wire system where even the pilot's manual control activity is effected through electronic computers. If the fly-by-wire computers are common with the guidance

computations (central integrated system), then the concept of pilot back-up is no longer tenable.

The pilot's monitoring ability is generally superior to the best automatic monitoring systems because of his unique talent in correlating a variety of information (displays, vehicle motions, sounds, etc.) to detect anomalous system performance. Even this talent loses significance or is extremely difficult to exploit in the integrated avionics complex being recommended or suggested for space shuttle vehicles.

The pilot's function as a system performance monitor was within the scope of the Study of Landing Techniques for Space Shuttle Vehicles. The pilot was used to observe automatic system performance from the simulator cockpit by viewing the progress of the flight on the vertical and horizontal situation display instruments. Raw position and velocity information is displayed on these instruments. They also provide flight director command cues that permit the pilot to control the vehicle in response to the computed steering commands. The value of a flight director or semiautomatic mode is questionable since the same computers and sensors solve the fully automatic problem. Nevertheless, this mode was evaluated.

The transition from automatic to manual control in a failure situation was looked at, but not in great depth. Loss of raw position and velocity data, or computed flight path data in IFR conditions would be catastrophic for the unpowered vehicle. Loss of the integrated computer complex which includes the fly-by-wire mechanization would also be catastrophic. Consequently, the simulation of a failure condition that permits continued operation of the vehicle contradicts the multiple fail-operative concepts that have been entertained by space shuttle avionics designers. (A failure should not have resulted in the loss of a function.) The manual conditions that were simulated presumed the availability of a fly-by-wire control system that was independent of the integrated computer complex. It also assumed the availability of basic data such as speed, altitude, attitude, and deviation from desired vertical and lateral paths as raw information separate from the computer complex. The availability of raw information regarding flight path deviation may be a reasonable assumption for lateral control but most candidate landing guidance systems will require on-board computation to generate

vertical flight path deviation. These are questions of avionics philosophy that were not addressed in the performance of this study. Thus, a back-up manual mode was mechanized and evaluated in the simulator but the avionics system architecture associated with such a mode was considered to be outside of the study scope.

B. DISCUSSION OF EQUILIBRIUM GLIDE APPROACH PATHS

1. Historical Perspective

The techniques of unpowered landings date back to the earliest aircraft and glider flight experience. The use of a high energy or steep angle glide path followed by a flare to a shallow landing path has always been a recommended landing procedure for engine out conditions in most aircraft. In the early 1960's these techniques were developed as the standard operating procedures for experimental, high performance vehicles. The X-15 research program and the preliminary design activity associated with manned lifting reentry vehicles in the late 1950's and early 1960's stimulated many investigations of unpowered landing techniques for relatively low L/D vehicles (References 17, 18, 19 and 20). Various analytical approaches to some of the aerodynamic aspects of unpowered landing techniques have been formulated (References 21 and 22, for example) and simulations have demonstrated successful, unpowered landings with innumerable vehicles. Automatic guidance and control for terminal area energy management and automatic landing of lifting reentry vehicles was developed for the unmanned, initial flights of the X-20 DynaSoar (Reference 23) and that system was built in 1963 before cancellation of the DynaSoar program. Since the mid 1960's the NASA Flight Research Center has been performing lifting body (HL-10, M2-F2, M2-F3, X-24) unpowered landings on almost a routine basis and the USAF Aerospace Research Pilot School includes F-104, low L/D, unpowered approaches as a key training activity.

With the advent of the space shuttle programs and increased interest in unpowered horizontal landing for large aircraft, the USAF Flight Test Center and NASA Flight Research Center have conducted joint flight evaluation programs with various aircraft that demonstrated candidate unpowered landing techniques (References 16, 24, and 25). Also much of the steep angle and biangular approach flight tests performed in recent years as part of air traffic and airport noise abatement studies have much in common with the unpowered landing technology which is of interest to the space shuttle program. It is therefore apparent that the

study results reported herein do not involve any pioneering aerospace concepts. The essence of this study from the perspective of more than a decade of continuing research in related technologies is the formulation and evaluation of a practically realizable navigation, guidance and control system that can provide space shuttlecraft with a fully automatic or manual capability for unpowered terminal area descent and precision horizontal landings. Verification of system concepts were bounded by two requirements: a) Performance had to be demonstrated with detailed simulations of candidate space shuttle designs that include all the generic classes of shuttlecraft (and all their aerodynamic peculiarities) under consideration. b) The system had to be consistent with state-of-the-art avionics technology in regard to landing guidance sensors, inertial, air data and other vehicle measurement requirements and practical flight control system constraints.

2. Flight Path Stability and Flight Path Angle Versus Speed

The ability of an aircraft to maintain a specified flight path angle (or climb and descent rate) is treated under the general subject of "airplane performance". The thrust or power required curves that specify aircraft performance capability also can be used to cover glider or zero thrust performance characteristics. These curves can be related to flight path stability and can be used as a convenient introduction to the theory of the equilibrium or energy management flight paths for the unpowered space shuttlecraft.

Figure 3-11 illustrates the form of thrust and power required curves for an aircraft in level flight. In this case the thrust must equal the drag to achieve level, non-accelerating flight. The speed for minimum drag corresponds to the speed that will yield the maximum L/D. The power required curve is obtained by multiplying the drag by velocity. There is significance to the slope of the thrust required curve in terms of flight path stability. This type of flight path stability referred to as operation on the front or back side of the thrust or power curve has an equivalent application to the unpowered, gliding vehicles. Figures 3-12 and 3-13 illustrate the flight path stability concept for a powered case. Consider an aircraft in level flight operating at speed V_{A_1} on Figure 3-12. If thrust were held constant and the aircraft were pitched up an amount $\Delta\theta$, a climb would be initiated with flight path angle γ, and vertical speed $\dot{h}$ changing as

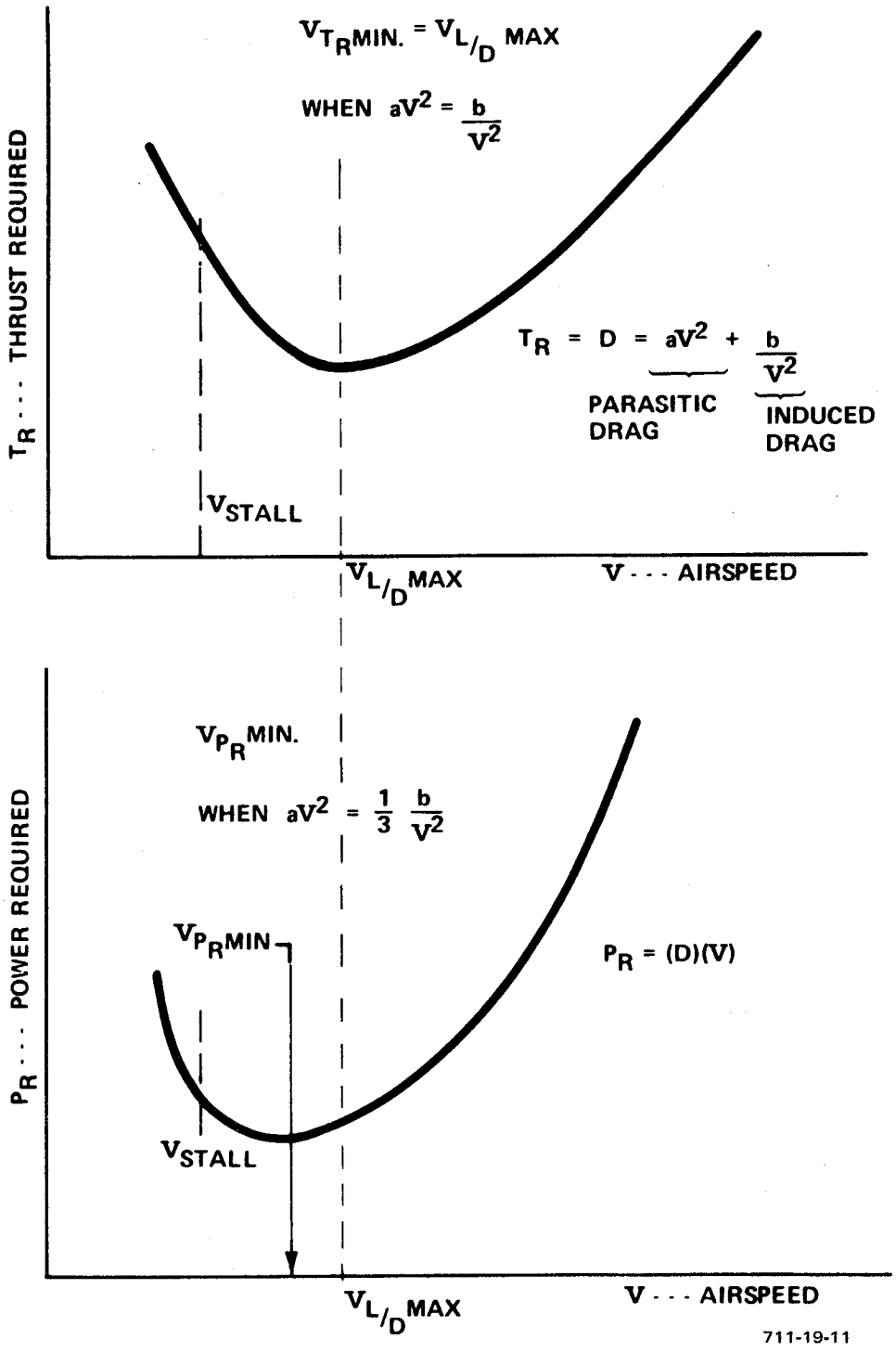

Figure 3-11
Thrust and Power Required Curves (Level Flight)

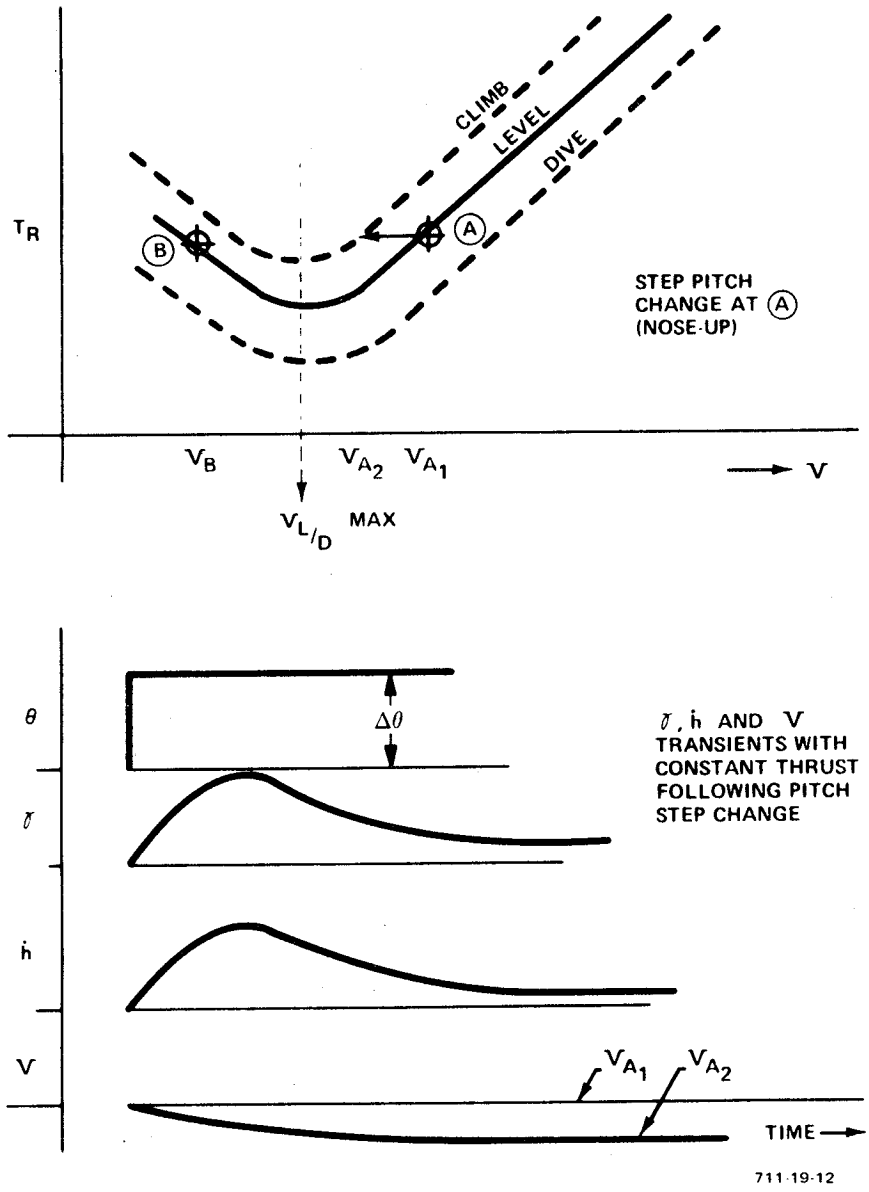

Figure 3-12
Flight Path Control on Front Side of Thrust Required Curve

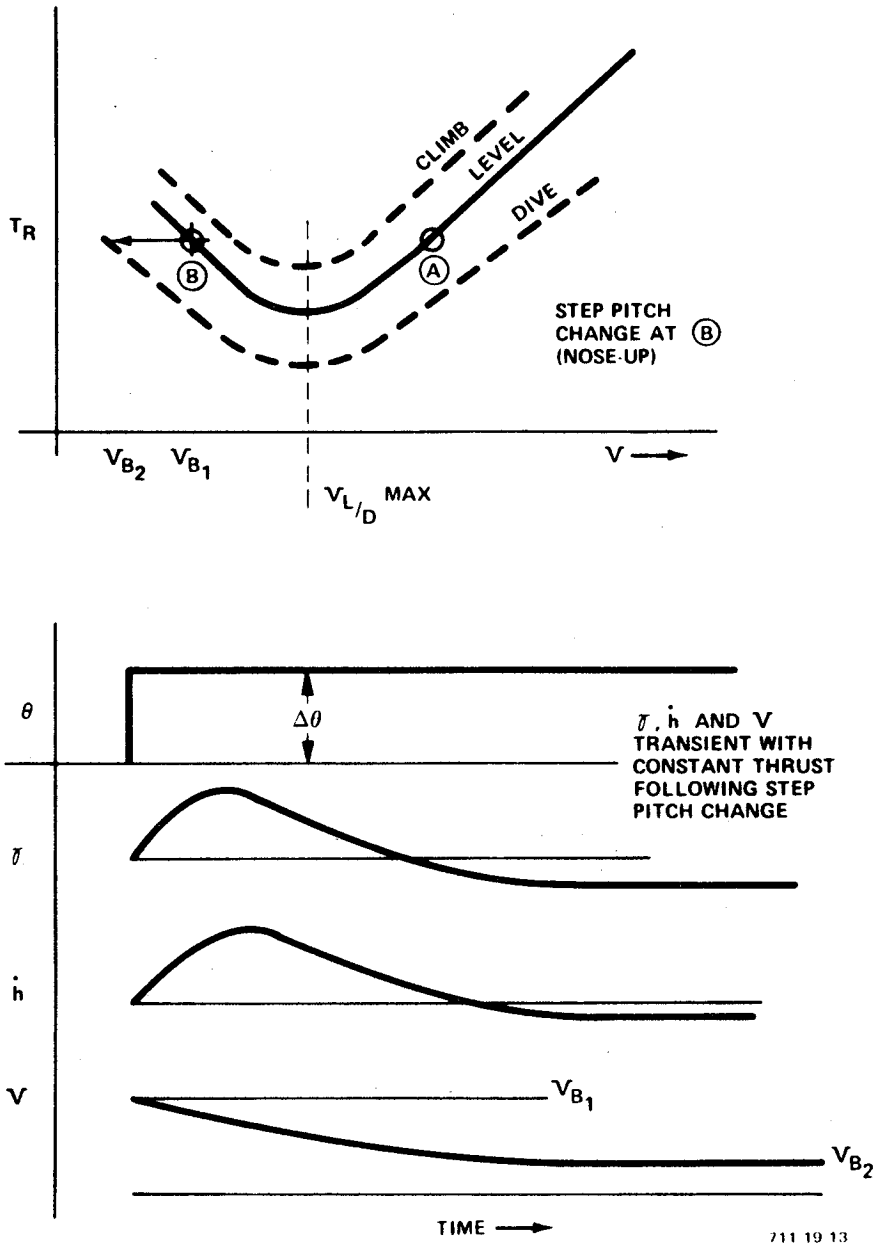

Figure 3-13
Flight Path Control on Back Side of Thrust Required Curve

shown on Figure 3-12. To maintain a climb, the thrust required equation must remain balanced in accordance with

$$T_R = D + W \cos \gamma = aV^2 + \frac{b}{V^2} + W \cos \gamma \qquad (3\text{-}1)$$

The thrust required, T_R, for climbs or dives are shown as dashed curves on Figure 3-12. They are offset from the level flight curve by an amount equal to W cos γ. With thrust held constant and a climb initiated, the aircraft speed will decrease until a new equilibrium speed V_{A_2} given by the relationship

$$aV_{A_1}^2 + \frac{b}{V_{A_1}^2} = aV_{A_2}^2 + \frac{b}{V_{A_2}^2} + W \cos \gamma \qquad (3\text{-}2)$$

is reached.

Now let us attempt the same maneuver on the other side of $V_{(L/D\ MAX)}$ (point B). Figure 3-13 illustrates the resulting response. With a step increase in pitch attitude, the flight path angle initially increases and a speed reduction begins. As the speed is reduced (with thrust held constant) the only equilibrium achievable is a dive at velocity V_{B_2} rather than the desired climb. If pitch attitude is constrained at the increased value $\Delta\theta$, a new equilibrium diving flight path angle and velocity will be reached. If we attempted to constrain the aircraft to an increased flight path angle by further increasing the pitch attitude, the speed reduction would be more rapid until the stall speed would be reached.

The designer of guidance systems for aircraft flight path control encounters this problem in automatic approach systems when the aircraft is being operated on the "back side of the power curve" but he recognizes the problem in the linearized transfer functions. As implied by the transient responses shown on Figures 3-12 and 3-13, the phenomenon should be seen in the pitch attitude-flight path angle relationship which in transfer function form is

$$\left(\frac{\gamma}{\theta}\right)(s) = \frac{s + \left(\dfrac{C_{D_1} C_{L_\alpha} - C_{L_1} C_{D_\alpha}}{C_{L_\alpha} \tau} - \dfrac{T_V}{m}\right)}{(s + \omega_1)(s + \omega_2)} \qquad (3\text{-}3)$$

where

$$\tau = \frac{m}{\rho S V} \tag{3-4}$$

T_V = thrust gradient = $\partial T/\partial V$

and subscript (1) refers to initial condition

Equation (3-3) shows that if we neglect the thrust gradient effect, the numerator zero moves into the right half plane when

$$C_{L_1} C_{D_\alpha} > C_{D_1} C_{L_\alpha} \tag{3-5}$$

which corresponds to operation at velocities below $V_{(L/D\ MAX)}$. Attempts to close a γ control loop under these conditions will force the system poles to move toward the right half plane zero. The time to double amplitude of the resulting divergent instability will depend upon the loop gain and how far into the backside of the thrust required curve the system is operating.

Now how does this relate to the unpowered, gliding vehicle? If we continued to add dive curves to the T_R versus V plot for steeper and steeper values of γ, these curves would intercept the $T_R = 0$ line. For each incremental γ there will be two values of V. The shallowest γ or minimum descent angle that intercepts the $T_R = 0$ line will be at $V_{(L/D\ MAX)}$. If we plotted the values of V for each value of γ we would get a curve of the form shown on Figure 3-14. (This curve corresponds to a relatively low L/D vehicle.) The significance of the curve from the standpoint of flight path control can be demonstrated by following an attempt to constrain the vehicle to a fixed glide path having an angle of about -17 degrees. Assume we are below the path and must shallow our descent to acquire the desired glide path as illustrated on Figure 3-15. If we are operating on the front side of the L/D curve at a speed of about 280 knots, we will follow the stable loop shown on Figure 3-14. As flight path angle decreases we move above the equilibrium curve. Operating above the curve results in a deceleration. The vehicle decelerates until it reaches the desired glide path. It then must increase its descent angle. This moves it below the equilibrium glide

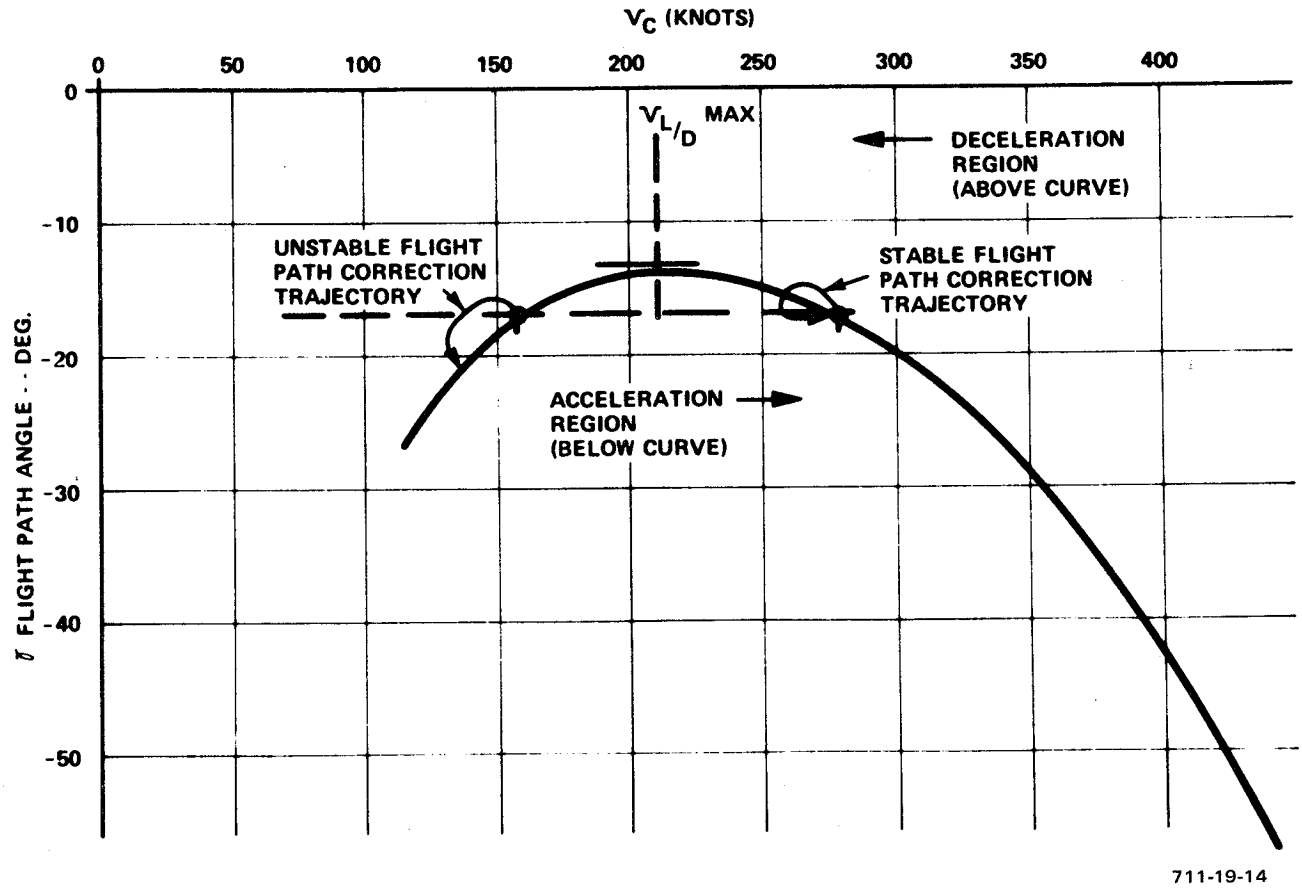

Figure 3-14
Equilibrium Terminal Glide Capabilities

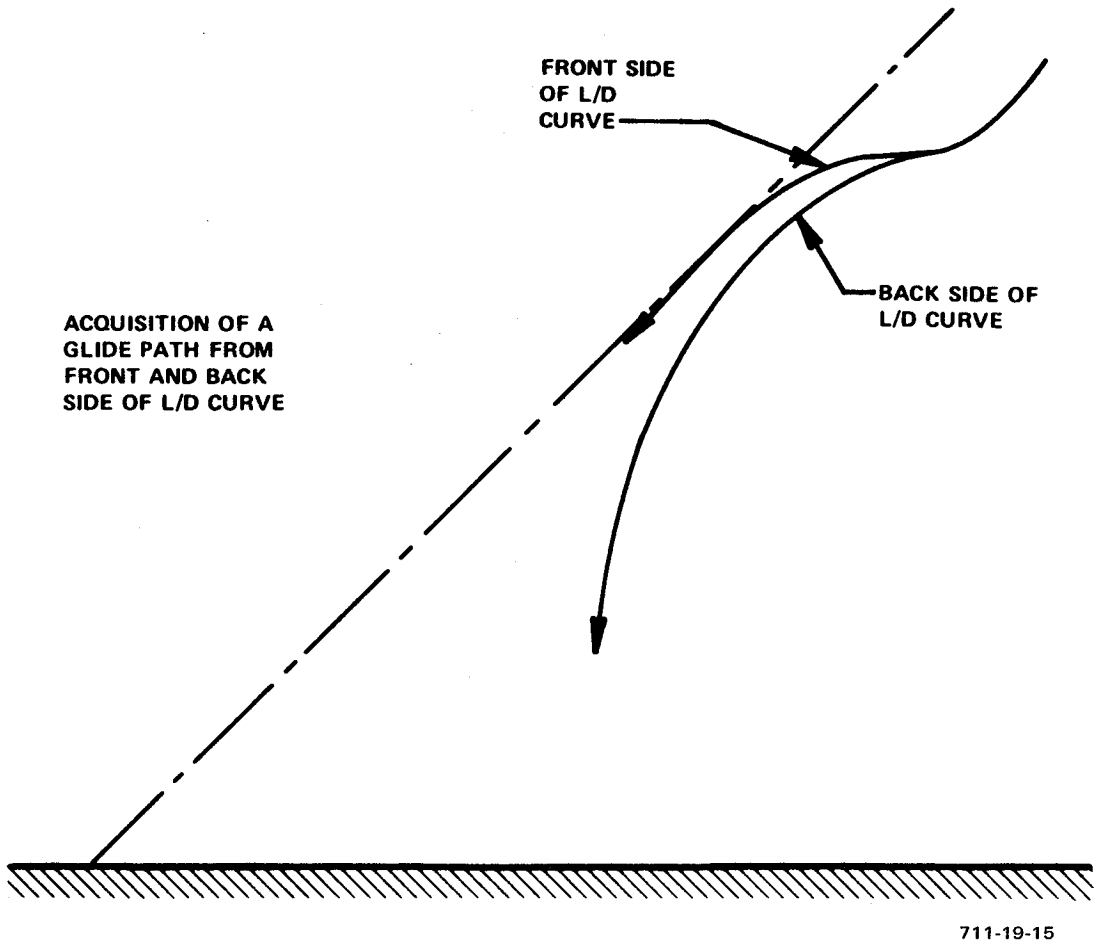

Figure 3-15
Acquisition of a Glide Path from Front and Back Side of L/D Curve

curve. Operation below the curve results in positive acceleration. The vehicle accelerates to reacquire the equilibrium speed of 280 knots on the desired glide path.

If we attempted to operate on the other equilibrium velocity below $V_{(L/D\ MAX)}$ for the -17 degree glide path, we obtain the divergent path illustrated on Figure 3-14. Nosing up results in a decelerating path. Equilibrium can be restored only by diving to a steeper angle than the desired glide path angle as illustrated by the unstable loop on Figure 3-14.

The significance of the equilibrium glide path curve of γ versus speed is the information that γ constraint above the curve leads to deceleration and γ constraint below the curve leads to an acceleration. If the accelerations along the constant γ lines intercept the curve the vehicle will reach speed equilibrium. If it does not intercept the curve, the vehicle will eventually stall. In the terminal guidance of the unpowered space shuttlecraft, operation above the curve and at angles considerably shallower than γ for L/D (max) does occur. However, it occurs during the final flareout phase where the speed reduction is part of the system design concept. In this case the vehicle is removed from an equilibrium state and placed in a transient state. The duration of the speed transient is a critical design parameter since touchdown must occur before the speed loss is excessive.

Since a fixed glide angle γ corresponds to an equilibrium airspeed, the guidance concept for landing unpowered vehicles is to aim that fixed glide angle at a point short of the desired landing point. Constraining the vehicle to the glide path formed in this manner ensures the simultaneous satisfaction of position and speed requirements prior to flareout. Figure 3-16 illustrates the geometry of the landing glide paths and defines the dynamic relationships which permit the derivation of the equilibrium glide angle versus speed curve. The well-known glider equation for equilibrium relates vehicle lift, L, drag, D, and flight angle, γ.

$$\tan \gamma = \frac{D}{L} = \frac{C_D}{C_L} \qquad (3\text{-}6)$$

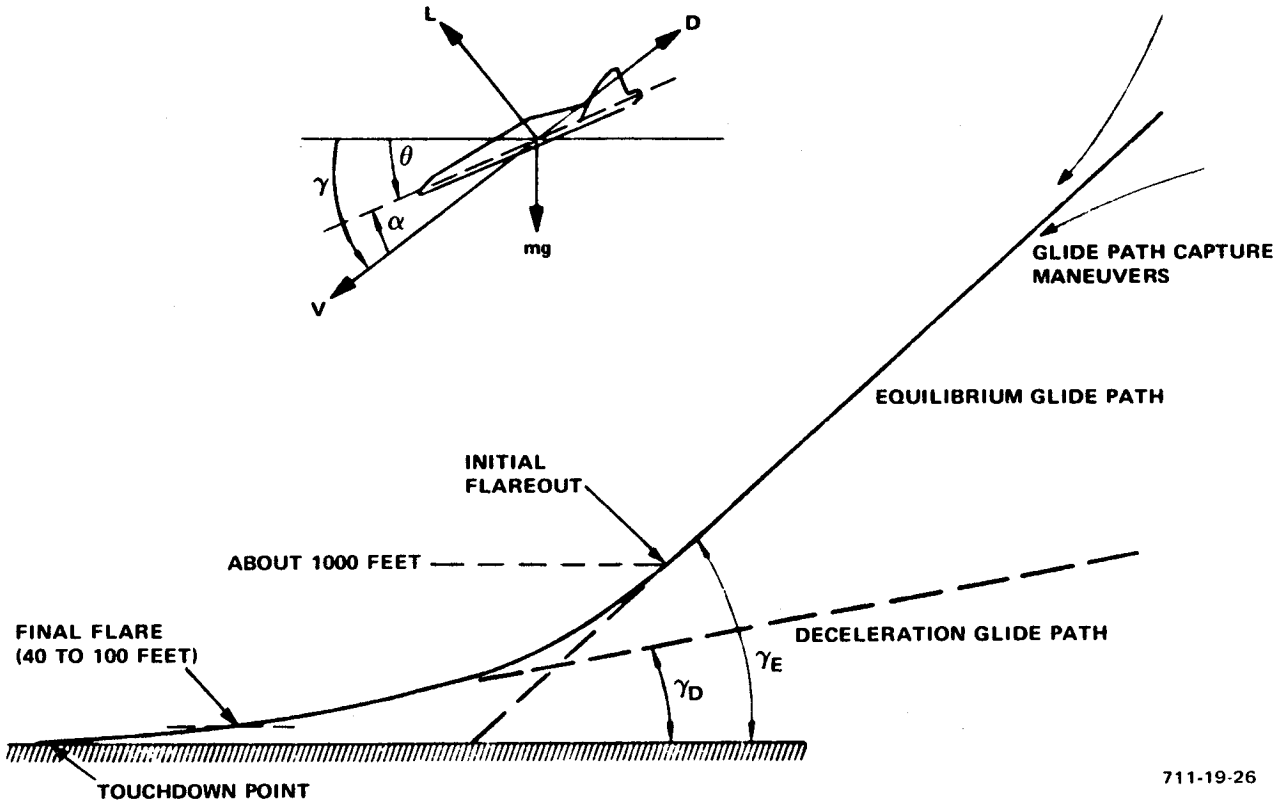

Figure 3-16
Geometry of the Two-Stage Glide Path Landing Concept

Approximating the drag coefficient C_D in terms of the lift coefficient C_L as

$$C_D = C_{D_o} + a\ C_L^2 \tag{3-7}$$

and combining with Equation (3-6) gives

$$\tan \gamma = \frac{C_{D_o}}{C_L} + a\ C_L \tag{3-8}$$

For zero lift acceleration

$$C_L = \frac{L}{QA} = \frac{W \cos \gamma}{QS} \tag{3-9}$$

Combining Equations (3-8) and (3-9), the relationship defining γ and Q dependence is Equation (3-10).

$$\sin^2 \gamma + \frac{Q}{a(W/S)} \sin \gamma - \left[1 + \frac{C_{D_o} Q^2}{a(W/S)^2}\right] = 0 \tag{3-10}$$

Typical curves derived from Equation (3-10) for various candidate shuttlecraft are shown in Figure 3-17. These curves were derived from early aero data which may have been subsequently modified. Calibrated airspeed rather than dynamic pressure is plotted on the abscissa. For each value of dynamic pressure Q in Equation (3-10), the appropriate compressibility correction is made for sea level to define impact pressure Q_C. From Q_C, the calibrated airspeed is determined using standard tables. The circled points on Figure 3-17 represent selected glide angle for the specific vehicles shown. It is desirable that an equilibrium point be selected sufficiently to the right of peak L/D to permit surplus energy for maneuvering and for headwind conditions. Lower L/D vehicles necessitate steeper descent angles and less speed margin. This requires higher acceleration flareouts and makes the flareout phase more critical in regard to tolerance of off-nominal conditions.

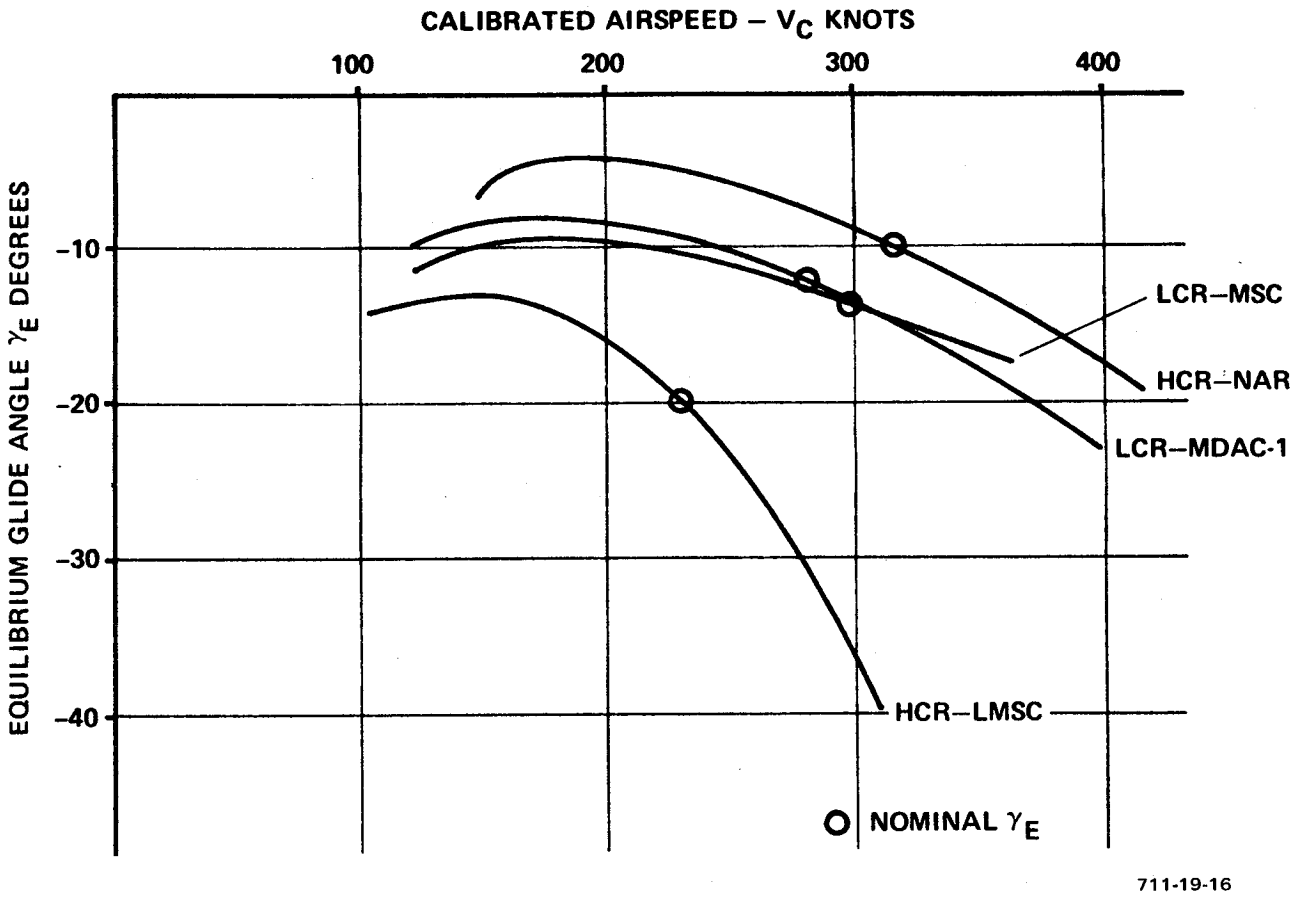

Figure 3-17
Equilibrium Glide Angles versus Calibrated Airspeed

The manner in which the constrained glide angle solves the position and speed requirements for landing the unpowered vehicle is illustrated in Figures 3-18 and 3-19.

The acquisition and tracking of the -10 degree glide path by the North American Rockwell HCR vehicle is shown on an altitude versus downrange plot. A window at 20,000 feet of almost 14 nautical miles in length is shown; however, as indicated on the individual trajectories, the velocity at first flare converges only to within ±15 percent of the nominal values. The acquisition maneuvers are constrained to prevent excessive angles of attack (back side of the L/D curve), and to prevent excessive dynamic pressure (Q). Position errors are brought to zero by the time the altitude reaches 7500 feet. As shown in Figure 3-19, however, speed convergence is considerably slower.

Dynamic pressure (Q) histories for these glide path acquisiton and tracking trajectories are illustrated in Figure 3-19. The nominal equilibrium glide descent (trajectory 4) maintains a relatively constant Q of about 325 pounds per foot^2 which corresponds to an equivalent airspeed of about 310 knots. During the acquisition maneuvers, the speed transients are severe, resulting in Q variations from near 100 to 575 pounds per foot^2. Convergence toward the equilibrium value is not complete at the time the first flare altitude is reached. The flareout system is designed to modify the maneuver commands as a function of off-nominal velocities. Convergence toward the equilibrium velocity is very low in this particular vehicle because of a very low value of C_{D_o} [in Equations (3-7 and (3-10)]. Updated aero models of this NAR vehicle did not have this low drag. The use of speed brakes during the glide path tracking phase of the flight can provide a more rapid convergence to the desired equilibrium airspeed. The spread in speed at the point of the first flare to the shallow glide path (Figure 3-16) restricts the range of headwinds and tailwinds that can be accommodated. Speed brakes therefore expand the capability for coping with winds. The absence of speed brakes in the particular NAR vehicle illustrated by the trajectories of Figures 3-18 and 3-19 necessitated higher nominal touchdown speeds (about 195 knots) than desirable.

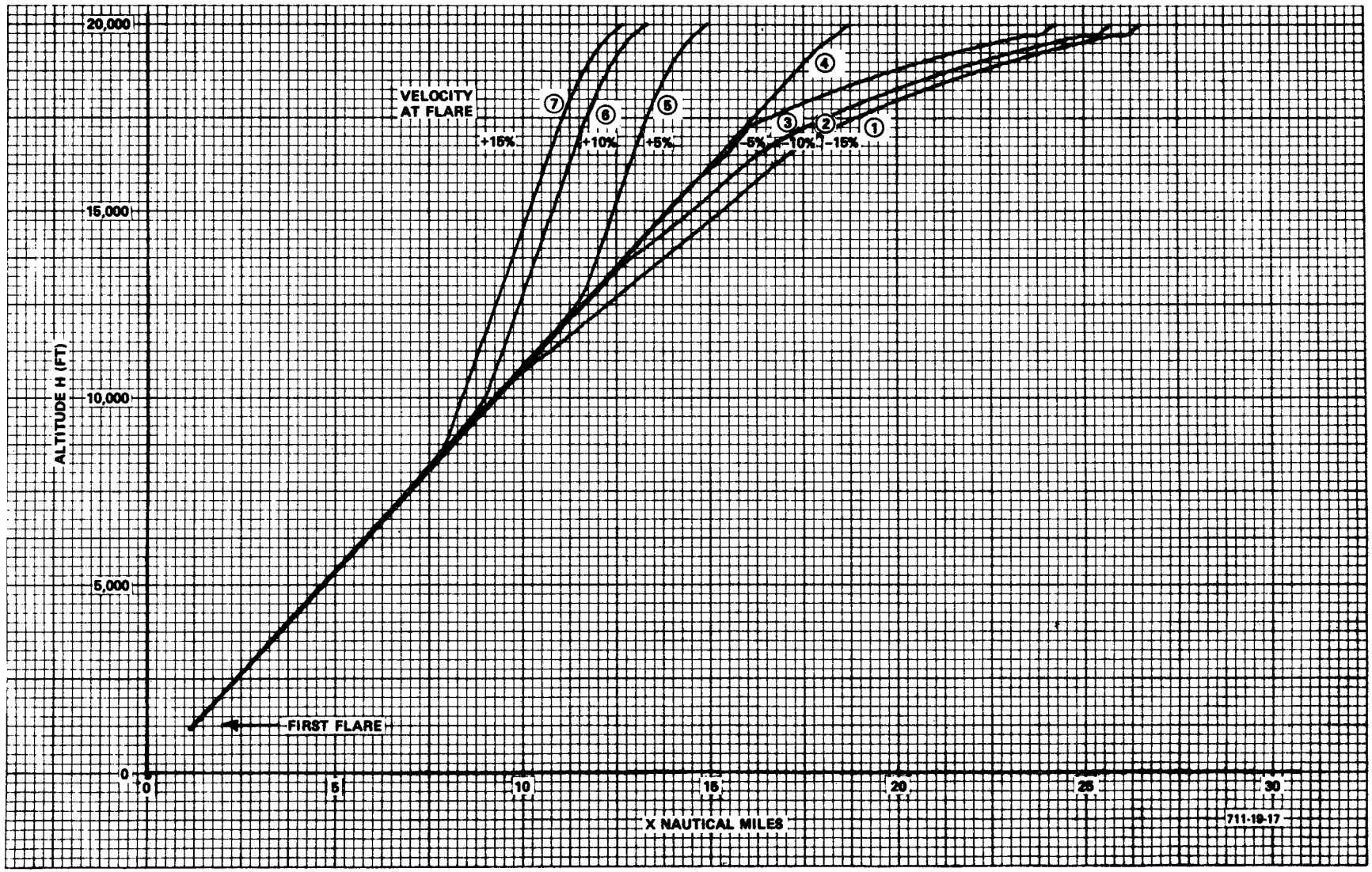

Figure 3-18
NAR-HCR Orbiter Glide Path Acquisition Trajectories

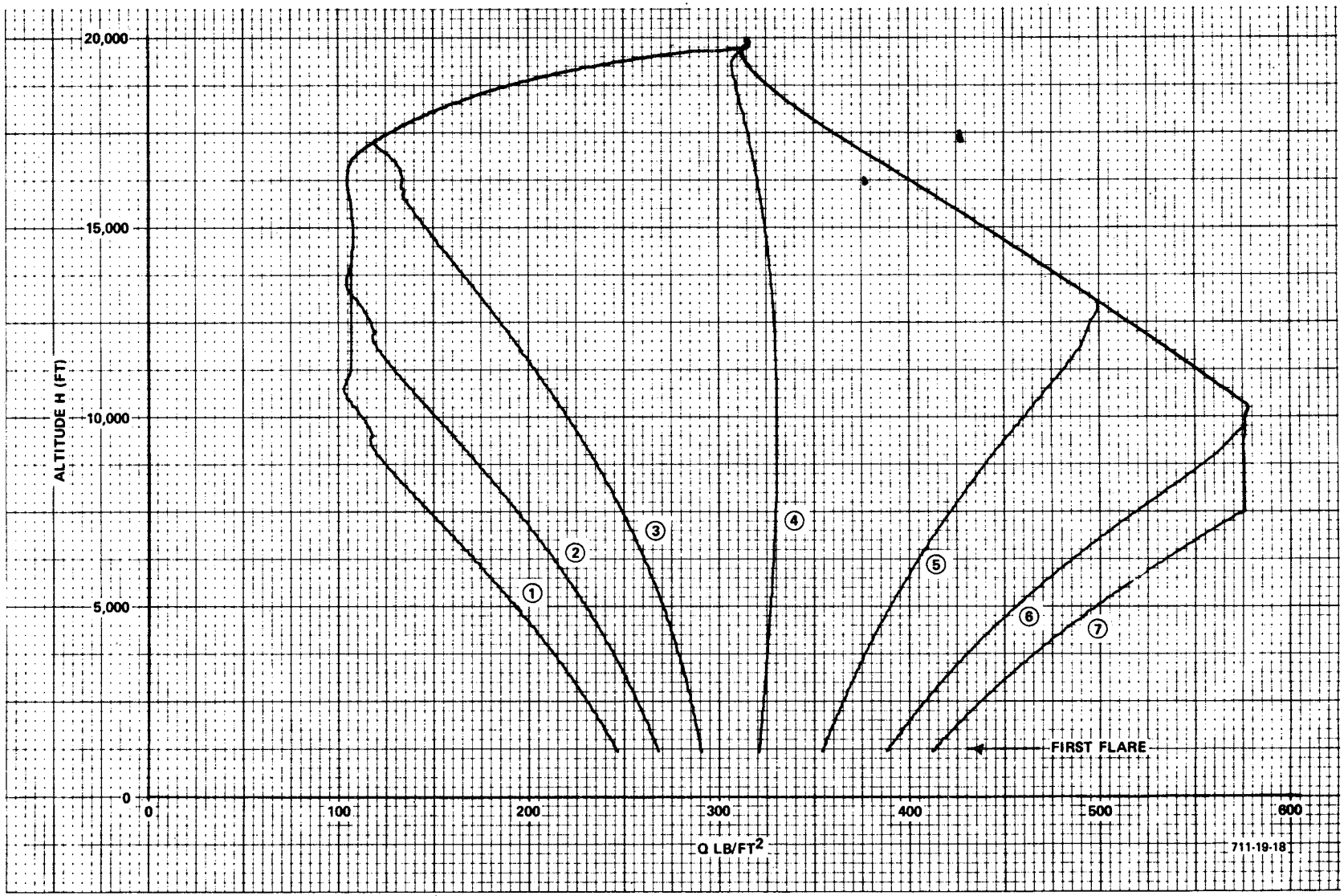

Figure 3-19
NAR-HCR Orbiter Dynamic Pressure for Glide Path Acquisitions

Figures 3-14, 3-17 and Equation (3-10) imply that an equilibrium speed exists at a constrained flight path angle. Even if the aerodynamics were constant through the range of decreasing Mach numbers, a fixed equilibrium speed would not exist. The glider equation that gives Equation (3-6) assumes equilibrium exists normal to and along the flight path. This results in a fixed Q for a fixed γ. However, if Q were fixed, the drag equation could not be in equilibrium. The extent of the departure from equilibrium can be demonstrated with the following analysis

$$Q = \frac{1}{2} \rho V^2 \tag{3-11}$$

Assume an approximate logarithmic model for the density ρ

$$\rho = \rho_o \, e^{-\beta h} \tag{3-12}$$

where $\beta \approx \frac{1}{23.500}$ is a reasonable approximation for altitudes between 20,000 feet and sea level.

$$\Delta Q = \left(\frac{\partial Q}{\partial V}\right) \Delta V + \left(\frac{\partial Q}{\partial h}\right) \Delta h = 0 \tag{3-13}$$

for a constant Q descent

$$\left(\frac{\partial Q}{\partial V}\right) = \rho_o \, e^{-\beta h} \, V \tag{3-14}$$

$$\left(\frac{\partial Q}{\partial h}\right) = - \frac{\beta \rho_o \, V^2}{2} \, e^{-\beta h} \tag{3-15}$$

Substituting (3-14) and (3-15) into (3-13) yields

$$\frac{dV}{dh} = \frac{1}{2} \beta V \approx \frac{V}{47,000} \text{ ft/sec/ft} \tag{3-16}$$

For an initial V of 600 feet per second, this relationship shows a ΔV of 255 feet per second for a Δh of 20,000 feet. The $\dot{V}$ for the range of speed under consideration is approximately 0.05 g rather than zero as assumed by the

glider equation. The result in complete simulations of typical vehicles is a slight departure from the constant Q equilibrium when the vehicle is constrained to a fixed glide path. Part of the variation is caused by aerodynamic changes with Mach number which require changes in angle of attack and Q to maintain the glide path. However, because the drag equation cannot be in equilibrium the vehicle usually tends to find a pseudo equilibrium between constant Q and constant V: that is, Q tends to increase slightly and V decreases but not as much as it would with a constant Q descent.

C. GUIDANCE AND CONTROL CONCEPT

1. Autopilot and Attitude Stabilization Loops

a. Pitch Stabilization and Control (Aerodynamic Flight Phases)

The pitch guidance and control block diagram in general form is shown in Figure 3-20. A displacement plus integral elevator control law provides pitch attitude stabilization in response to body axis pitch rate and local vertical oriented pitch attitude error. The pitch stabilization system receives both the steering commands based on the guidance computations and the maneuver commands inserted by the pilot for semi-automatic control modes. Guidance inputs are pitch commands with appropriate attitude, attitude rate, and control surface feedforward compensations to minimize errors in the closed loop process. Manual inputs command attitude rate (that is, rate of change of the attitude reference proportional to applied force) with appropriate adjustment of the command sensitivity as a function of velocity. The gains k_θ and k_q are functions of dynamic pressure.

The control equations are developed in terms of a sequence of loop closures which result in an elevator (or elevon) control law. The elevator control equation is

$$\delta_{E_{COMMAND}} = G_1(s)\ k_\theta \left[\theta_E + k_q/k_\theta\ G_2(s)\ q_E\right]\left[1 + \frac{k_{INT}}{s}\right] + \delta_{FF} \qquad (3\text{-}17)$$

where $G_1(s)$ provides for special lead-lag filters as required by the servo system dynamics. Also, k_{INT}, the elevator integration term may be accomplished through the actuation of a separate trim channel. In many cases, practical mechanization considerations require that the trim integration be performed in an on-off manner. This necessitates the use of threshold logic (deadzone plus hysteresis) plus a lag filter, the discrete output of which commands a fixed up or down rate of the trim actuator. An example of such an on-off integration requirement would have occurred with the McDonnell Douglas LCR vehicle which used an elevator plus a moving horizontal stabilizer for pitch control. The autopilot output would drive the elevator but the steady state output must be

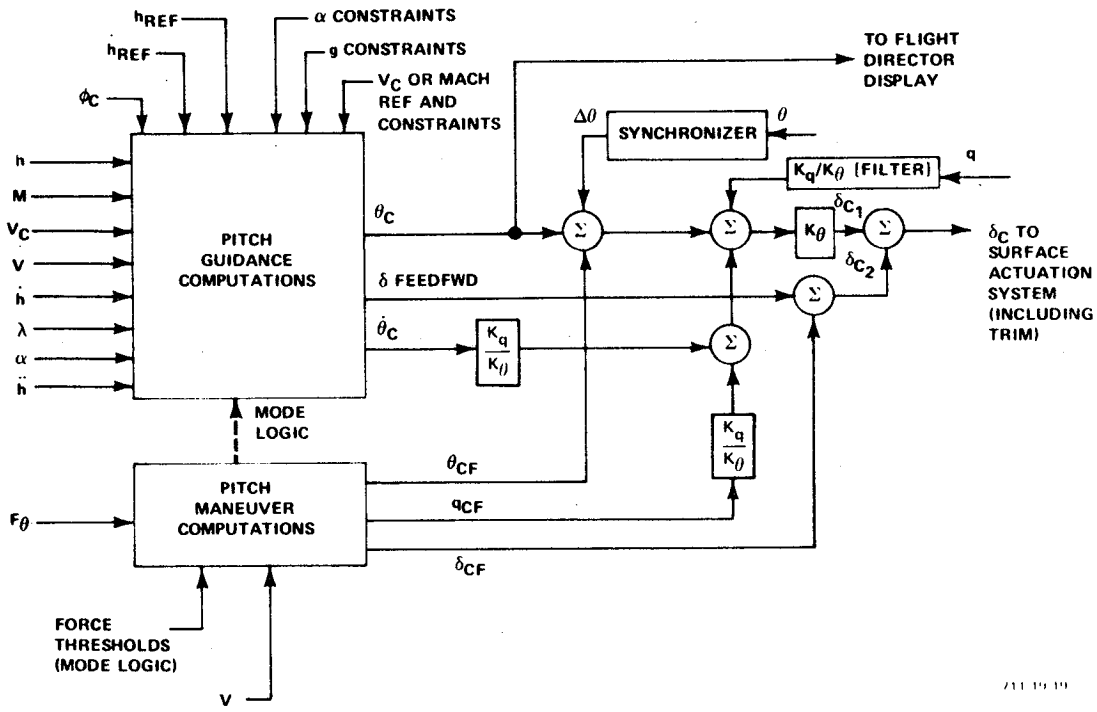

Figure 3-20
Pitch Guidance and Control,
Automatic and Automatic/Manual Block Diagram

off-loaded to the horizontal stabilizer. The horizontal stabilizer would be driven up or down by fixed rate trim actuators. From the standpoint of performance it would have been most desirable to pulse rate modulate the horizontal stabilizer actuator motors in order to achieve the linear integration equivalent of equation (3-17). However, if practical considerations precluded such a proportional drive, then the simpler on-off mechanization would have been used. The integral law always results in a performance compromise manifested by slight overshoot tendencies and long time constant "tails" on the steady state pitch response. It is used not for achieving any transient performance objectives but to automatically maintain steady state trim in the presence of large speed changes.

The elevator to elevator command transfer function is determined by the type of actuation systems employed. It may be expressed as

$$\left(\frac{\delta_E}{\delta_{E_{COMMAND}}}\right)\left(s\right) = H_{\delta_E}(s) = \left[\frac{1}{\left(\frac{s}{\omega_p}+1\right)}\,\frac{}{\left(\frac{s}{\omega_s}+1\right)}\right] H_2(s) \qquad (3\text{-}18)$$

where $1/\omega_p$ is a first order lag representation of a power actuator and $1/\omega_s$ is a first order lag representation of a secondary actuator that is used for manual and automatic control. The remaining high frequency dynamics in both power and secondary actuator loops are incorporated in the term $H_2(s)$. These higher order dynamic terms were not incorporated in the simulations used in the present study but they are included in equation (3-18) as a reminder that it is the higher order control dynamics that interact with elastic mode dynamics to dictate the control system's maximum attainable gains. If $H_2(s)$ were not included in equation (3-18), the clever autopilot designer would be tempted to use lead-lag compensators that cancel the ω_p and ω_s poles and replace them with new poles at any desired frequency. Not only do the $H_2(s)$ dynamics restrict the indiscriminate use of bandwidth extension compensators but the rate limit constraints on the actuators pose additional hazards to a high gain system. Both the secondary and power actuators include velocity limits. The power actuator's rate limit is the more important one because it is usually lower; about 20 degrees/second for the

space shuttle applications. The secondary actuator rate limit may be in the 50 to 60 degree per second range. It is also interesting to note that space shuttle flight control system designs have been considering quad redundant, velocity summing, electromechanical actuators for the secondary actuator function. A simple first order lag representation is not very reasonable if 30 radian per second bandwidths are desired. For this frequency region the electromechanical actuator is more of a 2nd or 3rd order system. Typically, for hydraulic systems

$$\omega_p = 10 \text{ to } 20 \text{ radians/second}$$

$$\omega_s = 25 \text{ to } 50 \text{ radians/second}$$

Equation (2-17) implies control of two state variables, pitch attitude θ and pitch rate q plus an additional feedforward term δ_{FF} which is the predictive elevator for an intended maneuver. Both the pitch rate and pitch attitude terms are error quantities representing the difference between the commanded state and actual vehicle state as follows:

$$\theta_E = \theta_s - \theta_c \tag{3-19}$$

where θ_s is the synchronized value of pitch attitude defined as $(\theta - \theta_o)$, θ_o being the initial value of θ

and

$$q_E = q - q_c \tag{3-20}$$

The command quantities are generated by both the guidance (or steering) computations and the pilot's maneuvering computations (which are shown in Figure 3-20 as derived from stick force sensors). The pitch rate loop includes a filter defined as $G_2(s)$ which contains a washout that eliminates the azimuth rate component into body axis pitch rate during turning maneuvers. The form of $G_2(s)$ is

$$G_2(s) = \left(\frac{\tau_1 s}{\tau_1 s + 1}\right) G_3(s) \tag{3-21}$$

where $G_3(s)$ is an elastic mode filter which would be added during a detailed autopilot design but is beyond the scope of the present study.

The pitch and pitch rate commands are the steering inputs to the stabilization loop. Pitch guidance equations are derived from the various inputs shown in Figure 3-20.

$$\theta_c = \sum_{j=1}^{n} \theta_{c_j} \tag{3-22}$$

where θ_{c_j} represents individual pitch steering commands associated with specific modes. Upon mode transition the previous value of θ_c is used as the initial condition for the new set of θ_c's. This acts as an "easy engage/disengage" function which is incorporated in conventional autopilots for smooth mode transitions. When required, the residual command of a previous mode may be decayed to zero after the next mode has been engaged.

b. Lateral-Directional Stabilization and Control, (Aerodynamic Flight Phases)

The lateral-directional guidance and control block diagram is shown in general form in Figure 3-21. Roll attitude stabilization is provided as a function of body axis roll rate and local vertical oriented roll attitude error. The roll stabilization system receives both the steering commands based on the guidance computations and the maneuver commands inserted by the pilot. As in the case of the pitch system, appropriate feedforward commands are generated to minimize errors in the closed loop process. Manual commands result in roll rates proportional to applied force. The rudder control provides for dutch roll damping (in combination with the roll stabilization system), turn coordination, and artificial directional stability. Body axis lateral acceleration, roll-yaw crossfeed, and computed turn rate command contribute to the turn coordination capability. As in the pitch control loop, the gains k_ϕ and k_p are made functions of dynamic pressure.

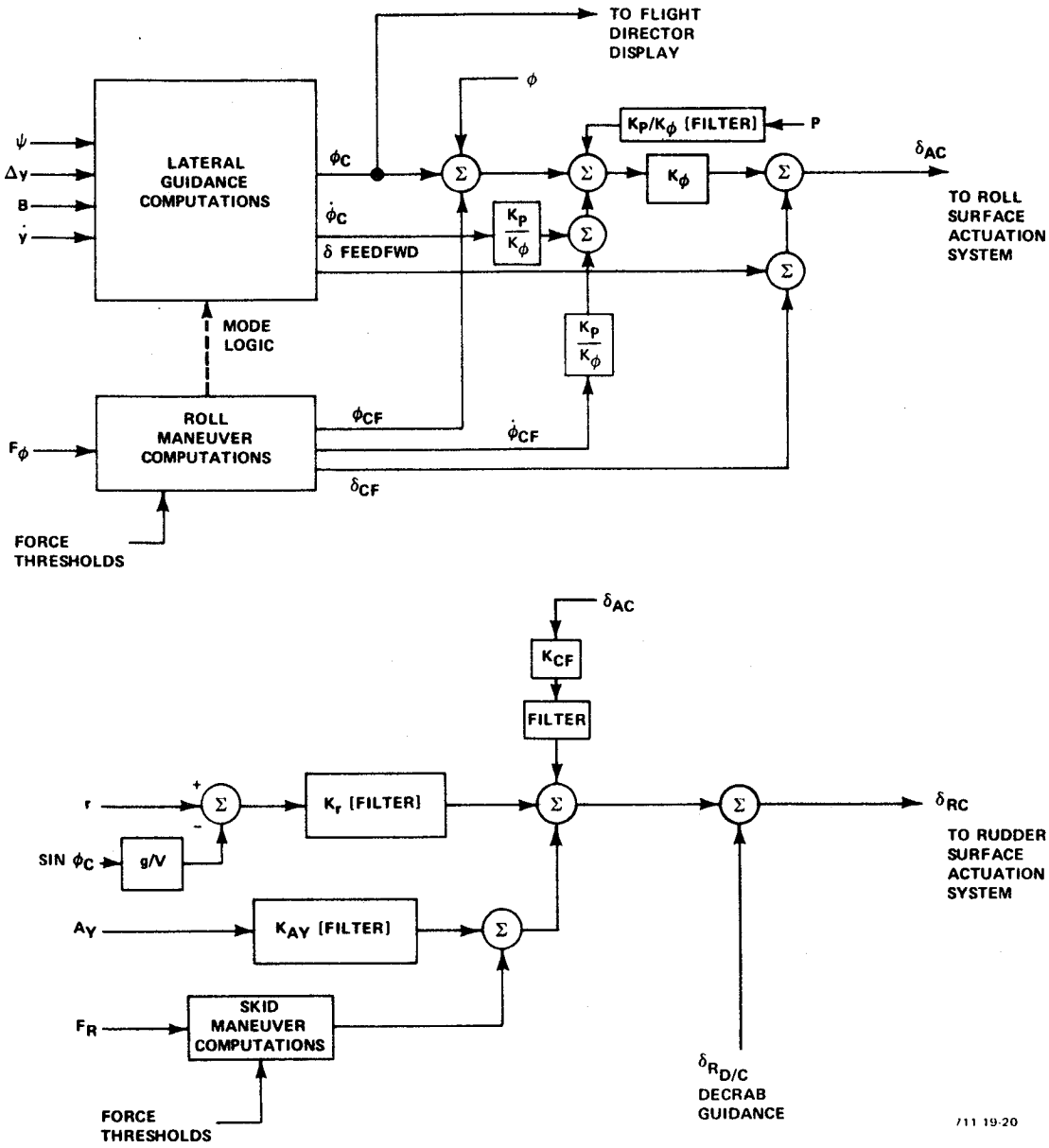

Figure 3-21
Lateral-Directional Guidance and Control,
Automatic and Automatic/Manual Block Diagram

The roll surface (aileron or elevon) control law is

$$-\delta_{A_c} = \left\{ \left[pG_4(s) - p_{COM} \right] \frac{k_p}{k_\phi} + (\phi - \phi_c) \right\} k_\phi + \delta_{A_{FF}} \tag{3-23}$$

where $G_4(s)$ is a roll rate elastic mode filter, the design of which is not covered in this study. The aileron/aileron command transfer function is similar to the elevator servo dynamics and in the case of elevons they would actually be identical (except for differences in authority limiting).

$$\left(\frac{\delta_A}{\delta_{A_c}} \right) \left(S \right) = \left[\frac{1}{\left(\frac{s}{\omega_p} + 1 \right)} \right] \left[\frac{1}{\left(\frac{s}{\omega_s} + 1 \right)} \right] H_2(s) = H_{\delta_A}(s) \tag{3-24}$$

where $\dot{\delta}_A$ maximum is about 30 deg/sec to 50 deg/sec typically.

The rudder control provides for dutch roll and turn coordination. The rudder control law is

$$\delta_{R_{COM}} = k_r \left[rH_3(s) - r_{COM} \right] \frac{\tau_4 s}{\tau_4 s + 1} + A_y G_5(s) + \delta_{A_{COM}} G_6(s) + \delta_{R_{D/C}} \tag{3-25}$$

where

$$r_{COM} = \frac{g}{V} \sin \phi_c \cos \theta \approx \frac{g}{V} \sin \phi_c \tag{3-26}$$

(a term added to distinguish a body axis yaw rate that should not be opposed by rudder deflections because it can occur in a coordinated turn. It helps provide a rudder deflection to improve coordination during turn entry and it permits increasing the yaw rate washout time constant τ_4 to values that do not compromise dutch roll damping.)

$$G_5(s) = k_{A_y}\left(\frac{1}{\tau_5 s + 1}\right) \tag{3-27}$$

$$G_6(s) = k_{RA}\,\frac{\tau_6 s}{(\tau_6 s + 1)\,(\tau_7 s + 1)} \tag{3-28}$$

The A_y feedback is used to improve turn coordination performance but in vehicles with low or negative directional stability it is an essential term for maintaining adequate stability in the lateral-directional dynamics. The k_{RA} term is a rudder to aileron crossfeed that is used to improve turn coordination during turn entry and exit. The $\delta_{R_{D/C}}$ is a computed rudder deflection needed to align the aircraft with the runway (decrab).

The gains k_r and k_{A_y} are functions of dynamic pressure but k_{A_y} is extremely sensitive and must be carefully programmed with such factors as Mach number and/or angle of attack as required to maintain adequate stability margins. The sensitivity of k_{A_y} arises from the need for very high gains at low dynamic pressure, high angle of attack flight conditions. As transonic and subsonic flight is reached the required gain reduction is generally larger than that provided by the dynamic pressure gain program alone.

The comments on elevator and aileron servo dynamics also pertain to the rudder dynamics. A summary of the various transfer functions for the lateral-directional stabilization loops is given in Figure 3-22.

2. Pitch Steering Versus Pitch Rate Steering Systems

The guidance inputs to the pitch stabilization system as shown in Figure 3-20 appear as pitch attitude commands. This is consistent with a long standing practice with transport autopilots. There is nothing sacred about pitch attitude steering rather than pitch rate steering since an equivalent autopilot system could be designed which achieves the same guidance performance objectives using pitch rate steering. The McDonnell Douglas recommended space shuttle autopilot system, for example, (Reference 26) uses pitch rate steering. There are actually

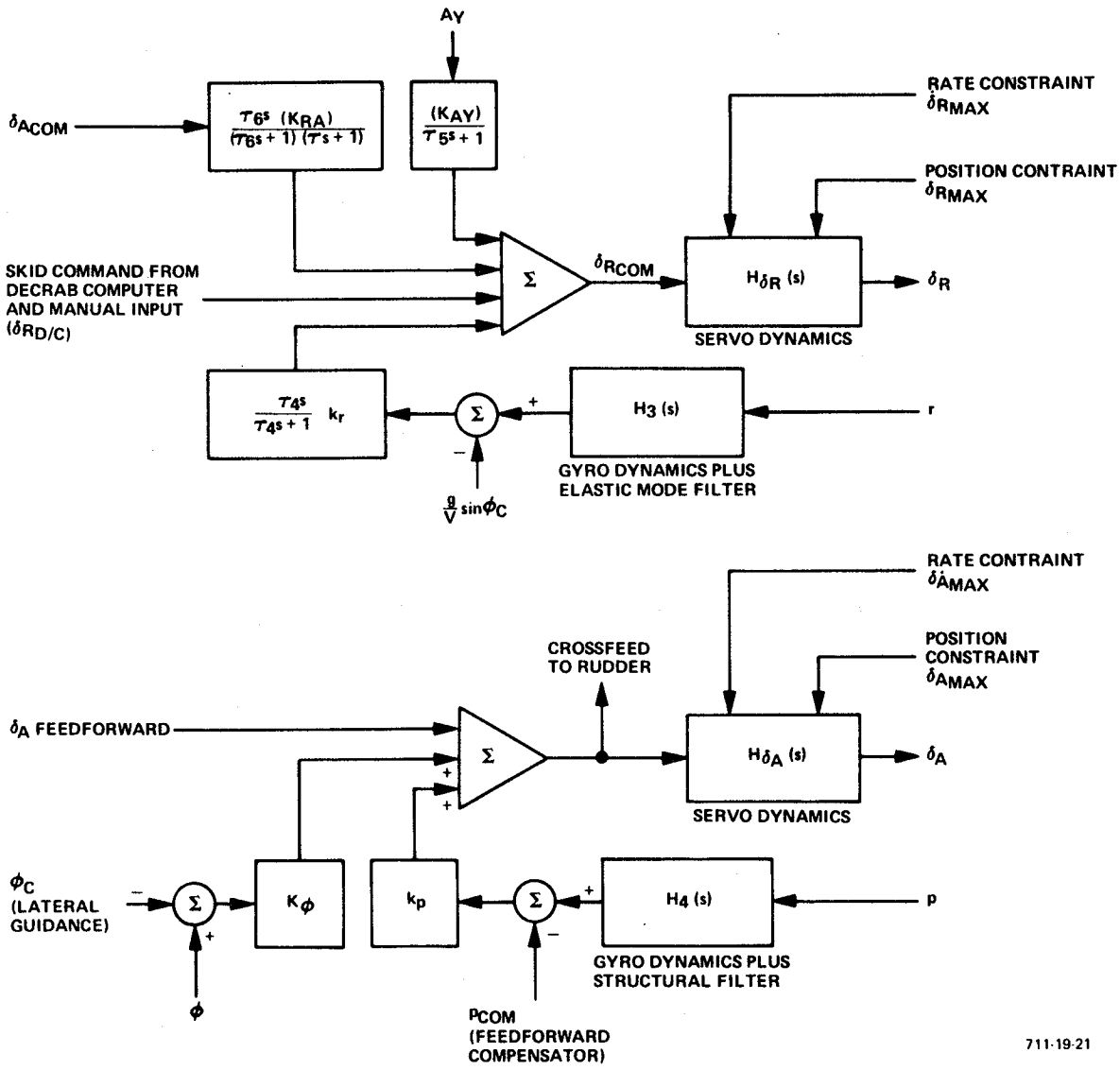

Figure 3-22
Lateral Stabilization Block Diagram

some advantages to the pitch rate command system over the pitch attitude command system defined in this study although these advantages may be outweighed by other considerations. The discussion which follows compares both types of systems, shows how they are almost mathematically identical and reviews the pros and cons of both approaches.

A typical pitch rate control inner loop (Reference 26) has a control equation of the following form:

$$\delta_{E_C} = k_1 \left[\frac{(s + 1)}{(0.1s + 1)\ s}\right]\left[\dot{\theta} - \dot{\theta}_C\right] \tag{3-29}$$

In this system, all guidance inputs appear as pitch rate commands. The measurement of pitch rate as a body axis quantity or Euler angle rate is an important consideration that will be discussed later.

If Equation (3-29) is rewritten in terms of pitch attitude using the identity

$$\dot{\theta} = s\theta \tag{3-30}$$

and eliminating the command inputs for the time being, then the control equation becomes

$$\delta_{E_C} = k_1 \left(\frac{s + 1}{0.1s + 1}\right)\theta \tag{3-31}$$

If this block diagram reduction is continued to an equivalent pitch rate plus pitch attitude form, we obtain the sequence of block diagrams shown in Figure 3-23(a). The resultant block diagram is essentially the same as the pitch attitude control block diagram defined previously by equation (3-17) except for the addition of the trim integrator in the attitude system. Figure 3-23(b) illustrates, for comparison purposes, the equivalent attitude system used in the work reported herein. The frequency response comparison between Figures 3-23(a) and 3-23(b) is illustrated on Figure 3-24. The following differences are observed:

- The attitude system differs at low frequency because of the inclusion of the trim integration. The trim integrator can also be added to the rate system so that this difference is not fundamental.

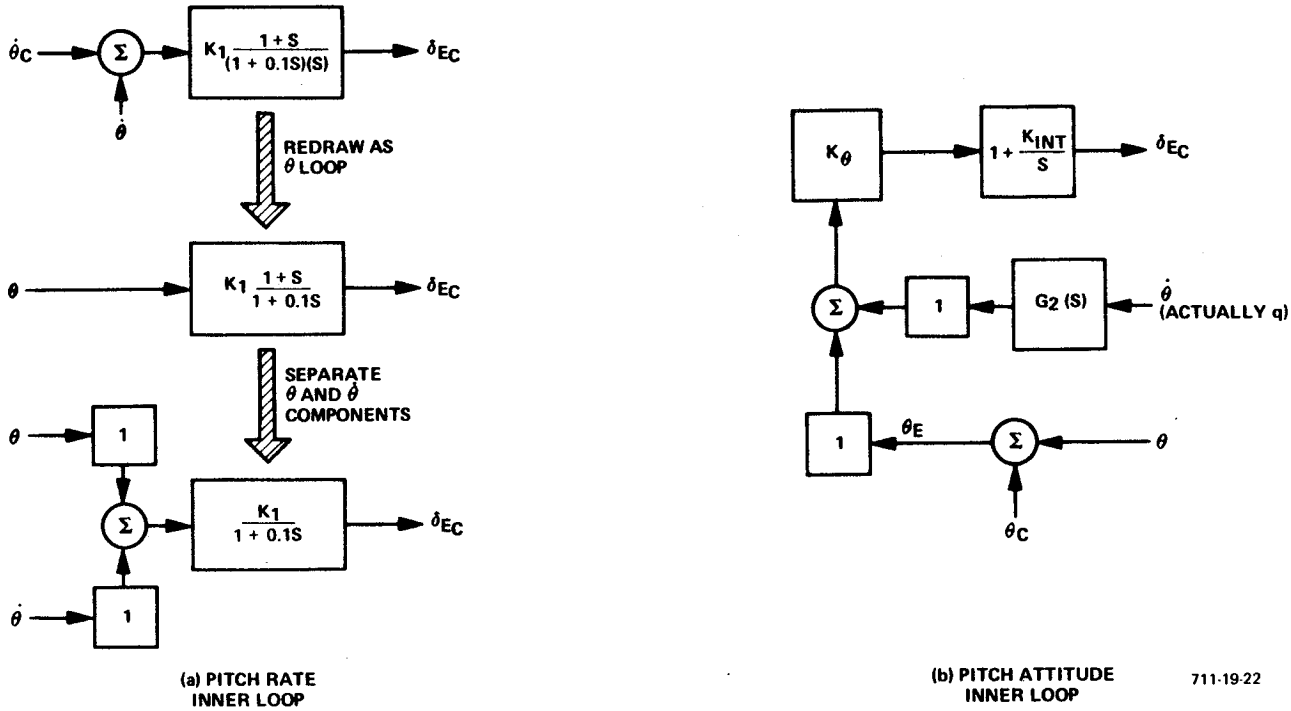

Figure 3-23
Comparison of Pitch Rate and
Pitch Attitude Inner Loop Block Diagram

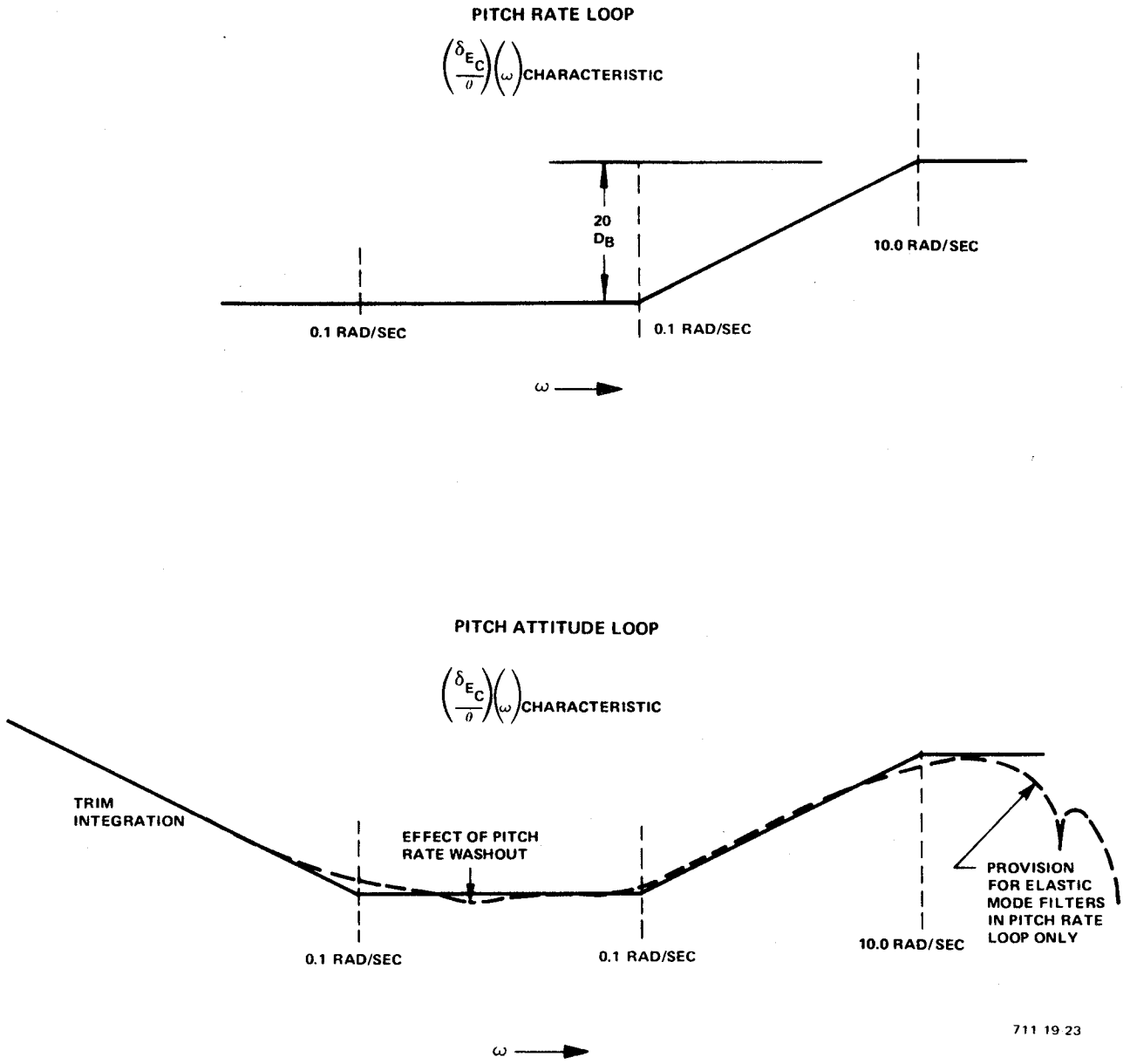

Figure 3-24
Frequency Response Comparison, δ_{E_C} per Pitch Attitude Error
for Pitch Rate and Pitch Attitude Control Systems

- The attitude system uses washed out, body axis pitch rate. For a 2.5 second washout time constant and for the gains shown, there will be an imperceptible dip in the frequency response between 0.1 and 1.0 rad/sec.

- The attitude system uses a high frequency roll-off filter on the rate signal only so that the roll-off for both systems may be made identical. A body axis rate sensor, strategically located for proper bending mode sensing is assumed for the attitude system and provision is made for elastic mode compensators. This capability may not exist for the attitude rate system if Euler angle rate, $\dot{\theta}$ is derived from a platform. If the attitude rate system is based on body axis pitch rate, then the inability to use a washout results in the azimuth rate coupling problem during turns.

It is apparent that there is little mathematical difference between the two systems from the standpoint of attitude stabilization. Let us compare the effect on guidance inputs and use a flight path angle, γ loop for the comparison. Figure 3-25 illustrates the two types of steering loops from the standpoint of stability. If the $\dot{\theta}/\dot{\theta}_C$ closed loop dynamics are represented by a double pole, then the root loci appear as in Figure 3-25(a). Considerable margins exist for good responses with a fairly wide range of gains. If the θ/θ_C closed loop dynamics of the pitch attitude system is also represented by a double pole, then a stable system exists as shown in Figure 3-25(b). However, this root locus does not show the fact that large steady state errors will exist because of the lack of an integration in the loop. The integration is inherent in the attitude rate system but absent in the attitude system. If a γ error exists, a pitch rate is required until γ error goes to zero. In the pitch attitude system, a γ error commands a proportional pitch attitude but as γ error is reduced the corrective pitch attitude would be reduced, thereby causing the γ error to again increase. The steady state result is a γ standoff. The solution to this problem is the incorporation of an integral term in the γ error control law as shown in Figure 3-25(c). Relatively high integral gains can be tolerated without compromising stability. The result is a response equivalent to that which is obtained with the pitch rate system.

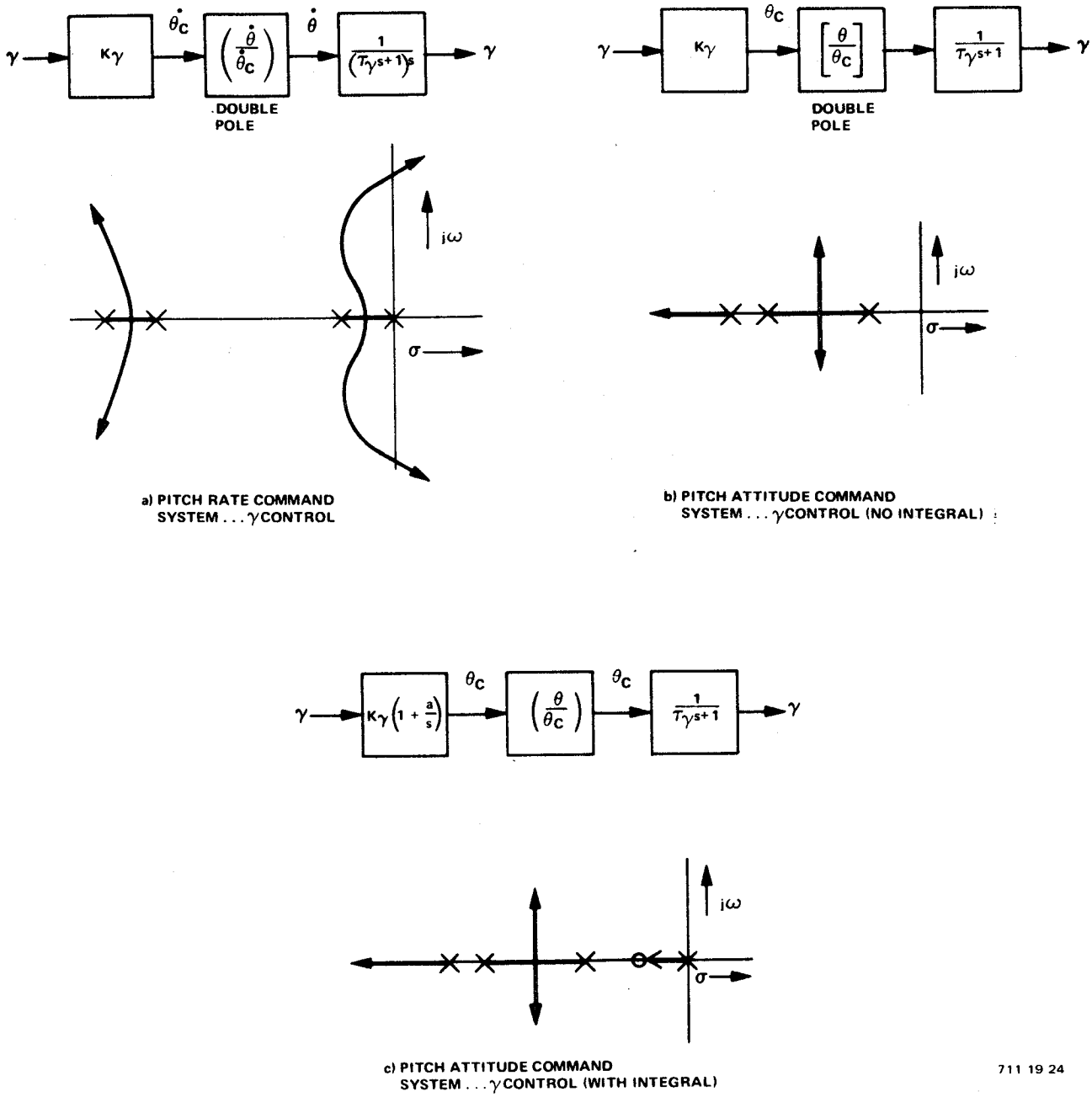

Figure 3-25
Stability Comparison of γ Control with
Pitch Rate and Pitch Attitude Steering

It should be noted that the qualitative root loci used to illustrate the γ control stability problem are very approximate, neglecting such phenomena as the γ reversal due to elevator lift, long period speed (phugoid) dynamics and the more exact closed loop pitch stabilization dynamics. However, the point of this analysis is that both systems end up with similar types of responses. One further point may be made regarding the lack of the pitch attitude system's inherent integration capability for closing a γ error loop. The computation capability of a digital autopilot almost eliminates the need for the integral function shown in Figure 3-25(c). This can be illustrated with the following example. Assume the vehicle starts in level flight ($\gamma = 0$) and is commanded to a γ of -10 degrees. With the pitch rate system the 10 degree γ error will cause a proportional pitch rate until the vehicle γ is equal to -10 degrees. With a pitch attitude system containing the integral loop of the type shown in Figure 3-25(c) the same response will be obtained. In the pitch attitude steering systems used in this study, an additional input is used to minimize the role of the integrator. If the flight path angle is to be changed -10 degrees, the system computes the required $\Delta\theta$ as

$$\Delta\theta = \Delta\gamma + \Delta\alpha \tag{3-32}$$

where $\Delta\gamma$ = -10 degrees and $\Delta\alpha$ is determined by the lift increment needed to perform the maneuver and maintain the desired flight path in the presence of speed changes. In effect, this predictive pitch term should provide for flight at the new flight path angle in an open loop sense. The closed loop system that operates on γ error is, in effect, a high gain vernier on the predictive loop. The combination of predictive or feedforward loops plus closed loop error control results in a tight guidance system with dynamic responses considerably faster and more accurate than those obtainable with closed loop systems alone.

In summary therefore, the pitch rate and pitch attitude systems can be synthesized so that they are mathematically equivalent with both providing equivalent guidance response capabilities. In this study the attitude system was used for the following reasons:

- Body axis pitch rate with washout rather than derived Euler angle rate because of anticipated space shuttle body mode stabilization phase requirements and special sensor location requirements.

- Potential for lower pitch rate gains ... higher pitch displacement gains ... easier to stabilize in elastic mode environment.

- Low gain integration on pitch attitude error for automatic trim capability ... allowing possibility of separate trim channel to unload limited authority incremental control servos.

- The use of pitch attitude rather than pitch rate steering involves some complexity penalties. A digital control system makes some of these penalties less important since the computations required are simple for a digital computer. These computations involve extensive use of feedforward or predictive pitch commands plus accumulation or storage of previous commands without requiring easy engage and disengage mechanizations.

- The use of a basic pitch attitude inner loop is consistent with large transport autopilot practice.

3. Terminal Glide Path Acquisition and Tracking

Acquisition of the steep angle approach glide path nominally occurs at an altitude of 20,000 feet. The high altitude energy management system will guide the vehicle toward an ideal intercept with the approach path somewhere above 20,000 feet. Typical logic criteria for initiating acquisition of the terminal glide path are:

for $h > 20{,}000$ feet

and $\left|(\psi_{RUNWAY} - \psi)\right| < 45$ degrees

start glide path acquisition

if $h_{ERROR} \leqslant 1000$ feet

for $h \leqslant 20{,}000$ feet

and $\left|(\psi_{RUNWAY} - \psi)\right| < 45$ degrees

start glide path acquisition

Various techniques were studied to predict the precise acquisition maneuver that will result in a glide path intercept that results in simultaneous satisfaction of zero h and $\dot{h}$ error (tangential intercept). However, it was found that the simplest acquisition maneuver is the closed loop guidance law (less the integral loop). Thus if the acquisition criteria are satisfied, the pitch command guidance law is

$$\theta_C = k_\gamma \left(\gamma_{REF_1} - \gamma \right) + k_h \, h_E \left(1 + \frac{a_2}{S} \right) + \theta_P + \theta_{CL} \qquad (3\text{-}33)$$

where a_2, the integral gain is equal to zero until on-course tracking criteria are satisfied, θ_P is the predictive change in pitch attitude required to fly the reference path, and θ_{CL} is a closed loop command limit used to prevent excessive angle of attack and speeds. In this case θ_P may be made equal to the required change in γ, neglecting the $\Delta\alpha$ component defined in equation (3-32). Note that

the gain k_h is made inversely proportional to velocity to permit the tightest control loop consistent with stability requirements.

$$\theta_P = \left(\gamma_{REF_1} - \gamma_0\right) \tag{3-34}$$

where γ_0 is the initial value of γ when the acquisition mode is initiated.

The total pitch command is rate constrained to limit the maneuver g as follows:

$$\dot{\theta}_{C_{MAX}} = \left(\text{sgn } \theta_C\right)\left(\frac{N_{Z_{MAX}}}{V}\right) (57.3) \text{ deg/sec} \tag{3-35}$$

where $N_{Z_{MAX}} = N_{Z_{MAX}}(+)$ for sgn θ_C = (+)

$$= N_{Z_{MAX}}(-) \text{ for sgn } \theta_C = (-) \tag{3-36}$$

Reasonable values of $N_{Z_{MAX}}$, the incremental normal acceleration limits are about 0.5g. The g constraints may also be applied to the γ_{REF} term in equations (3-33) and (3-34). This could be accomplished by constraining the rate at which γ_{REF} changes from the initial value of γ such that

$$\dot{\gamma}_{REF} = \text{sgn}\left(\gamma_{REF} - \gamma_0\right)\left(\frac{N_{Z_{MAX}}}{V}\right) (57.3) \text{ deg/sec} \tag{3-37}$$

If γ_{REF} is constrained in this manner then smoothing filters would not be required for the θ_P term in equation (3-34).

Additional constraints must be applied to prevent excessive angles of attack (penetration of back side of L/D curve) and excessive diving speeds. This is accomplished through the term θ_{CL} of equation (3-33). The following types of limits are imposed:

α_{LIM} $\begin{cases} \alpha_{MAX} - \text{corresponds to } \alpha \text{ for peak L/D} \\ \alpha_{MIN} - \text{corresponds to aerodynamic limit for vehicle} \end{cases}$

γ_{LIM} $\begin{cases} \gamma_{MAX} - \text{typical} = -5 \text{ degrees} \\ \gamma_{MIN} - \text{prevents excessive dive angles - typical} = -25 \text{ degrees} \end{cases}$

Q_{LIM} Q_{MAX} or $V_{C_{MAX}}$ = dynamic pressure or calibrated airspeed limit

$$\left.\begin{array}{ll} \Delta\alpha = (\alpha_{LIM} - \alpha) & \text{when } \alpha \text{ exceeds limit} \\ \Delta\alpha = 0 & \text{when } \alpha \text{ is within limit} \end{array}\right\} \quad (3\text{-}38)$$

$$\left.\begin{array}{ll} \Delta\gamma = (\gamma_{LIM} - \gamma) & \text{when } \gamma \text{ exceeds limit} \\ \Delta\gamma = 0 & \text{when } \gamma \text{ is within limit} \end{array}\right\} \quad (3\text{-}39)$$

$$\left.\begin{array}{ll} \Delta Q = (Q - Q_{LIM}) & \text{when } Q \text{ exceeds limit} \\ \Delta Q = 0 & \text{when } Q \text{ is within limit} \end{array}\right\} \quad (3\text{-}40)$$

$$\theta_{CL} = k_\alpha \Delta\alpha \left(1 + \frac{b_1}{S}\right) + k'_\gamma \Delta\gamma \left(1 + \frac{b_2}{S}\right) - k_Q \Delta Q \left(1 + \frac{b_3}{S}\right) \quad (3\text{-}41)$$

When the vehicle has acquired the glide path, the tracking phase starts by turning on the integral term a_2 of equation (3-33). The criteria for initiating the tracking phase are:

$$|h_{ERROR}| < 50 \text{ feet}$$

and

$$|\gamma_{ERROR}| < 1.5 \text{ degrees}$$

or

$$|\gamma_{ERROR}| < 1.5 \text{ degrees for 10 seconds}$$

Figures 3-18 and 3-19 discussed previously showed acquisition and tracking responses for a -10 degree glide path using these guidance laws. The α_{LIM} and Q_{LIM} constraints operated on these trajectories although the N_Z constraints were not used.

4. First Flare - Shallow Glide Path Acquisition and Tracking

The flare to the shallow glide slope, defined as γ_{REF-2} on Figure 3-26 occurs at the first flare altitude, h_2. A nominal value of -2.5 degrees has been used for γ_{REF-2}. The determination of a nominal h_2 is based on the following considerations:

- Desired normal acceleration for the maneuver
- Initial velocity
- Desired velocity at final flare
- Drag aerodynamics including landing gear, drag brakes, and flaps
- Landing gear and flap deployment altitudes
- Drag brake control procedures
- Desired time (or distance) on shallow glide path

The last four items dictate the basic geometry of the two glide paths; that is, the altitude at which they intersect. The first two items determine how high above the shallow glide path the first flare is initiated. As in the case of the steep glide path acquisition, it would appear to be theoretically possible to command a normal acceleration maneuver that terminates precisely on the glide path. The dynamic response limitations in achieving commanded accelerations restricts the precision of this type of maneuver. Nevertheless this has been the approach used to acquire the shallow glide path. At altitude h_2, control to h_{ERROR} on the steep glide path terminates but the γ loop is retained. The γ reference is transitioned to -2.5 degrees (from -10 degrees, the typical approach glide path angle) at a rate corresponding to the desired normal acceleration. The control law is

$$\theta_C = k_\gamma (\gamma_{REF} - \gamma) + \theta_P \tag{3-42}$$

where

$$\left.\begin{aligned} \gamma_{REF}(t) &= \gamma_1 + \int_0^t \dot{\gamma}_C \, dt \\ &\text{for } \gamma_{REF}(t) < -2.5 \text{ degrees} \end{aligned}\right\} \tag{3-43}$$

$$\dot{\gamma}_C(t) = 0 \quad \text{when } \gamma_{REF}(t) = -2.5 \text{ degrees} \tag{3-44}$$

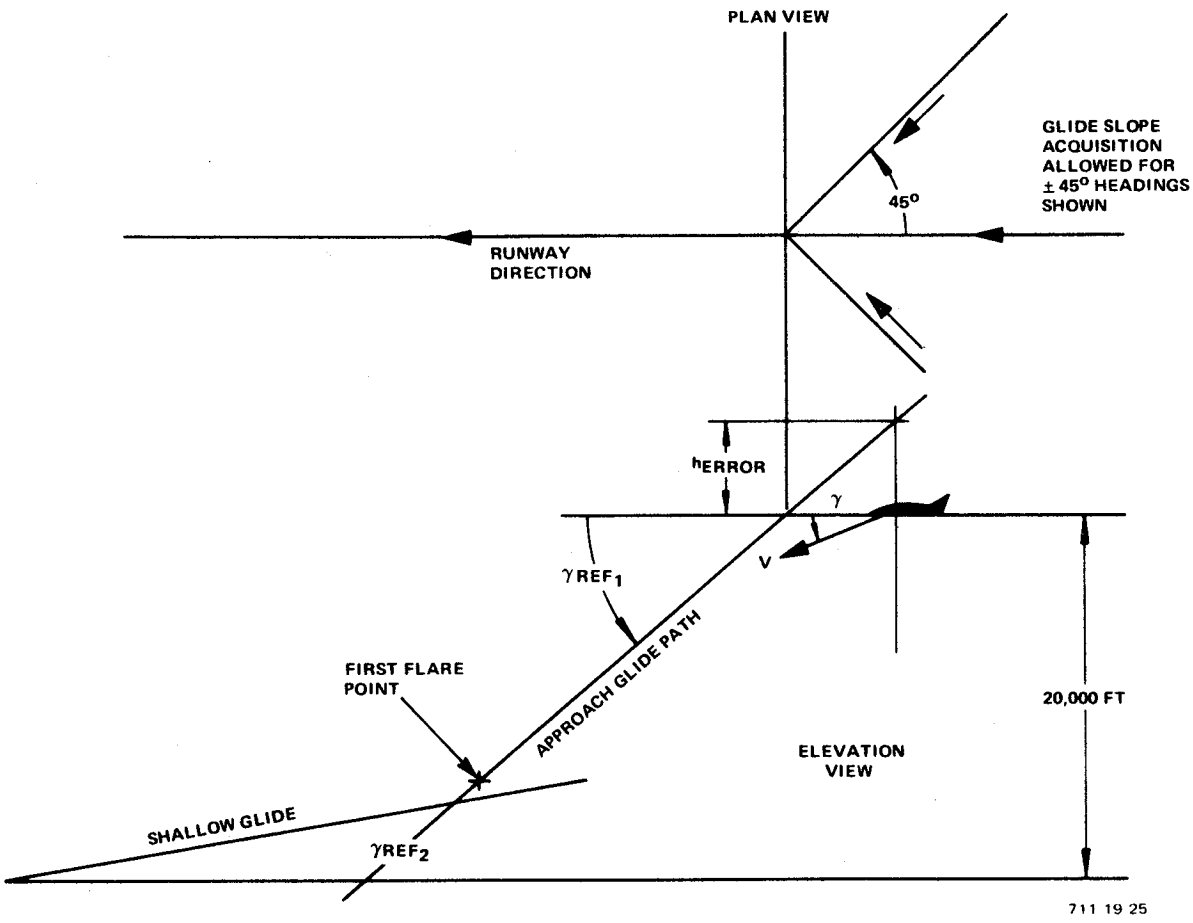

Figure 3-26
Glide Path Acquisition and Tracking Geometry

$$\dot{\gamma}_C(t) = \text{sign}\left[\gamma_{REF-2} - \gamma\right] \left|\dot{\gamma}_{MAX}\right| \tag{3-45}$$

$$\dot{\gamma}_{MAX} = 57.3 \frac{N_{Z_{MAX}}}{V} \text{ deg/sec} \tag{3-46}$$

The predictive pitch command, θ_P, provides the $\Delta\gamma + \Delta\alpha$ required in the maneuver. Thus,

$$\theta_P(t) = \int_0^t \dot{\gamma}_C \, dt + \Delta\alpha\,(t) \tag{3-47}$$

noting that $\dot{\gamma}_C$ becomes zero when γ_{REF-2} is achieved. We can make an approximate estimate of $\Delta\alpha(t)$ by solving the linearized lift equation as follows:

$$L = W\,(N_Z + \cos\gamma) = C_L\,(\alpha, \delta_E)\,QS \tag{3-48}$$

where N_Z, the incremental normal acceleration is in units of g.

For $N_Z = 0$,

$$L = W\cos\gamma_1 = C_{L_1}\,QS \tag{3-49}$$

which defines initial conditions prior to the maneuver.

$$\Delta L = W\left[N_Z + \frac{\partial\,(\cos\gamma)\,\Delta\gamma}{\partial\gamma}\right] = \left(\frac{\partial L}{\partial\alpha}\right)\Delta\alpha + \left(\frac{\partial L}{\partial\delta_E}\right)\Delta\delta_E + \left(\frac{\partial L}{\partial V}\right)\Delta V \tag{3-50}$$

Eliminating the δ_E term with the trim relationship

$$\Delta\delta_E = \frac{C_{m_\alpha}}{C_{m_{\delta_E}}}\,\Delta\alpha \tag{3-51}$$

gives

$$W(N_Z - \Delta\gamma\sin\gamma) = \left(C_{L_\alpha} + C_{L_{\delta_E}}\frac{C_{m_\alpha}}{C_{m_{\delta_E}}}\right)\Delta\alpha\,QS + \left(\frac{\partial L}{\partial V}\right)\Delta V \tag{3-52}$$

$$L = C_L \, QS = \frac{C_L \, \rho \, V^2 \, S}{2} \tag{3-53}$$

$$\left(\frac{\partial L}{\partial V}\right) = C_L \, S \, \rho \, V \tag{3-54}$$

From equation (3-48),

$$C_L = \frac{W}{QS} \, (N_Z + \cos \gamma_1) \tag{3-55}$$

so that

$$\left(\frac{\partial L}{\partial V}\right) \Delta V = 2W \, (N_Z + \cos \gamma_1) \, \frac{\Delta V}{V} \tag{3-56}$$

Substituting the term

$$C_x = \left[C_{L_\alpha} + C_{L_{\delta_E}} \left(\frac{C_{m_\alpha}}{C_{m_{\delta_E}}} \right) \right] \tag{3-57}$$

into (3-52) yields

$$W(N_Z - \Delta \gamma \sin \gamma) = C_x \, QS \, \Delta \alpha + 2W(N_Z + \cos \gamma_1) \, \frac{\Delta V}{V} \tag{3-58}$$

or

$$\Delta \alpha = \frac{W(N_Z - \Delta \gamma \sin \gamma)}{QS \, C_x} - \frac{2W(N_Z + \cos \gamma_1)}{QS \, C_x} \, \frac{\Delta V}{V} \tag{3-59}$$

Defining

$$\Delta V = \int_0^t \dot{V} \, dt \tag{3-60}$$

allows us to write $\Delta \alpha$ in terms of constants and measured variables as follows (in degrees):

$$\Delta \alpha = \frac{57.3 \, d_1}{Q} \left(1 - \frac{\Delta \gamma \sin \gamma}{N_{Z_{REF}}} \right) - 57.3 \int_0^t \left(\frac{\dot{V}}{V} \right) \left(\frac{d_2}{Q} \right) dt \tag{3-61}$$

where

$$d_1 = \frac{W\, N_{Z_{REF}}}{C_x S} \tag{3-62}$$

and

$$d_2 = \frac{2W}{C_x S}\left(N_{Z_{REF}} + \cos \gamma_1\right) \tag{3-63}$$

Note that $N_{Z_{REF}}$ represents the desired acceleration for the maneuver. When the acceleration maneuver is completed, $d_1 = 0$. The complete predictive pitch term for the first flare maneuver is [referring back to equation (3-47)] :

$$\theta_P(t) = \int_0^t \dot{\gamma}_C \, dt + 57.3 \frac{d_1}{Q}\left(1 - \frac{\Delta\gamma \sin \gamma}{N_{Z_{REF}}}\right) - 57.3\, d_2 \int_0^t \left(\frac{\dot{V}}{V}\right)\left(\frac{1}{Q}\right) dt \tag{3-64}$$

Note that d_1 and d_2 are approximate constants that are not calculated in the guidance computer but are fixed values for a given vehicle. Equations (3-48) through (3-63) may be used to obtain a first cut at the required values but simulator studies including the non-linear aerodynamics are needed to optimize these constants.

When the shallow glide path has been acquired and the first flare maneuver is completed, the last part of equation (3-64) must be retained in the guidance equation but with a new value of d_2 that reflects the reduction of $N_{Z_{REF}}$ to zero. First, however, we must define the criteria for initiating closed loop tracking to the shallow glide path. These criteria are:

- $h_{E_2} \geqslant 0$ and $\gamma \leqslant \gamma_{REF_2}$

  (altitude is below the shallow glide path and the descent is steeper than γ_{REF_2})

or

- $h_{E_2} \leq 0$ and $\gamma \geq \gamma_{REF_2}$

  (altitude is above the shallow glide path and the descent is shallower than γ_{REF_2})

The closed loop tracking equation for the shallow glide path is identical to that used for the steep glide path except for predictive commands that compensate for the deceleration, gear deployment and flaps (if they are provided). The tracking equation is:

$$\theta_C = k_\gamma \left(\gamma_{REF_2} - \gamma \right) + k_h \, h_E \left(1 + \frac{a_2}{S} \right) + \theta_{P_2} \tag{3-65}$$

where, as in the case of the steep glide path tracking, k_h varies inversely with velocity.

$$\theta_{P_2} = -57.3 \frac{d_1}{Q} \left(1 - \frac{\Delta\gamma \sin \gamma}{N_{Z_{REF}}} \right) - 57.3 \, d_3 \int_0^{t_{FF}} \left(\frac{\dot{V}}{V} \right) \left(\frac{1}{Q} \right) dt + e_1 \, \delta_{LG} \tag{3-66}$$

The first part of θ_{P_2} cancels the identical term that existed during the flare maneuver. The cancellation is necessary if the guidance computer uses the previous value of θ_C as the initial condition for mode transition. If we merely let d_1 become zero prior to engagement of the shallow glide path tracking phase, then this cancellation would not be required. The value of d_3 is

$$d_3 = \frac{2W}{C_x S} \cos \left(-2.5 \text{ deg} \right) \approx \frac{2W}{C_x S} \tag{3-67}$$

Provision must be included to increase d_3 if flaps or gear are deployed with aerodynamic effects that alter C_x. The term e_1 is another compensation for change in pitching moment or lift as a result of landing gear deployment. It would also be used for flap deployment where the value of e_1 would be significant (as compared to the relatively small influence of the landing gear).

5. Final Flareout Techniques

a. General Discussion of the Flareout Problem

If the two phase or segmented flareout sequence is performed properly, the unpowered vehicle, as it descends below 100 feet, arrives at a position and energy state that is not significantly different from that of a jet aircraft immediately prior to flareout. Thus, the final flareout maneuver that must arrest the vertical speed to reasonably low values is the same for unpowered shuttlecraft and conventional aircraft. This situation is, of course, only true if the first flare to the shallow, decelerating glide path is achieved precisely and in the absence of disturbances. The unpowered vehicle is considerably more sensitive to off-nominal conditions than the conventional, powered aircraft. Indeed, the early experimenters with automatic landing systems soon learned the futility of attempting to achieve good autoland performance without precise throttle controls. An automatic landing system for unpowered vehicles must incorporate more sophisticated control laws that detect and respond to the many off-nominal conditions that may occur. Three types of flareout controllers were evaluated during this study program. Results obtained with two of them (acceleration controller and vertical velocity controller) are documented in this report. The exponential controller ($h + \dot{h}$) was evaluated in the preliminary studies with the MSC 245 LCR configuration, but this approach was dropped in subsequent studies of the other vehicles. All three types could be made to work perfectly in an undisturbed environment with nominal conditions prior to initiation of flareout. They all required additional logic and corrective loops to cope with off-nominal conditions. There are some basic similarities as well as differences in the types of flareout controllers investigated. The discussion which follows is concerned with these similarities and differences.

In general, all flareout control laws are based on steering commands as a function of the feedback state variables h, $\dot{h}$ and $\ddot{h}$ where h is the height above the runway. If these steering commands are viewed as pitch commands, then the flareout law may be generalized in the following form

$$\theta_c = f_1 (h, \dot{h}, \ddot{h}) + \theta_p (t, h) \qquad (3\text{-}68)$$

where:

θ_c = pitch command

θ_p (t, h) = predictive component of the steering command that is based on either a posteriori data or calculated pitch angle required to give the desired h and $\dot{h}$ response.

Other forms of this generalized control law appear. Sometimes it is written entirely as an elevator command

$$\delta_E = f_3 (h, \dot{h}, \ddot{h}, \theta, \dot{\theta}) \tag{3-69}$$

and in some mechanizations, the pitch function θ is removed. The functions f_1, f_2 and f_3 include a variety of filters and compensators as well as gain functions. The gain coefficients may be constant, programmed or continuously computed as a function of the errors from the desired state.

A basic flareout control law that encompasses almost every conceivable flareout scheme can be defined. Surprisingly enough, that control law is fairly specific. It is shown in block diagram form in Figure 3-27. Note however, that this figure does not show some of the logic switching functions required to smoothly transition from a glide path tracking phase to the flareout. The basic control law, when written as a Laplace Transformed pitch command is of the form

$$\theta_c = k_F \left[h_R + k_{\dot{h}} (\dot{h} - \dot{h}_F) \right] \left[1 + \frac{k_{INT}}{S} \right] + k_{\ddot{h}} \ddot{h}_E + \theta_p(s) \tag{3-70}$$

where:

k_F = The h, $\dot{h}$ flare equation loop gain

h_R = Radio altitude (height above the runway)

$k_{\dot{h}}$ = Ratio of vertical speed to vertical position gain. It is also the key parameter that defines the geometry of a reference exponential flareout path.

$\dot{h}_F$ = Nominal touchdown (final) vertical velocity reference or a programmed $\dot{h}$ command

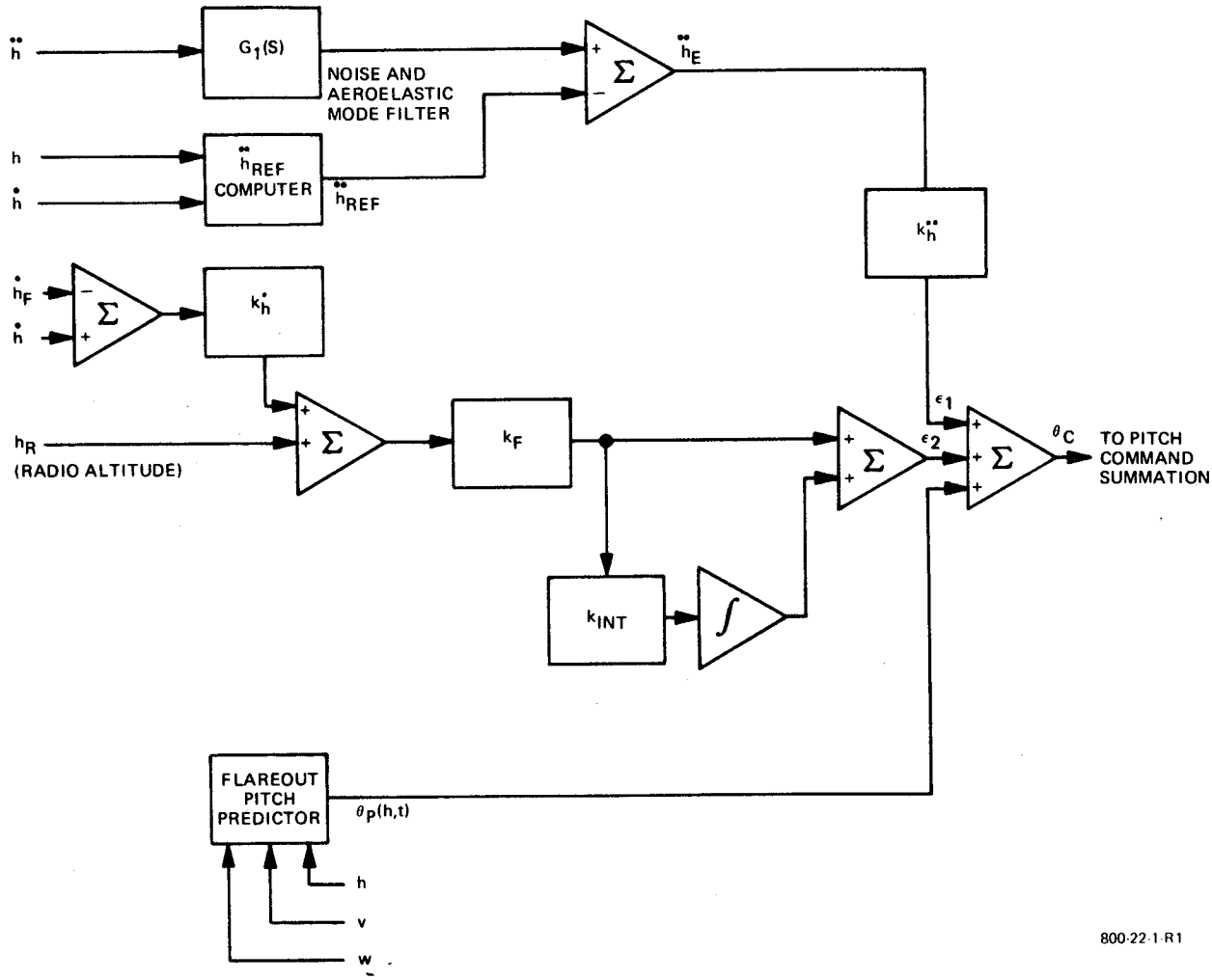

Figure 3-27
Basic Pitch Command Flareout Block Diagram

k_{INT} = Control law integral gain

$k_{\ddot{h}}$ = Vertical acceleration loop gain

$\ddot{h}_e$ = Difference between actual and commanded vertical acceleration

$\theta_p(s)$ = The Laplace Transform of a predicted pitch maneuver $\theta_p(t, h)$ which, if performed under nominal conditions, will ensure that the reference flight path is achieved with zero error. It may be a function of h representing additional altitude constraints on the predictive time program.

Equation (3-70) encompasses all types of flareout controllers from the simplest open loop systems to very sophisticated final value guidance schemes and optimal controllers. In the simplest case, all closed loop feedbacks are eliminated ($k_F = 0$) and the predictive pitch command (with or without a predictive $\ddot{h}$ command) is used to achieve the flareout. The next level of improved capability is obtained with the $\dot{h}$ loop, but without the h or position loop. In this case, at the time of flareout initiate, $\dot{h}_F$ is entered as the new vertical speed reference. Prior to that time, the vertical speed reference was that required to track the glide slope. A more sophisticated version of this approach may introduce a time program (continuous or in discrete steps) for $\dot{h}_F$. The next level of sophistication makes this $\dot{h}_F$ program a function of discrete altitude steps. If the discrete altitude steps are changed to a continuous altitude function we have the $h + k_{\dot{h}}\dot{h}$ control law. Thus far the use of constant gains are satisfactory. However, as we introduce additional computational procedures that attempt to satisfy terminal constraints, then the various state variable feedbacks of equation (3-70) remain intact but the gains are continuously adjusted. There is nothing sacred about expressing the flareout control law as a pitch command. As long as the basic autopilot uses a pitch attitude inner loop, the specification of steering inputs as pitch commands has physical significance. The control law could have been specified as a surface command, and indeed, for those systems that eliminate the pitch feedback, the surface command form would be more appropriate.

b. Bandwidth, Wavelength and Effectiveness of Closed Loop Flareout Control

In Reference 26, the question of flareout flight path controllability is discussed in terms of a control wavelength. The point of that discussion was that the basic closed loop dynamic process of controlling an aircraft's vertical position was limited by stability and other practical considerations to a frequency of below 1.0 radian/second. The value for a large aircraft would be below 0.628 radian/second (10.0 second period). If the vertical position loop were critically damped with time constant τ, it would require 4τ seconds for a disturbance error to settle to zero. Likewise, a second order system with 0.5 damping would have a settling time of about one cycle. In Reference 26, the transformation from time to distance was made. A closed loop frequency, ω, was interpreted as a wavelength as follows

$$\lambda = VT = \frac{2\pi V}{\omega} \tag{3-71}$$

where T = flight path control period,

The closed loop vertical path control process having a 10-second period and a final approach speed of 180 knots (304 feet/second) corresponds to a wavelength of 3040 feet. A reasonably damped system will require at least one wavelength to settle to its final value; but one wavelength is approximately equal to the entire downrange distance of the flareout.

The fact that flight path dynamics are sluggish has motivated many research efforts aimed at improving flight path response. Techniques using control law compensators are theoretically feasible but they encounter the elastic mode stabilization problem with high gain acceleration loops. A demonstration of the problem is the acceleration response to a step elevator for two candidate space shuttle orbiters that were studied (Figure 3-28) (the MSC 245 straight wing and the LMSC delta wing). Note the reversal and the loss of about 1 second before the desired polarity is achieved. Work with Direct Lift Control (DLC) has shown that the reversal due to elevator can be eliminated with DLC surfaces, thereby improving the acceleration response capability by a factor of about 2:1. None of the space shuttle vehicles studied, however, had provision for DLC.

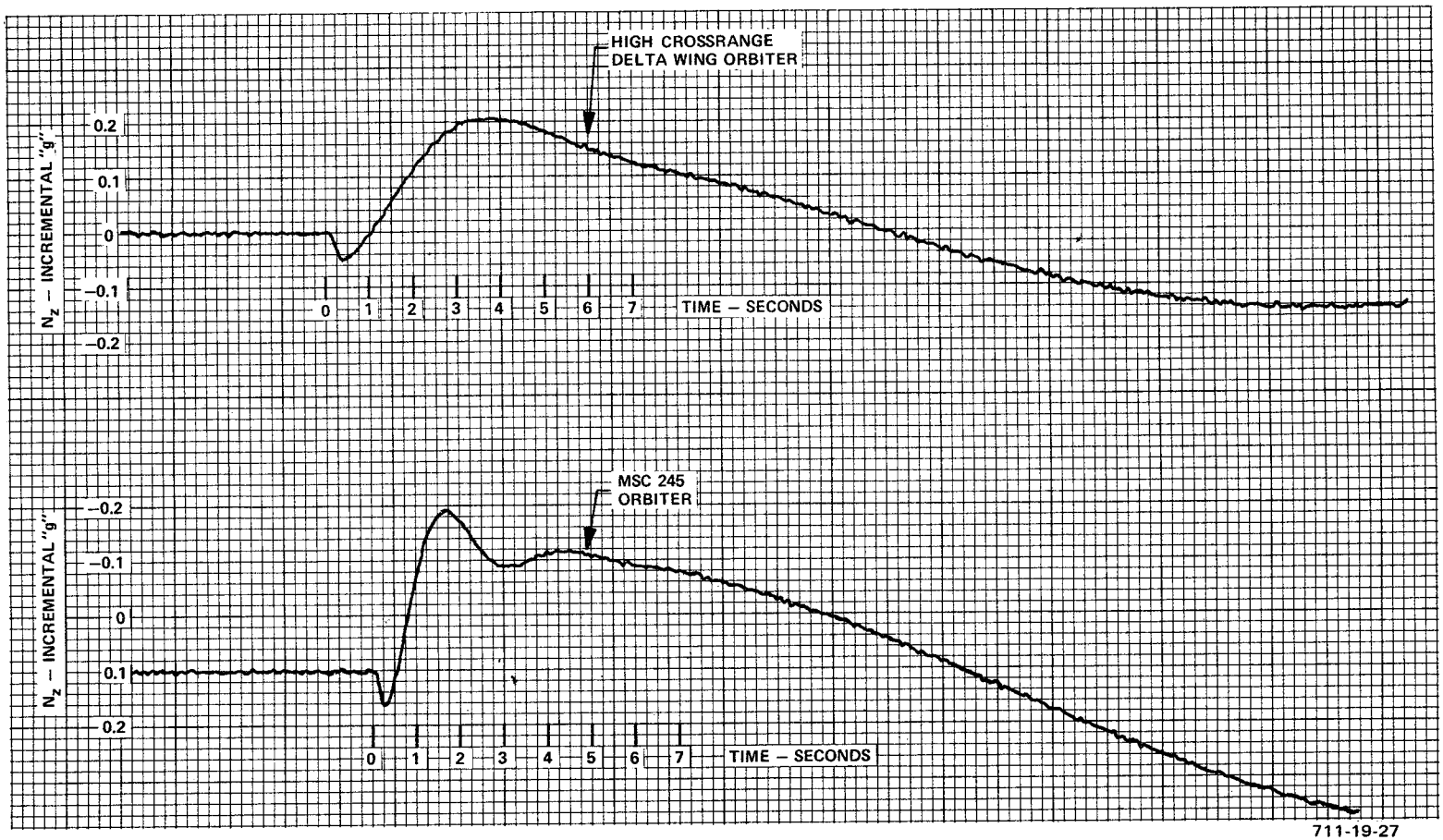

Figure 3-28
g Responses to Step Elevator Deflections
for Two Space Shuttle Vehicles

The point made here is that a flareout system cannot be dependent upon closed loop control exclusively to achieve its precision objectives. The essential elements of a successful flareout system may be summarized as follows:

- Start with a precisely aimed vehicle (proper altitude, velocity and vertical velocity)

- Use an open loop predictive input that can completely satisfy the flareout maneuver requirement with all position and velocity feedback loops open. Use all available vehicle data (weight, speed, aerodynamic characteristics) to compute this predictive command.

- Use the tightest vertical speed and position feedbacks augmented with vertical acceleration that are consistent with stability and the data measurement capability. The tight closed loop system helps correct errors more rapidly but, more important, it prevents the development of errors in a gust and windshear environment. In regard to stability, it is acceptable to use unstable loops immediately prior to touchdown if the period of the instabilities exceed several seconds.

c. The Exponential Flareout Controller

The flareout control law for the exponential controller is initiated at a critical altitude (dependent upon the specific vehicle). The control equation is equation (3-70) with constant gain coefficients. Equation (3-70) defines a reference flight path having an exponential decay of altitude with respect to time. This path reference, h_{REF} is

$$h_{REF}(t) = (h_o + k_{\dot{h}} \dot{h}_F)\, e^{-t/k_{\dot{h}}} + k_{\dot{h}} \dot{h}_F \qquad (3\text{-}72)$$

The term $\dot{h}_F$ represents a vertical speed bias that calls for a finite sink rate at touchdown. It may also be viewed as an altitude bias that shifts the exponential altitude path to a steady state value below the ground level. For a value of $k_{\dot{h}} = 5.0$, and a vertical rate bias of -1.5 feet/second, and if

the flareout starts at 40 feet, then equation (3-72) yields the following typical path reference:

$$h_{REF}(t) = 47.5\ e^{-0.2t} - 7.5 \tag{3-73}$$

The steering law that exercises closed loop control to this reference path is the loop gain k_F and the displacement plus integral (k_{INT}) term of equation (3-70). In most systems the key to a successful flareout is the feedforward or predictive pitch program, $\theta_p(t)$. In its ideal application, this open loop pitch command will cause the aircraft to follow a path such that

$$h + k_{\dot{h}}\ (\dot{h} - \dot{h}_F) = 0 \tag{3-74}$$

If this were to occur, the error signal ϵ_2 on Figure 3-27 would be zero throughout the flareout. The $h + \dot{h}$ control loop may therefore be interpreted as a vernier control on the basic feedforward or predictive command. The optimum predictive command is dependent upon vehicle aerodynamics, initial velocity, initial sink rate, vehicle weight and flare initiating altitude. When any of these parameters depart from the nominal values, the predictive command should be adjusted to minimize dependence upon the $h + \dot{h}$ closed loop vernier. Such an adjustment capability is implied by the inputs to the Flareout Pitch Predictor shown on Figure 3-27. A procedure for adjusting the predictive commands for off-nominal conditions is

- Compute $\theta_p(t)$ by integrating the aircraft equations of motion with constraints in h, $\dot{h}$ and $\ddot{h}$ that yield an instantaneous h that satisfies equation (3-72). The resultant pitch angle defines $\theta_p(t)$, or if desired $\delta_{E_p}(t)$.
- Establish a perturbation guidance logic by perturbing the trajectory with initial condition errors in V, weight h and $\dot{h}$ plus errors in h and $\dot{h}$ at discrete time intervals. The result is a control law of the form

$$\theta_p(t) \text{ or } \delta_{E_p}(t) = \delta_{E_p}(t)_{\text{nominal}} + [C]\begin{bmatrix} \delta V \\ \delta W \\ \delta h \\ \delta \dot{h} \end{bmatrix} \tag{3-75}$$

where

$$[C] = \left[\frac{\partial \delta_E(t)}{\partial V_o}, \frac{\partial \delta_E(T)}{\partial W}, \frac{\partial \delta_E(t)}{\partial h(t)}, \frac{\partial \delta_E(t)}{\partial \dot{h}(t)} \right] \tag{3-76}$$

By attempting to modify the predictive command as a continuous function of the state variables rather than a function of initial errors in the state variables, we have closed a feedback loop. The new h and $\dot{h}$ gains may be incorporated into the existing $h + \dot{h}$ vernier control law. What we have done in equation (3-75) is establish a strategy for correcting $\theta_p(t)$ or $\delta_{E_p}(t)$ for initial condition errors plus a strategy for adjusting the gains of the $h + \dot{h}$ control loop in accordance with measured deviations from the desired trajectory. This would appear to be a fruitful approach if we had reason to believe that the nominal trajectory is a desirable one in response to flight path errors.

In this study perturbation logic for off-nominal conditions was carried to corrections for V_o, W, and $\dot{h}_o$. These will be discussed later.

d. The Vertical Velocity Flareout Controller

By dropping the h_R term in equation (3-70) we have a flareout controller that tries to acquire the touchdown vertical velocity and only tries to control vertical velocity (with help from an $\ddot{h}$ damping loop). The predictive command determines the altitude at which the final vertical speed will be reached. Nominally the terminal vertical speed should be reached about 3.0 seconds prior to touchdown. Overshooting the terminal vertical speed reference or reaching that reference at too high an altitude can cause excessive longitudinal touchdown dispersion.

e. The Acceleration Terminal Controller

This controller is contained within the $\ddot{h}$ reference computer block on Figure 3-27. At the start of this study the possibility of combining this controller with the flareout controller as shown on Figure 3-27 was investigated. The concept was to compute the $\ddot{h}$ reference that continuously satisfied the exponential flareout requirement. When this was attempted, the $h + \dot{h}$ loop and the $\ddot{h}$

loop would develop opposing controls in some types of wind disturbances. Thus, in order to use the acceleration controller, k_F on Figure 3-27 is made zero.

The acceleration terminal controller concept is to force solution to the nominal exponential flareout geometry but, if disturbed from the original path, seek a new exponential path that satisfies the $h + \dot{h}$ control equation. That is, if equation (3-74) is always satisfied, we will ensure the terminal $\dot{h}$ requirement. The development of the required terminal controller is as follows:

Differentiating equation (3-74) gives

$$\dot{h} + k_{\dot{h}} \ddot{h} = 0 \text{ or } \ddot{h} = -\frac{\dot{h}}{k_{\dot{h}}} \tag{3-77}$$

Thus, if we are to follow the desired path at every instant, an acceleration defined by equation (3-77) must be maintained. This acceleration becomes the $\ddot{h}$ command of the $\ddot{h}$ loop on Figure 3-27. The term $k_{\dot{h}}$ is actually a parameter of the exponential path as well as a control law gain. If we wish to constrain the aircraft to an exponential path with time constant $k_{\dot{h}}$, in the presence of position and velocity errors, then from equation (3-74) we know that

$$k_{\dot{h}} = \frac{-h}{(\dot{h} - \dot{h}_F)} \tag{3-78}$$

Substituting this into equation (3-77) yields:

$$\ddot{h}_{ref} = \left(\frac{\dot{h}^2}{h} - \frac{\dot{h}_F \dot{h}}{h} \right) \tag{3-79}$$

The typical $\ddot{h}$ control loop will be of the form

$$\theta_{c_1} = \left(\frac{\ddot{h}}{\tau s + 1} - \ddot{h}_{ref} \right) k_{\ddot{h}} \tag{3-80}$$

where the filter on the $\ddot{h}$ signal is for noise and aeroelastic mode decoupling. It is obviously desirable that the $\ddot{h}$ loop gain, $k_{\ddot{h}}$ be made as high as possible. This involves some difficult stability considerations associated with the inherent sluggish g response of the vehicle to elevator commands (Figure 3-28).

f. Comparison of Flareout Controllers

The three types of flareout controllers described above can provide satisfactory performance when properly optimized. It is difficult, however, to make a judgment on which is best. All three systems are actually quite similar. They depend upon the predictive term for most of the flareout maneuver while the closed loop controls act as a vernier. Ultimately, the best system is the one that provides the tightest flight path control in the presence of wind and turbulence disburbances and perhaps measurement errors. The mode of operation of all three systems can be described in terms of the h, $\dot{h}$ phase plane. Figure 3-29 shows these phase planes for each system. The exponential flareout system [Figure 3-29(a)] always tries to control to a fixed line on the phase plane. A large vehicle has difficulty in achieving an $h + 5\dot{h}$ line. (It typically can achieve an $h + 2\dot{h}$ line.) Also an $h + 2\dot{h}$ controller will give higher accelerations than an $h + 5\dot{h}$ system. The higher gain in $\dot{h}$ is desired for control tightness but it does not give the best trajectory. What is more significant, however, is that if the aircraft has deviated from the reference $h + k_{\dot{h}}\dot{h}$ line, it generally does not have the control bandwidth to reacquire that line in the remaining time. This is where the acceleration controller [Figure 3-29(c)] should have some advantage. It does not try to recover to the original reference line but always computes the minimum acceleration needed to complete an exponential flareout. This controller, however, is also restricted by the large aircraft's inability to achieve rapid acceleration changes.

Figure 3-29(b) shows the vertical speed controller's phase plane trajectory. It only tries to achieve the terminal $\dot{h}$ reference. It should nominally reach $\dot{h}_F$ at about 8 feet from touchdown. If it flares too high it will tend to land at $\dot{h}_F$ but with a penalty in fore-aft excursion on the runway. If it flares too low it may not reach the touchdown reference $\dot{h}$. There are techniques for adding additional intelligence to this controller so that it can minimize these penalties. The adjustment of the flare initiation altitude as a function of initial $\dot{h}$ errors is one of these techniques that will be described later. In all three controllers illustrated in Figure 3-29, the flare initiation is changed to accommodate off-nominal initial sink rates. Another adjustment is to change the predictive commands for variations in the initial speed.

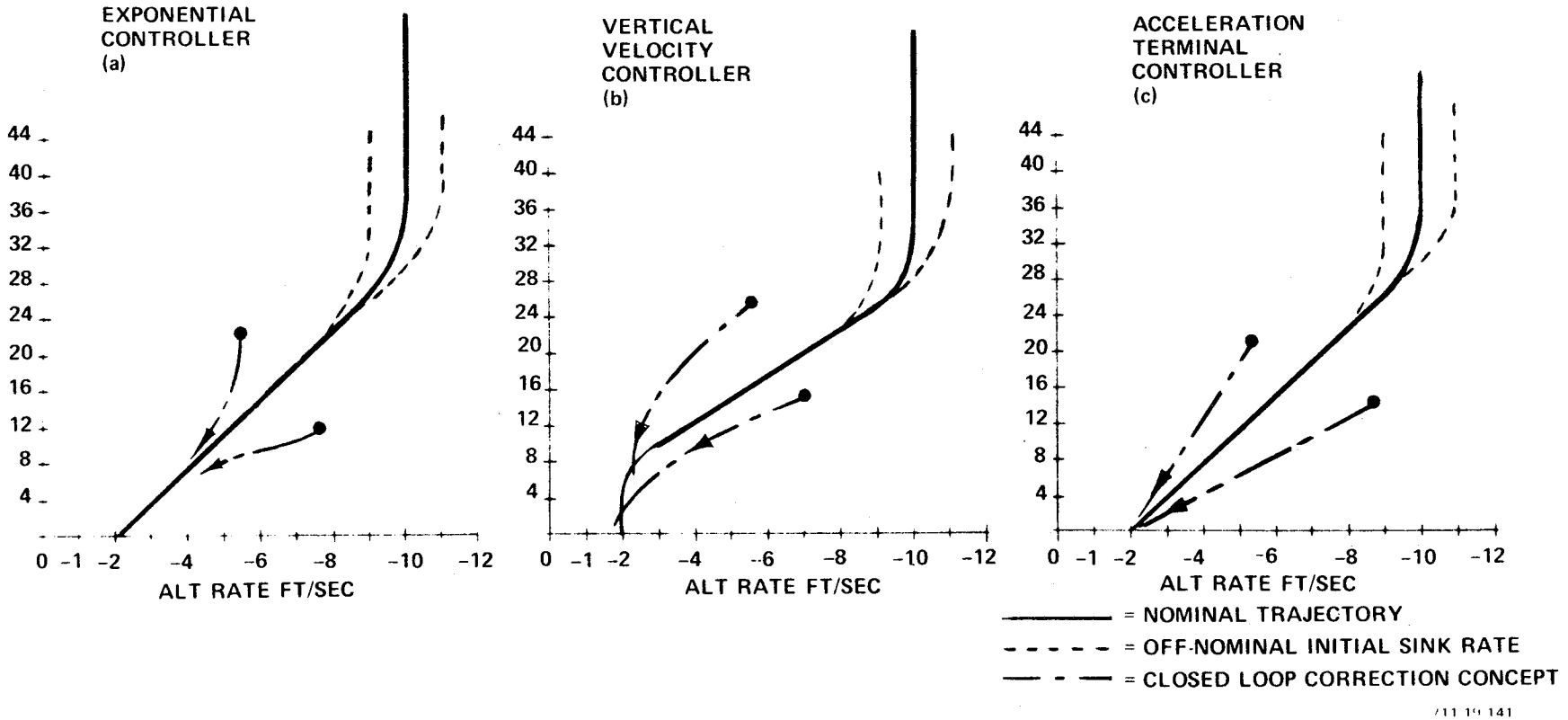

Figure 3-29
Phase Plane for Three Types of Flareout Controllers

Most of the specific vehicle design studies on this program mechanized and evaluated the acceleration flare controller and the vertical velocity controller. The emphasis was shifted to the vertical velocity after tests in a wind gust environment indicated that the acceleration controller tended to develop larger touchdown $\dot{h}$ dispersions. Various logic corrections that were designed to improve the performance of the acceleration controller ended up by making the system look like the vertical velocity controller for most of the flareout. The $\ddot{h}$ reference computation was cut-out until $\dot{h}$ reached a threshold value, the initial maneuver being made by the predictive pitch command only. Then if $\dot{h}$ reached about -2.5 feet/second, control was switched to the vertical velocity control law. The acceleration flare controller, however, did show some promise in the mechanization of a single flareout system rather than a two-phase system. For a low L/D vehicle where acquisition of the shallow glide path is achieved at best for a few seconds, the single flare approach showed reasonable results. In that case, the acceleration controller had considerably more time to stabilize on a properly controlled exponential trajectory since flareout started at an altitude of several hundred feet.

g. Flare Initiate Optimization and Predictive Command Compensation

The vertical velocity flare controller has the following equation

$$\theta_c = k_{\dot{h}}\left(\dot{h}_{REF} - \dot{h}\right)\left(1 + \frac{a}{S}\right) - k_{\ddot{h}}\ddot{h} + \frac{f_1}{1 + \tau S} + 57.3\,\frac{f_2}{V}\left(\frac{1}{S}\right) \qquad (3\text{-}81)$$

where the f_1 and f_2 gains represent the predictive pitch commands.

The flareout is initiated at an altitude h_F given by the logic equation:

$$\text{Engage flare when } h + \dot{h} - B \leqslant 0 \qquad (3\text{-}82)$$

The value of B is selected to initiate flare at the nominal flare altitude for a nominal $\dot{h}$. Thus, for a nominal h_F of 60 feet (C.g., height), and a nominal $\dot{h}$ of -15 feet/second, equation (3-82) will be

$$h + \dot{h} - 45 \leqslant 0$$

A form of compensation that was used on f_1 is

$$f_1 = f_1' + \left(\dot{h}_{REF_o} - \dot{h}_o\right) c_1 + (V_{REF} - V_o)\ c_2 \qquad (3\text{-}83)$$

where typical nominal values of $f_1 = f_1'$ are about 1.5 degrees. The zero subscript indicates the values at flare initiation ($h = h_F$).

The combination of flare altitude adjustment and predictive command compensation allowed all combinations of headwind and tailwind landings for a delta wing vehicle to be achieved with a touchdown vertical speed dispersion of 0.5 foot/second and position dispersion of 100 feet. Turbulence would of course increase these dispersions but no techniques can correct this problem unless we can improve the bandwidth of the flight path control loop.

6. Runway Alignment Techniques (Decrab Guidance)

a. Discussion of Candidate Techniques

Two techniques for automatic runway alignment have resulted from work in automatic landing. (Reference 26) These are described as follows:

- Skid Decrab

This technique involves roll control to track the lateral path through coordinated turns (zero sideslip) down to a "decrab" altitude of approximately eight feet. In the presence of cross winds, a zero sideslip crab angle will develop. At the decrab altitude, the lateral guidance commands are removed and zero roll angle is commanded. At the same time, rudder commands are used to align the aircraft with the runway heading (decrab). Predictive commands are added to both the rudder and aileron channels to provide surface deflections that will compensate for roll and yaw moments resulting from the sideslip developed during the maneuver. The system is normally designed so that touchdown occurs when approximately 70 to 80 percent of the crab angle is removed. At this time, the crab angle is small and the aircraft has a yaw rate established in the direction of the remaining crab angle. This results in low side forces on the gear at touchdown and does not allow time for the aircraft to develop a significant cross runway drift velocity.

- Forward Slip

The "forward slip" technique involves aligning the aircraft heading with the runway heading by applying roll and yaw commands at an altitude of approximately 200 ft. The roll commands used for lateral guidance combined with the rudder commands used for alignment result in a sideslip equal to the original crab angle. The vehicle can be landed on one gear truck in the forward slip configuration provided maximum bank angle constraints (imposed by wing scrape limitations) are observed. In fact, this is the normal manual landing technique for transport aircraft. Because of restrictions on roll attitude resulting from wing and engine pod clearances, techniques have been developed to reduce the touchdown roll attitude to an acceptable value with an additional skid maneuver. Systems have been developed combining the forward slip and the skid decrab maneuver.

- Selection of a Runway Alignment System for the Space Shuttle

The forward slip maneuver is the preferred runway alignment technique for manual control. Pilots have found it easier to minimize lateral drift with this technique than with the skid decrab. For the skid decrab to be done properly, a critical and precise sequence of rudder and roll commands must occur in the final three seconds prior to touchdown. Automatic systems can, in general, perform this maneuver with less difficulty than a pilot because they can utilize precise measurements and computations to develop the necessary roll and yaw controls.

For automatic control, the forward slip maneuver has the disadvantage of interacting with the lateral guidance. While rudder control is maintained to keep the vehicle heading aligned with the runway heading, roll commands are used to command sideslip for lateral guidance. To avoid large lateral errors in the presence of wind shear and gusts, cross feed is required between the rudder channel and the roll channel. Experience has shown that the definition of these cross-feed terms is critical and that small errors in these parameters can result in lateral guidance errors which are more dangerous than incorrect heading alignment at touchdown. Another factor which weighs against the forward slip maneuver for the unpowered shuttle is the large drag which will result during the extended period of high sideslip. For a 25 knot cross wind at a typical final approach speed of 200 knots, a steady sideslip of over seven degrees is required. Data on drag due to β, δ_A, and δ_R has not been available in the vehicle aero model used to date. The seven degrees of β will obviously result in a large drag and hence have an impact on the shallow glide slope speed management.

For the above reasons, the skid decrab technique has been chosen for runway alignment of both shuttle classes of vehicles.

b. Mechanization and Performance of Decrab System

Figure 3-30 is the block diagram of the aileron and rudder control configuration for decrab. The aileron channel includes closed loop control for roll (ϕ) and roll rate (p) commands identical to the roll control for other modes. For decrab, the roll and roll rate commands are zero to command a roll

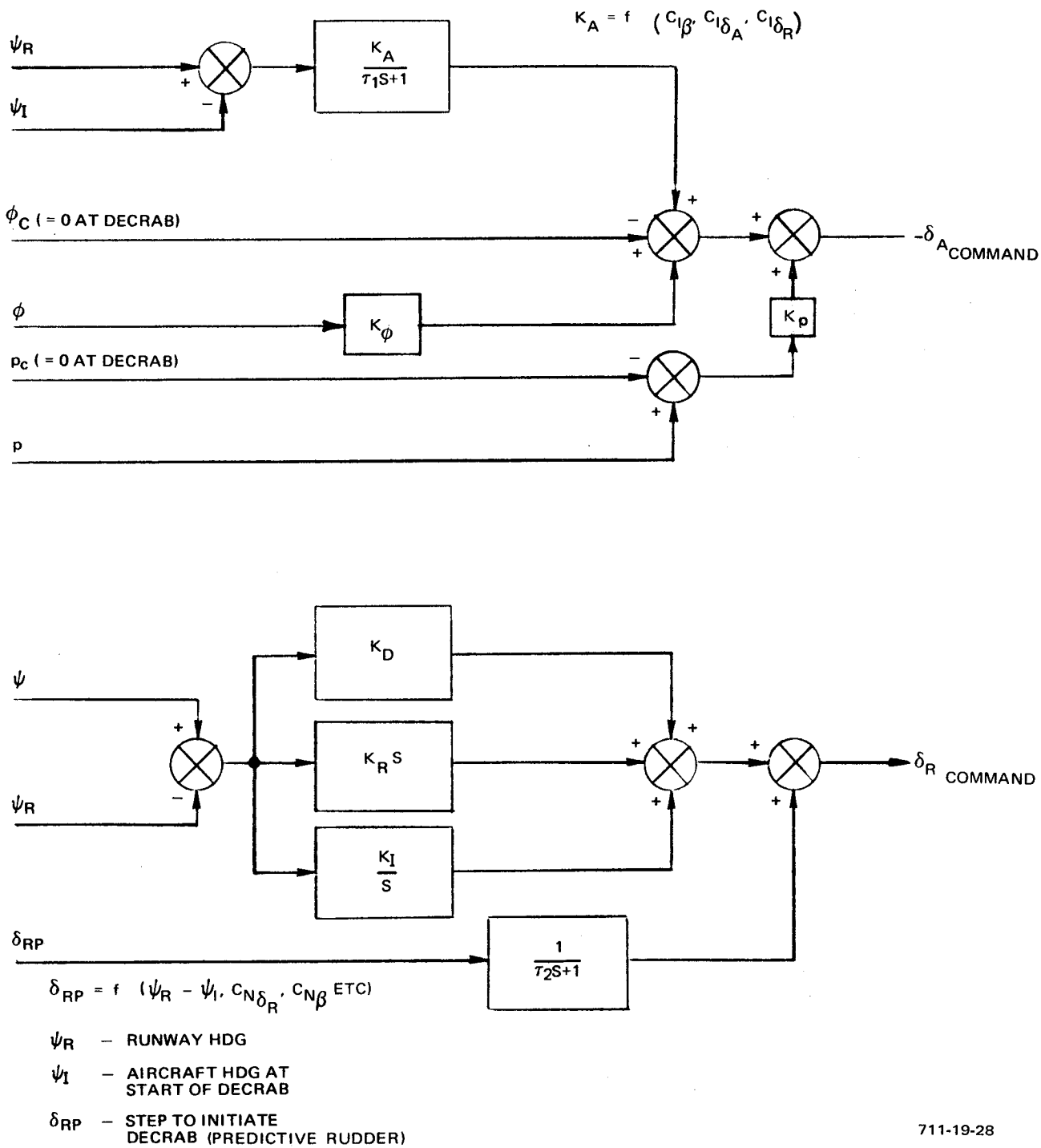

Figure 3-30
Decrab Control System

level attitude. In addition, a predictive command is added to provide a rolling moment to counteract the moments caused by sideslip and rudder deflections during the skid maneuver. Since both sideslip and rudder deflection during decrab are proportional to the initial crab angle, the aileron prediction term is proportional to $(\psi_R - \psi_I)$ as shown in Figure 3-30.

The rudder channel uses rate, displacement, and integral control to skid the aircraft into alignment with the runway heading. Provisions are also made for a predictive rudder command to cancel the yawing movements due to sideslip during the maneuver. For the North American delta wing vehicle however, static directional stability C_{n_β} is almost zero during this condition so that the rudder predictive term is not required.

A typical application of a decrab system design can be illustrated using the version of the NAR high crossrange, delta wing vehicle that was studied on this program. The decrab gains selected for that vehicle are:

K_A	1.73 deg per deg	Aileron Predictive Command
τ_1	1.0 sec	Aileron Predictive Command Time Constant
K_ϕ	2.5 deg/deg	Normal Roll Gains used for other modes
K_p	2.5 deg/deg/sec	Normal Roll Gains used for other modes
K_D	0.8 deg/deg	Decrab Displacement Gain
K_R	0.985 deg/deg/sec	Decrab Rate Gain
K_I	0.05 deg/sec/deg	Decrab Integral Gain
δ_{RP}	Not used	Rudder Predictive Command
τ_2	Not used	Rudder Predictive Command Time Constant

In subsequent work with a more complete NAR vehicle simulation the rate gain K_R was increased to 2.5 and the integral gain was dropped to zero.

A time response of the decrab maneuver is shown in Figure 3-31. By slightly overcorrecting with the aileron predictive command and exploiting the rolling moment due to rudder, the wing into the wind is held down slightly. This technique reduces the cross runway drift that builds up after the crab angle is removed. The decrab maneuver will be initiated when the aircraft is eight feet from touchdown. The traces in Figure 3-31 illustrate that with an initial 5 degree crab angle a good touchdown will result if the vehicle touches down anytime between 2.5 seconds and approximately 6.5 seconds after decrab initiation. During this period, more than 70 percent of the crab angle has been removed, cross runway drift is less than 20 feet, and the cross runway drift rate is less than 10 feet per second. The nominal time to touchdown is about four seconds from initiation of the skid maneuver. At that time the displacement from the runway centerline is approximately zero. The roll in the direction of the wind causes an initial translation into the crosswind. As the sideslip builds up, this translation velocity is reversed so that at the nominal touchdown time, the vehicle has translated back to the centerline. For nominal touchdown speeds, the crosswind represented in Figure 3-31 corresponds to about 17 knots.

7. Lateral Guidance

There are two types of lateral guidance modes used in the space shuttle terminal area guidance system. These same two types of modes (with various subset modes) are also used in conventional transport aircraft autopilots. Figure 3-32 identifies these two lateral guidance modes as a heading mode that generates roll command ϕ_{c1} and a flight path mode that generates roll command ϕ_{c2}. The roll commands are constrained to a maximum rate of change $(\dot{\phi}_c)_{max}$ and a bank angle command limit $(\phi_c)_{max}$. Typical bank angle limits are 45 degrees at the higher altitude, higher speed flight regimes, reduced to 30 degrees as the final approach paths are reached and reduced again to about 10 degrees in the last minute prior to touchdown. Roll rate command limits are likewise reduced from maximum values of about 20 degrees/second to 5 degrees/second prior to landing.

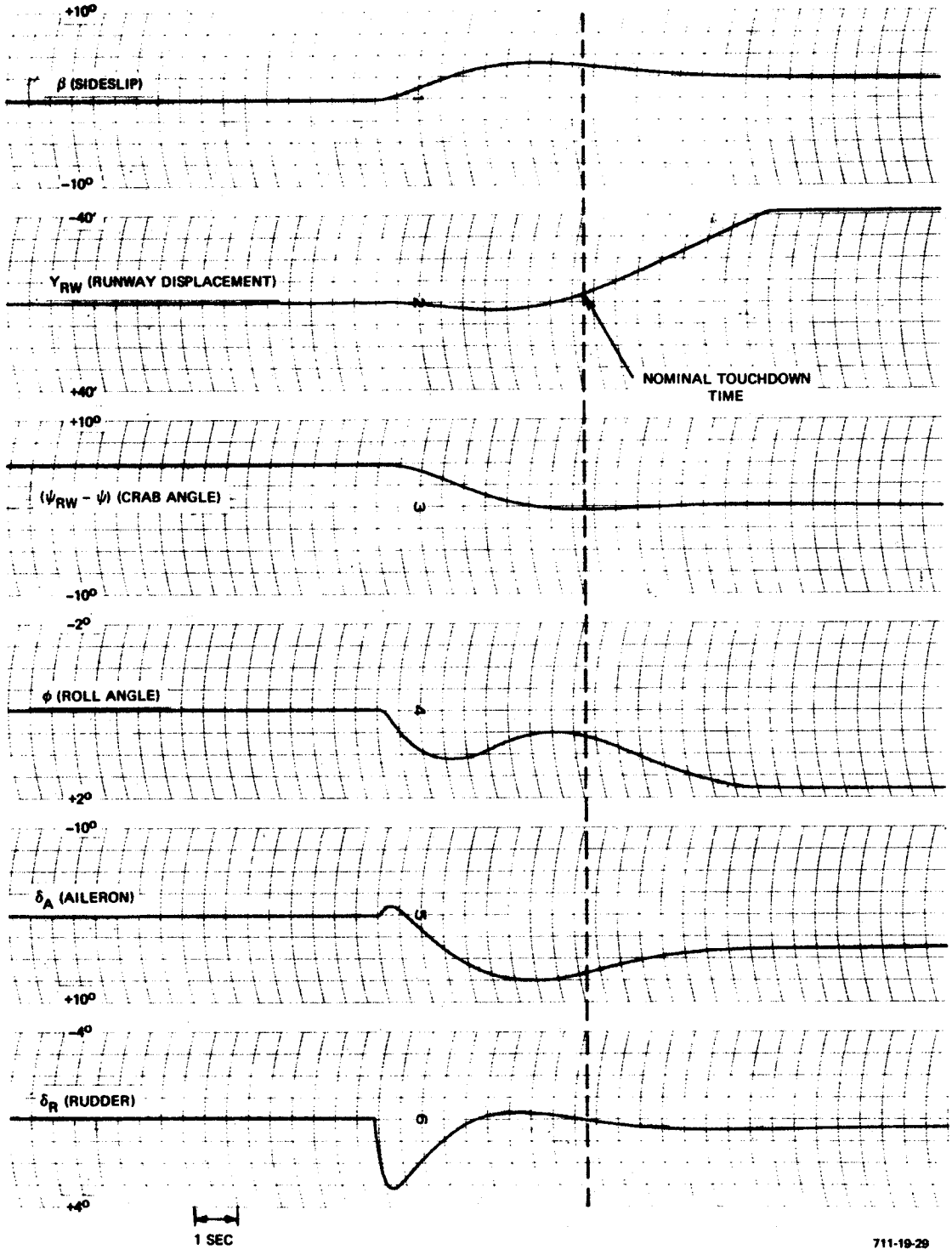

Figure 3-31
Decrab Maneuver HCR Orbiter, M = 0.3, h = 8 feet

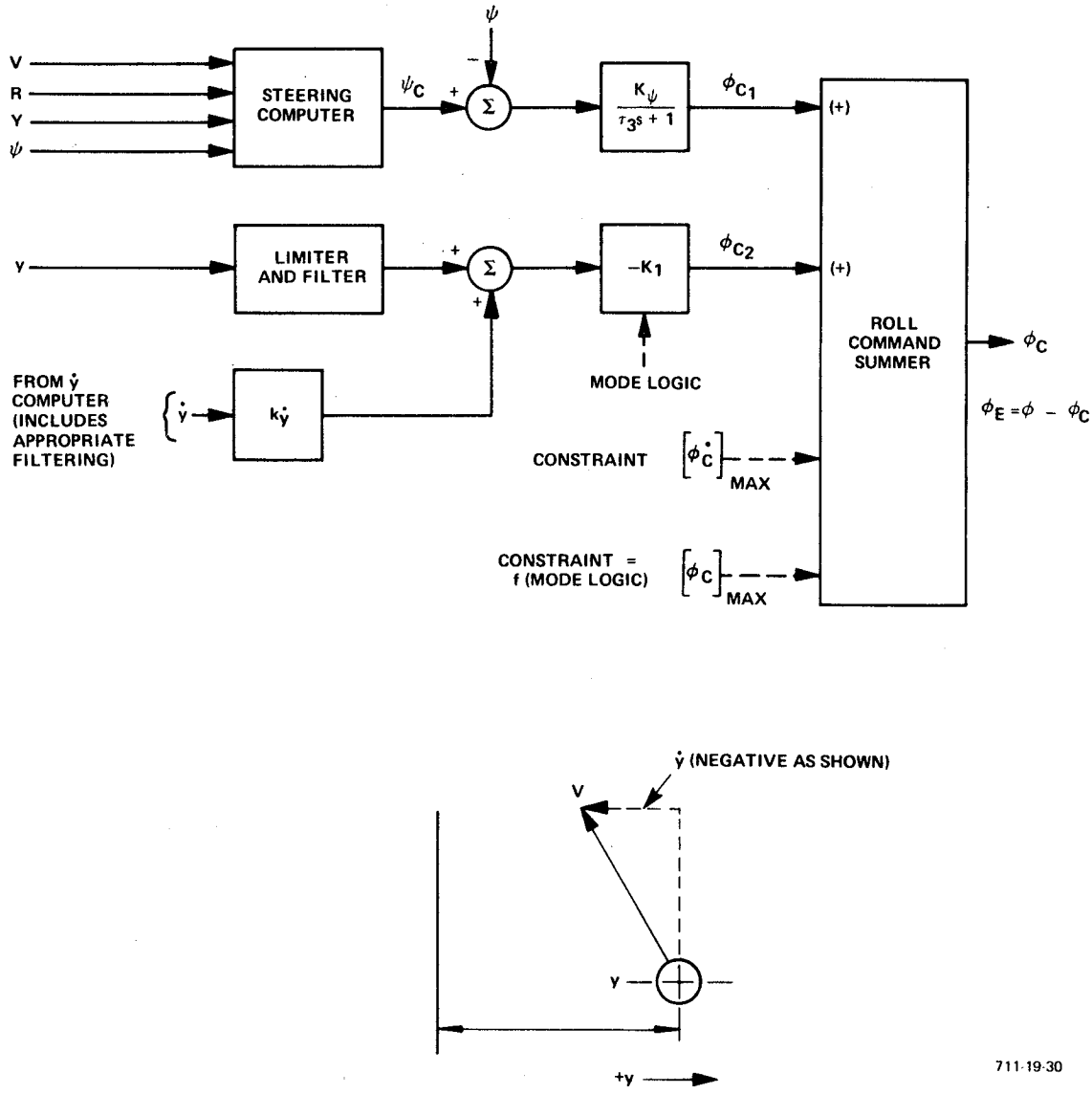

Figure 3-32
Lateral Guidance Block Diagram

The heading control law

$$\phi_{c_1} = \frac{k_\psi}{\tau_3 S + 1} (\psi_c - \psi) \tag{3-84}$$

requires a gain control that is proportional to velocity in order to compensate for the aircraft's turn rate variation:

$$\dot{\psi} = \frac{g}{V} \tan \phi \tag{3-85}$$

Therefore

$$k_\psi = k_{\psi_o} \left(\frac{V}{V_o} \right) \tag{3-86}$$

where V_o is typically 200 ft/sec and $k_{\psi_o} \approx 1.0$

This permits a nearly constant heading reponse (when in the linear control region) through large ranges of velocity since the heading loop gain Y(s) is represented by the following transfer functions

$$(Y)_{\substack{\text{OPEN} \\ \text{LOOP}}}(s) = \left(\frac{\phi_c}{\psi} \right) \left(\frac{\phi}{\phi_c} \right) \left(\frac{\psi}{\phi} \right)$$

$$= k_{\psi_o} \frac{v}{V_o} \left(\frac{1}{\tau_3 S + 1} \right) \left(\frac{\phi}{\phi_c} \right) \left(\frac{g}{v} \right) \tag{3-87}$$

where $\frac{\phi}{\phi_c}$ = closed loop roll dynamics

With the V gain control, the loop gain is invariant with velocity.

An important factor in the analysis of heading control stability is the definition of the heading angle ψ. If ψ is the euler angle determined by a yaw, pitch, roll sequence of rotations from a local vertical coordinate frame, then the heading control laws given in equations (3-84) and (3-86) are not adequately represented by the stability analysis of equation (3-87) for large angles of attack and large bank angles. The problem results from the fact that the turning

kinematics are only an approximation of the azimuth change experienced by the vehicle's X axis. To illustrate the problem without the required derivation of the geometrical relationships, consider the hypothetical case of an aircraft in horizontal flight with a 90-degree angle of attack (pitch angle = +90 degrees). Now perform a zero sideslip bank about the velocity vector. A bank about the velocity vector is all body axis yaw rate and zero body axis roll rate. Let the roll angle change about the velocity vector be 90 degrees. The initial result is that the angle of attack remains 90 degrees (no change in velocity vector) but the azimuth angle ψ has changed 90 degrees. This corresponds to a case where the azimuth rate is the rate of roll about the velocity vector rather than g/V tan ϕ, the relationship defined by the turning kinematics.

Thus if the specified control law is implemented using euler angle ψ, then serious stability problems can occur for high angle-of-attack flight conditions (at high velocities). To overcome this problem, the angle ψ can be interpreted as inertial velocity vector heading defined as:

$$\psi = \tan^{-1} V_{north}/V_{east} \tag{3-88}$$

This was done in the high altitude guidance modes where the vehicle is steered to various reference headings. Reasonable turn rate capability without stability problems was possible only when heading is defined as in equation (3-88).

The other type of lateral guidance involves following a specified ground track. The guidance law is

$$\phi_{c_2} = \left[(y)_{limited} + k_{\dot{y}}\,\dot{y}\right]\left[-k_1\right] + \phi_{cp} \tag{3-89}$$

This guidance law is similar to that used in autopilots for tracking localizer beams, VOR radials and INS generated ground track references. Filtering is required on both the y and $\dot{y}$ information but the extent of that filtering depends upon the data measurement source. In equation (3-89) it is assumed that appropriate y and $\dot{y}$ filtering has been accomplished within the navigation state estimation equations. The dynamic effect of these filters (lags) restrict the achievable gains for this loop. The term ϕ_{cp} is a predictive bank angle command

that is used to fly a curved track. The value of ϕ_{cp} is determined by the radius of curvature R_c of that track:

$$\phi_{cp} = \tan^{-1}\left(\frac{V^2 \cos \gamma}{gR_c}\right) \tag{3-90}$$

It is noted that equation (3-89) does not include an integral term on y. The only reason for using a path integration term would be to correct for errors in the measurement or synthesis of $\dot{y}$. At this time is is assumed that such $\dot{y}$ errors do not exist. If the integrator is used, it must be switched-on only after the tracking of the path is fairly well stabilized, with only small y errors existing (presumably because of the inaccuracy in the $\dot{y}$ information).

8. High Cross-Range Vehicle High Altitude Energy Management

a. Introduction

The high altitude energy management objective is to steer the vehicle between altitudes of 100,000 to 20,000 feet so that when it reaches 20,000 feet, it will be aligned with the terminal glide path. This alignment includes lateral and vertical position and velocity errors of approximately zero. implies lateral tions at 100,000 feet may vary in position and heading. The following discussions cover the results of the three key tasks associated with this energy management problem. These are:

- Define the theoretical energy management capacity of the high cross-range vehicle from 100,000 feet to 20,000 feet, where the 100,000 feet velocity is approximately 3,000 ft/sec. This capacity should be expressed as a position window at 100,000 feet with a nominal or target position defined for each initial heading.

- Define a system concept and the associated guidance laws that exploit the vehicle's energy management capability by steering the vehicle to achieve zero error alignment with the terminal glide path.

- Demonstrate the performance of the specified energy management system with simulations of the HCR vehicle and associated guidance laws.

b. Theoretical Energy Management Capability

- Undershoot Boundaries

The technique for defining the theoretical energy management window is illustrated in Figure 3-33a and 3-33b, the vertical and horizontal views, respectively, of the 100,000 feet to 20,000 feet trajectories. The 20,000 feet low key point is designated as the 0,0 coordinate in the horizontal plane. The landing runway is shown located with respect to the 0,0 coordinate. That runway is assumed to be aligned east-west and landing occurs at a heading of 270 degrees (west).

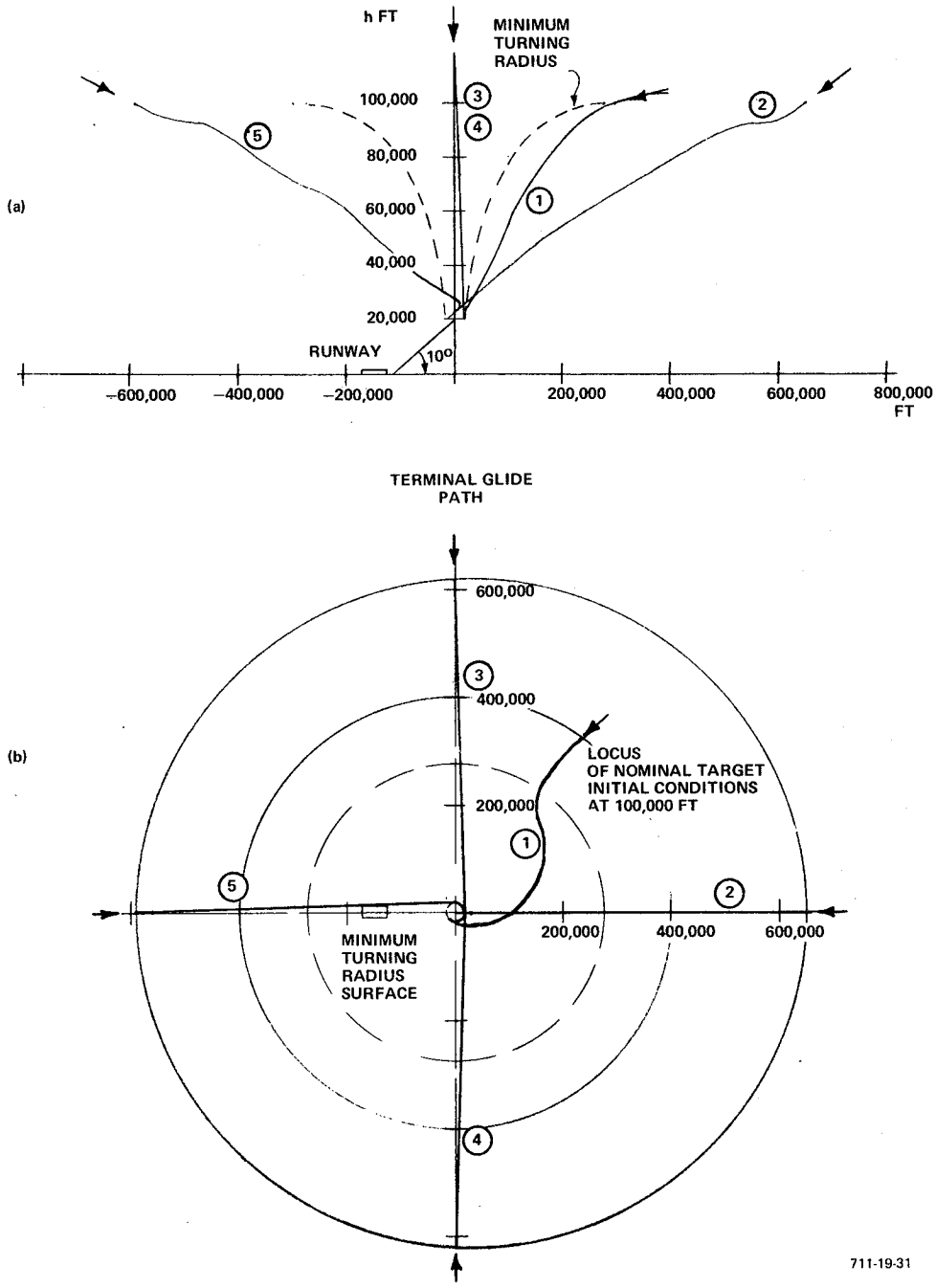

Figure 3-33
Definition of Energy Management Undershoot Surface

Consider trajectory (2) - it is a straight-in approach (heading of 270°). The vehicle is flown at maximum L/D from 100,000 feet to 20,000 feet. The resultant trajectory represents the maximum undershoot boundary for the 270° heading case. Thus, if the down-range displacement was greater than 660,000 feet at an altitude of 100,000 feet and a velocity of 3,000 ft/sec, the vehicle must fall short (or undershoot) the terminal 10 degree glide path.

Now, consider trajectory (5) on Figures 3-33a and 3-33b (90° heading). Again we fly maximum L/D toward the low keypoint, but prior to reaching 20,000 feet we make a 180° turn which exactly aligns us with the final approach path. The distance flown is approximately the same as for Case (2), but the down-range distance is shortened slightly by the circumference of the 180° turn. Trajectory (5) represents the maximum undershoot boundary for a 90° initial heading.

Trajectories (3) and (4) show similar maximum L/D trajectories for 180° and 0° initial headings where an appropriate final 90° turn is made to align with the final approach path. If we continue to run maximum L/D trajectories of this type for every heading, we define a conical type surface which represents the maximum undershoot boundary. If the vehicle ever falls outside of this distorted cone, it means that it can never reach the low keypoint. The large circle on Figure 3-33b represents the locus of positions for each heading such that the vehicle can fly on the undershoot surface only by maintaining maximum L/D at all times.

- Nominal 100,000 Feet Position Locus

There is also an overshoot boundary, but its definition is not as apparent from Figure 3-33. Assume again that we are approaching straight-in (270°), but now we are at 100,000 feet with down-range coordinates of near zero. (We are almost over the low keypoint.) We must initiate a turn immediately and achieve a trajectory heading toward the low keypoint without falling below the undershoot boundary. The turning radius for a 45 degree bank is

$$R_c = \frac{V^2 \cos \gamma}{g \tan \phi} = \frac{V^2 \cos \gamma}{g} \qquad (3\text{-}91)$$

Turning radii centered at the low keypoint for nominal velocities and γ's associated with each altitude are plotted as the dashed curve on Figures 3-33a and 3-33b. Since the nominal turning radius at 100,000 feet is about 300,000 feet, it is apparent that there is only a limited ability to achieve a 180° heading change for the overshoot case without passing through the undershoot boundary. The coordinates of the overshoot boundary will also be a function of heading. Thus, at 100,000 feet, somewhere between the undershoot boundary (large circle on Figure 3-33b) and overshoot boundary (to be described subsequently), there is a nominal desired position. The locus of the nominal 100,000 feet target positions for each heading is shown as the inner circle on Figure 3-33b.

There are some interesting implications to the fact that the nominal 100,000 feet target position is a circle rather than a point. Reentry guidance systems are generally expected to steer to a 100,000 feet (or Mach 3) target point. As seen in Figure 3-33b, that target point shifts with the heading that it is being approached. The implication is that the reentry guidance system should steer to a vertical line through the low key target point (20,000 feet) so that the proper heading is achieved at 100,000 feet.

- Overshoot Boundaries and 100,000 Feet Windows

If we repeat the process of initializing at 100,000 feet with a velocity of 3,000 ft/sec for the 270° initial heading, but this time move the vehicle down-range position forward from the 660,000 feet undershoot boundary toward the zero down-range coordinate, we can determine the overshoot boundary. This boundary can be found for a complete set of lateral displacements as well as the zero lateral displacement corresponding to the straight-in approach. In every case, we attempt a 180° turn maintaining peak L/D at all times (with appropriate dynamic pressure constraints). If we fall below the undershoot boundary as we turn back toward the low key target point, the initial position exceeded the overshoot boundary.

We can complete the 100,000 feet window definition by finding undershoot boundaries for various lateral offsets. (For large lateral offsets,

there is no distinction between an overshoot or undershoot condition.) The resultant window is the cardioid shape shown in Figure 3-34. Three windows differing slightly in the down-range dimension are shown. The longer window is for the straight-in case; the shortest is for the case where a 180° turn-back is required; and the middle curve is for the case where the initial heading is orthogonal to the landing runway (final flight path). The nominal trajectory starts at the center of the window and proceeds toward the low keypoint as indicated by the horizontal view of that trajectory identified as (1) on Figure 3-34.

Note that the symmetrical axis of the window, shown in Figure 3-34 corresponds with the initial heading. To establish the window for each heading with respect to the runway heading, we rotate the appropriate window of Figure 3-34 about the low keypoint. The result of this rotation is shown in Figure 3-35. The large circle corresponds to the locus of undershoot boundaries for all initial headings. The inner circle is the locus of 100,000 feet (high key) target points for all initial headings. These are the same circles discussed previously with regard to Figure 3-33. They are shown in Figure 3-35 with the respective windows for 0°, 90°, 180° and 270° initial headings with respect to the runway.

c. Guidance Laws

- Pitch Guidance

Pitch guidance is based on maintaining a dynamic pressure reference until a maximum descent flight path angle is reached. Then closed-loop control to flight path angle, γ, is maintained with Q and α constraints included to prevent penetration into excluded flight regions. The pitch command equations are of the following form:

$$\theta_C = K_Q\left(Q - Q_{REF}\right)\left(1 + \frac{a}{s}\right) + K_L\left(\frac{1 - \cos\phi}{\cos\phi}\right) \qquad (3\text{-}92)$$

$$\text{for } \gamma > \gamma_{REF}$$

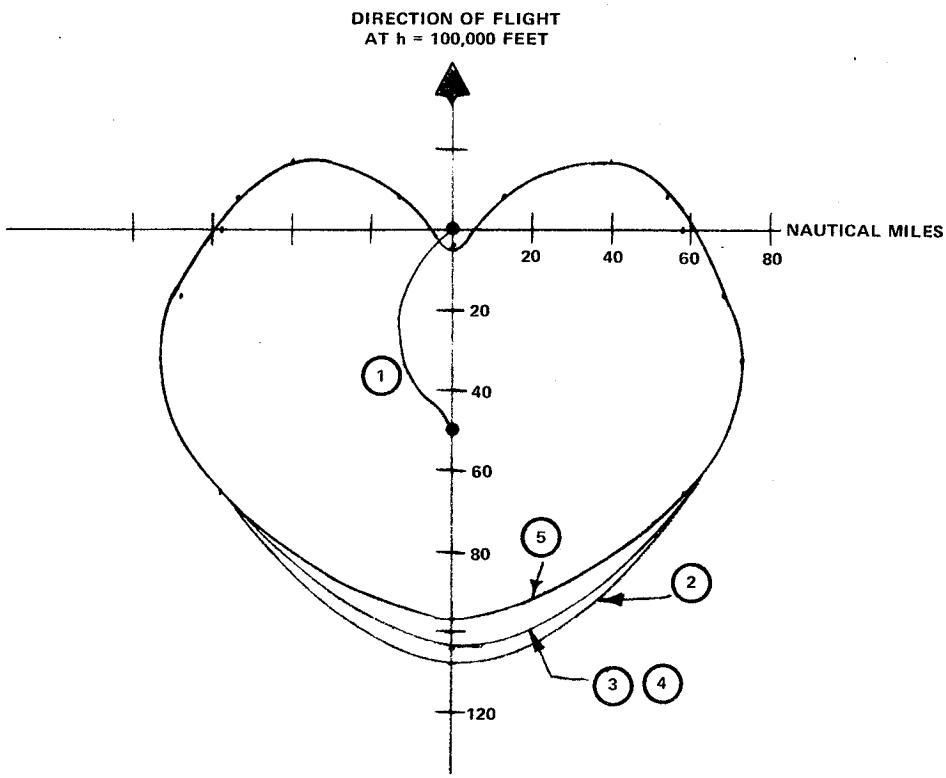

① = NORMAL TRAJECTORY

② = WINDOW FOR INITIAL HEADING ALIGNED WITH LANDING RUNWAY

③AND④= WINDOW FOR INITIAL HEADING 90° WITH RESPECT TO LANDING RUNWAY

⑤ = WINDOW FOR INITIAL HEADING 180° WITH RESPECT TO LANDING RUNWAY

711-19-32

Figure 3-34
Theoretical Energy Management Window at 100,000 feet

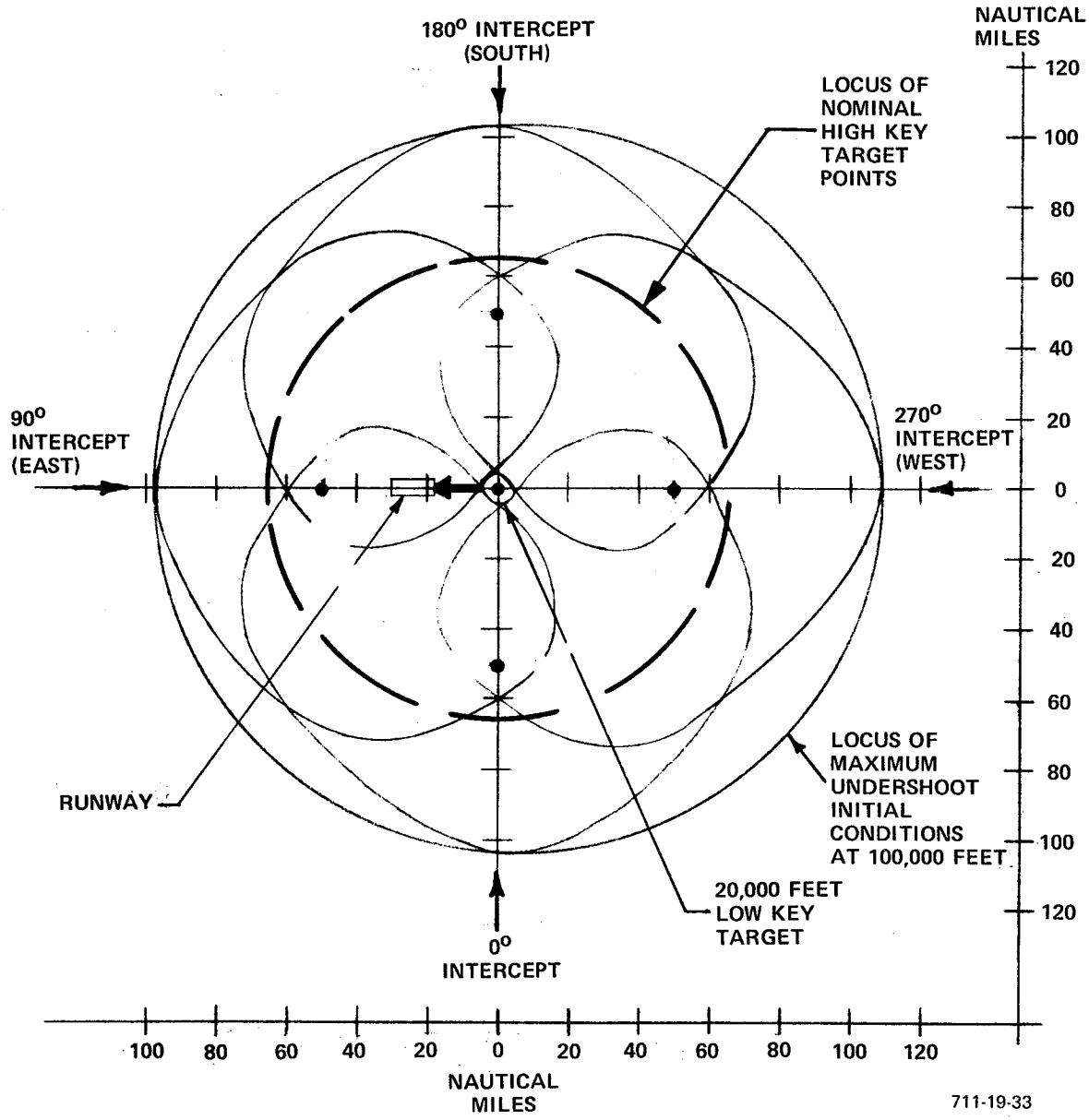

Figure 3-35
Energy Management Windows for 360-degree
Intercept Headings (with Landing Runway at 270 degrees)

$$\theta_C = K_\gamma \left(\gamma_{REF} - \gamma\right)\left(1 + \frac{b}{s}\right) + K_L \left(\frac{1 - \cos \phi}{\cos \phi}\right) \qquad (3\text{-}93)$$

$$\text{for } \gamma \leq \gamma_{REF}$$

where K_L is the gain of a lift compensation term for banking maneuvers (function of lift curve slope and dynamic pressure) and γ_{REF} is the terminal glide path (-10 degrees for the high cross-range vehicle being studied). The nominal Q_{REF} is about 150 lbs/ft^2 for most vehicles; but in Equation (3-92), Q_{REF} may be adjusted for energy management in accordance with

$$Q_{REF} = Q_{NOM} + \Delta Q \qquad (3\text{-}94)$$

$$\Delta Q = \frac{k_\alpha}{s} (\alpha - \alpha_{REF}) \qquad (3\text{-}95)$$

where

$$\alpha_{REF} = f(M, h, \Delta E) \qquad (3\text{-}96)$$

The Q loop is a convenient way of flying long term α control without exciting an aircraft's phugoid mode (which tends to occur with a tight α hold loop). Also, short term α computations or measurements may contain excessive errors and this technique helps to minimize the effects of these errors.

In the high altitude energy management simulations with the NAR vehicle, Equations (3-95) and (3-96) were not used. (A constant Q_{REF} was maintained.) In work with MDAC delta configuration, which will be documented in a supplement to this report, the ΔQ functions per Equation (3-95) and (3-96) were used. The α reference was programmed as a function of M, but some additional logic based on h and energy error, ΔE, could also have been useful. These latter terms are retained in Equation (3-96) because of their potential utility in an energy management system that starts at about 150,000 feet. Note that in practice, the Q loop would be converted to a Q_c (impact pressure) loop, which is the parameter that can be measured with a pitot-static probe.

- Lateral Guidance

The guidance concept for achieving the high altitude energy management is shown in Figure 3-36 and 3-37. The vehicle is steered toward a tangential intercept of a circle of radius r_o. The center of the circle is a short distance from the point at which the vehicle should intercept the glide path at 20,000 feet.

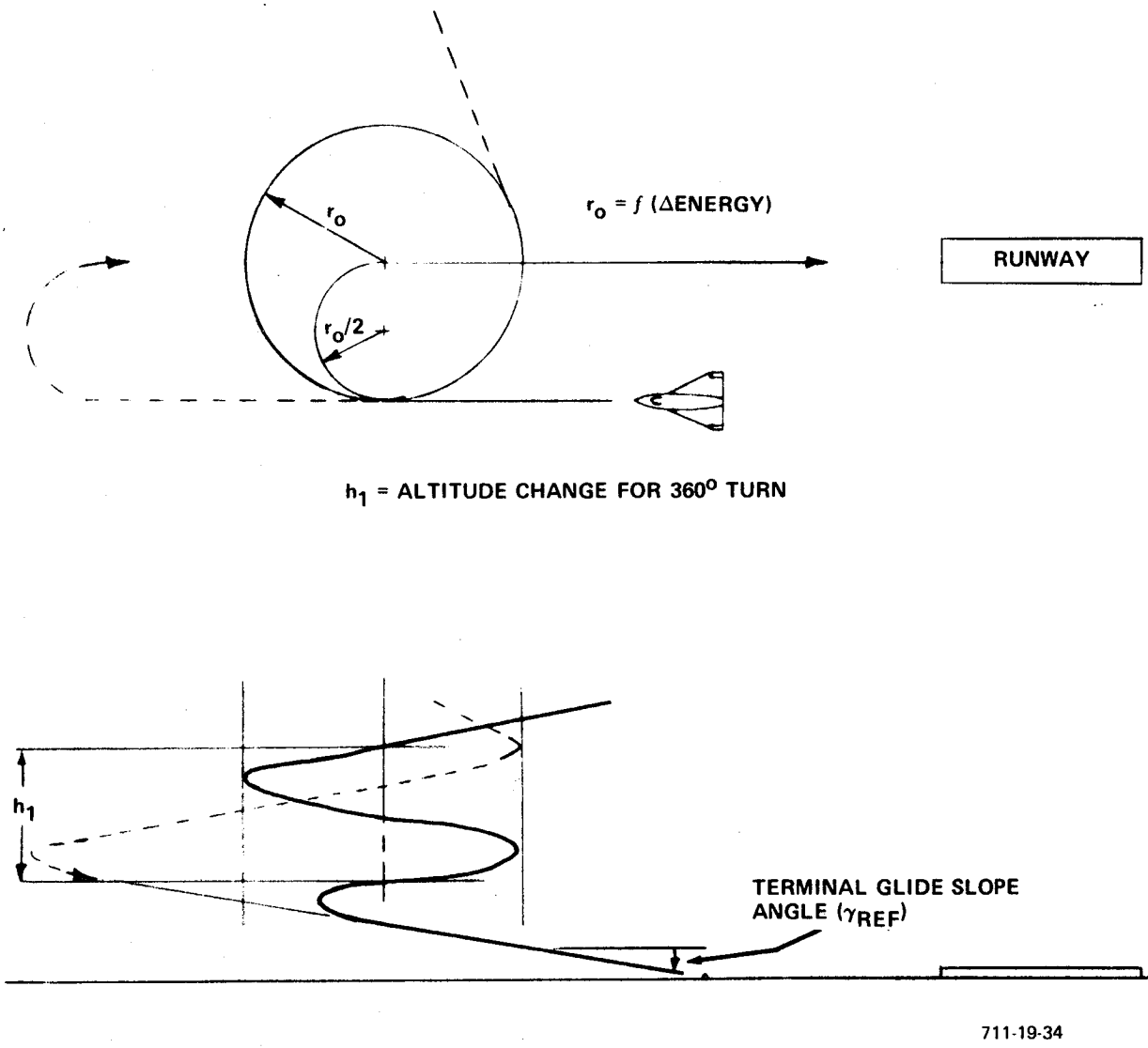

Figure 3-36
Typical Trajectories Showing Final Alignment
Maneuver with Terminal Flight Path

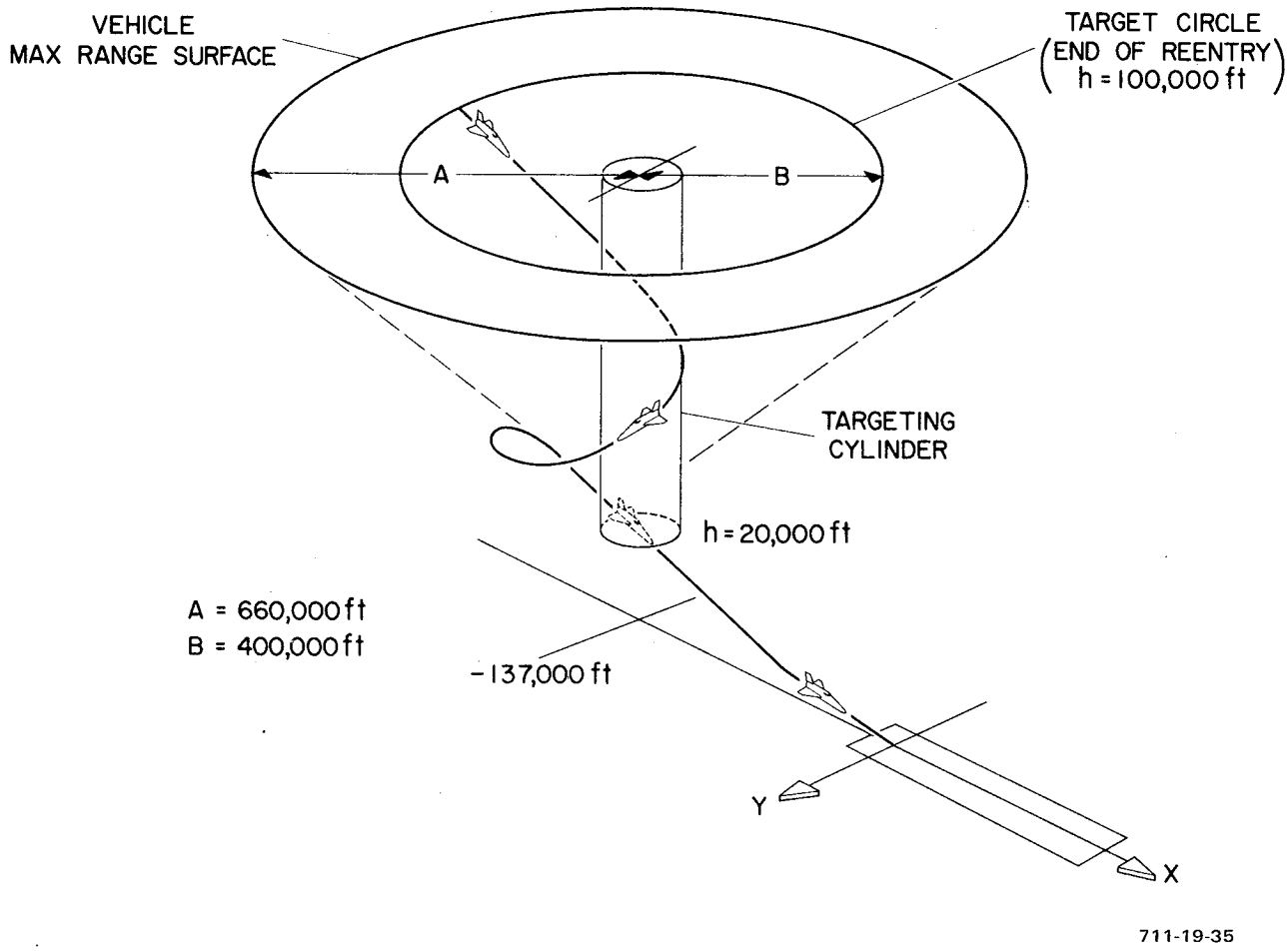

Figure 3-37
Three Dimensional View of Typical High Altitude
Energy Management Procedure

The radius r_o is a function of the vehicle's excess or shortage of potential and kinetic energy as referenced to a nominal trajectory. The guidance law steers the vehicle so that it attempts to descend in a spiral path that remains tangent to the shrinking circle of radius r_o. A predictive computation is continuously made to determine if a full circle can still be flown before intersecting the glide path. If not, the vehicle is steered along the dashed path, following a heading 180 degrees from the runway direction. At the proper time, a 180-degree turn with turning radius $r_o/2$ is performed such that the vehicle intercepts the center of the "localizer" path while simultaneously acquiring the terminal glide path. The three dimensional view of the trajectory illustrated in Figure 3-37 shows that the target circle is actually a target cylinder. Nominally, a high crossrange vehicle arrives at the targeting cylinder at an altitude of about 50,000 feet and a velocity of 900 feet/second.

The radius of the target circle or target cylinder shown in Figures 3-36 and 3-37 grows as a function of excess energy. The equation for the target circle radius is:

$$r = r_o + C_E \Delta E \tag{3-97}$$

where r_o is the nominal trajectory radius (20,000 feet) and ΔE is the energy error given by

$$\Delta E = W \left[h - C_1 (D_K) \right] + \frac{WV}{g} \left[V - C_2 (D_K) \right] \tag{3-98}$$

D_K = distance to low keypoint

$C_1 (D_K)$ = nominal altitude for each D_K

$C_2 (D_K)$ = nominal velocity for each D_K

The vehicle is commanded to fly a heading that is tangent to circle r in the direction that corresponds to clockwise turning. That heading, ψ_T, is computed from the knowledge of the magnitude and direction of D_K and the magnitude of r. The bank command is

$$\phi_C = \frac{C_1 (\psi_T - \psi)}{(\tau s + 1)} \tag{3-99}$$

which represents a conventional autopilot heading control mode where the gain C_1 is reduced as velocity decreases. (Bank commands are limited to ±45°.) Prior to the final turning maneuver that captures the terminal path leading to the runway, closed-loop control is established to the target circle of radius r_o as shown in Figure 3-36. The bank command guidance law is

$$\phi_{C_{LIMITED}} = \tan^{-1}\left(\frac{V^2 \cos\gamma}{r_o g}\right) + k_y\left[\left(r' - r_o\right)_{LIMITED}\right] + k_{\dot{y}}\,\dot{r} \qquad (3\text{-}100)$$

where: r' = distance of vehicle from r_o center and ϕ_C is limited to ±45°.

The circle of radius r_o is flown until the vehicle is heading 180° ± 30° from the runway and the altitude has reached the value where another complete 360° turn cannot be completed without descending below the terminal glide path. At this point, the heading is maintained (180° ± 30° from runway) until the vehicle has reached a height such that a 180° turn, flying a circle of radius $r_o/2$ establishes the vehicle on the terminal glide path and aligned with the runway center line (Figure 3-36). During the constant heading phase, the steering law is the same as Equation (3-99), but with the heading reference equal to the runway heading +180°. During the final turn on to the terminal path, the lateral steering law is

$$\phi_{C_{LIMITED}} = \tan^{-1}\left(\frac{V^2 \cos\gamma}{\frac{r_o}{2} g}\right) + k_y\left[\left(r'' - \frac{r_o}{2}\right) + k_{\dot{y}}\,\dot{r}''\right] \qquad (3\text{-}101)$$

where r'' = distance from $\frac{r_o}{2}$ center. Closed-loop control to the terminal path is initiated when the intercept heading falls below 30 degrees.

d. Simulation Results

Performance of the system using the above guidance laws is documented in Figures 3-38 through 3-43. Figures 3-38 and 3-39 show the vertical and horizontal views of nominal trajectories approaching the low keypoint from five different headings covering zero through 360 degrees. Figure 3-40 shows the corresponding velocity histories (versus altitude) for these trajectories. All start at 100,000 feet, with the same range from the low keypoint, but approaching from different directions. All trajectories fly tangent to the circle of radius

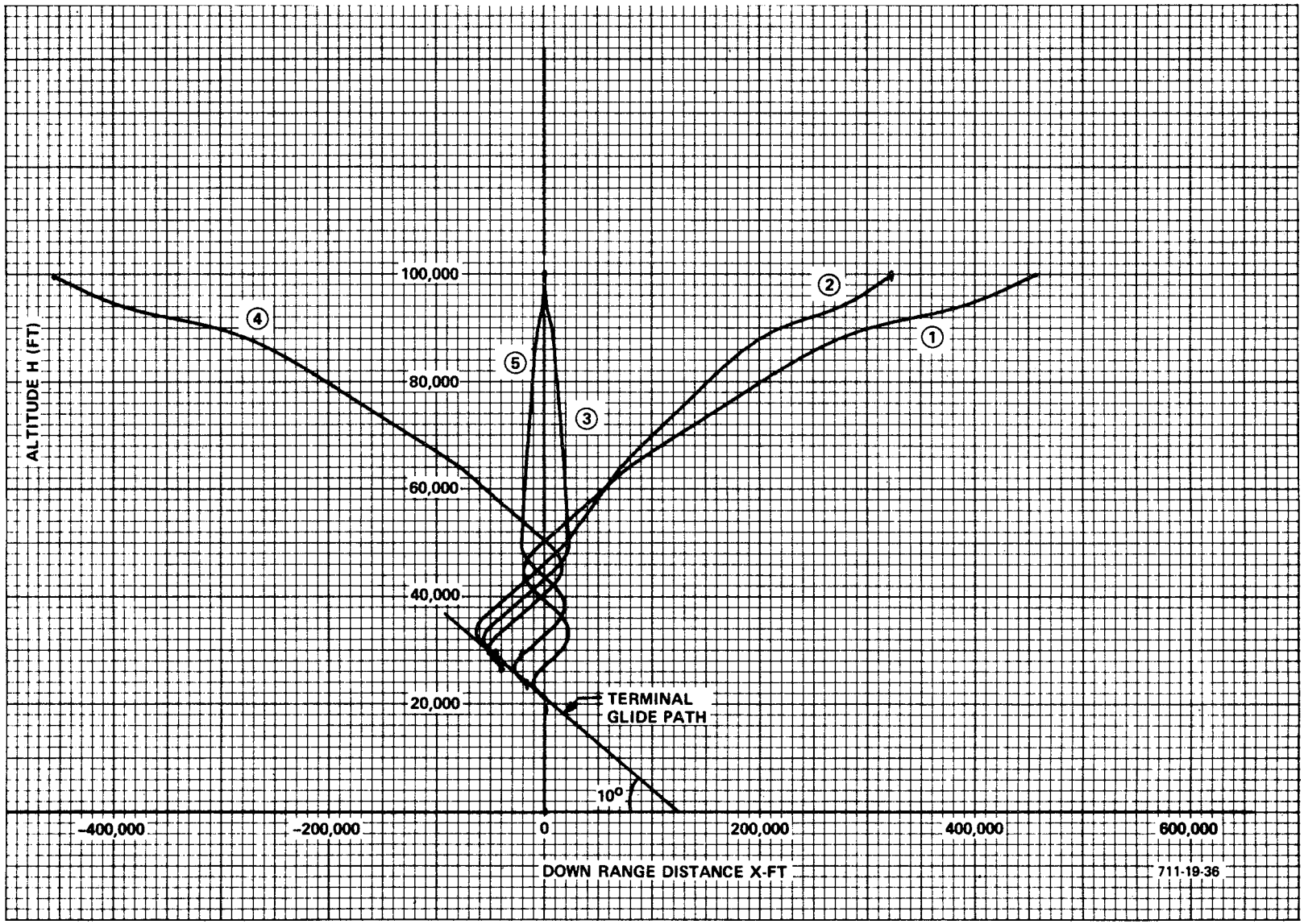

Figure 3-38
HCR Terminal Energy Management Steering (Vertical View)
for Terminal Glide Path Acquisition for Various Headings

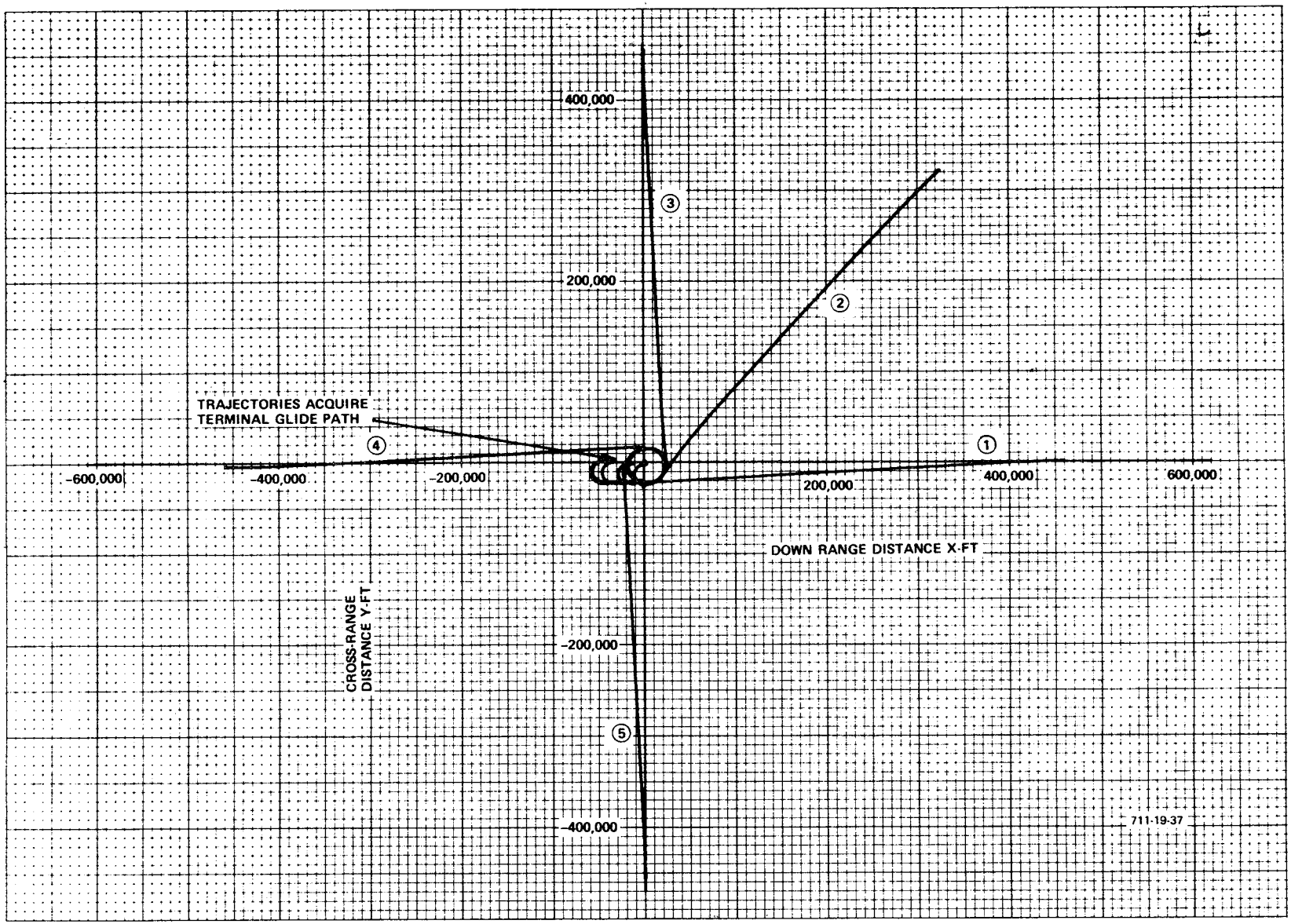

Figure 3-39
HCR Terminal Energy Management Steering (Horizontal View)
for Terminal Glide Path Acquisition for Various Headings

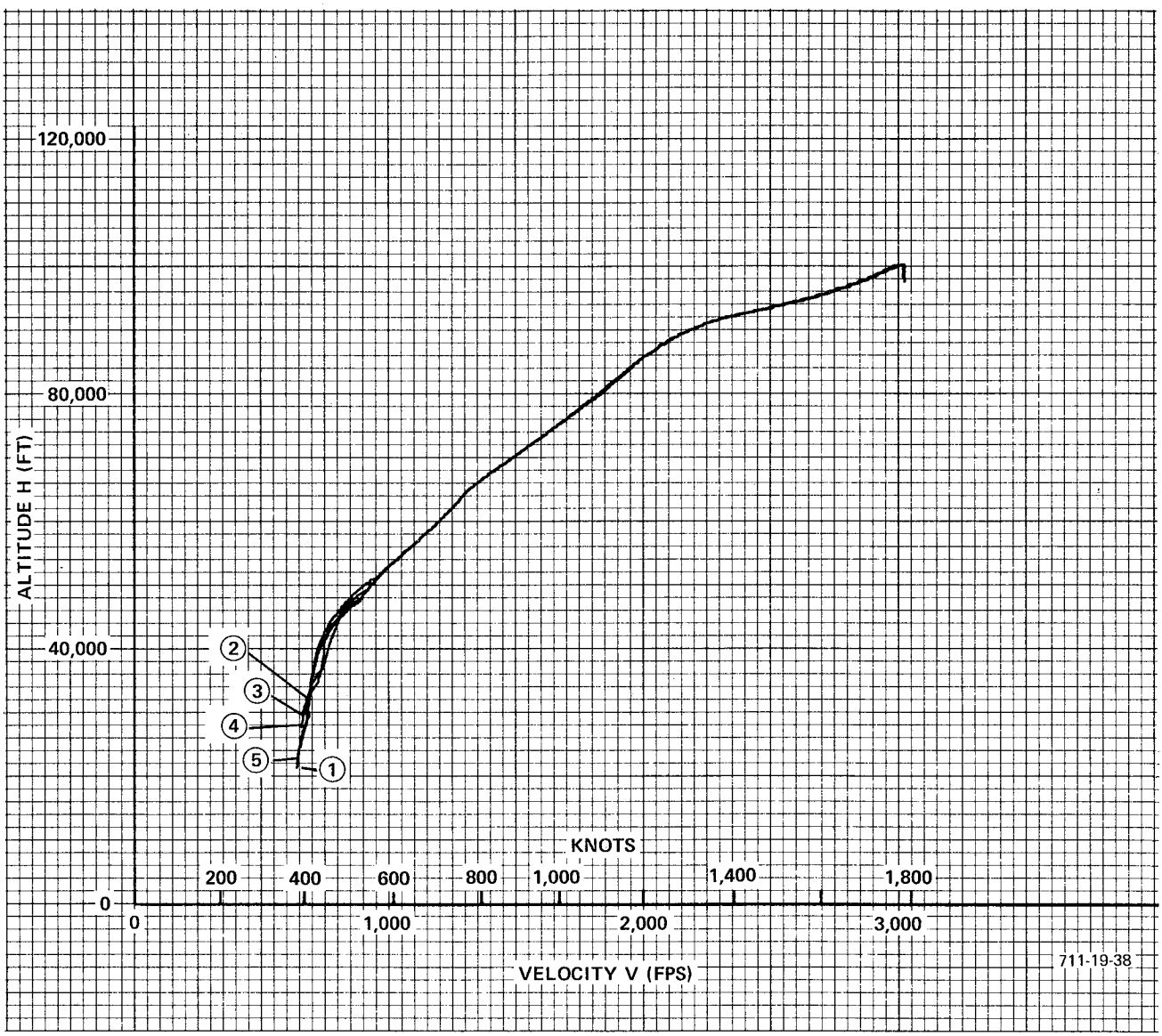

Figure 3-40
HCR Terminal Energy Management Steering
(Velocity Histories) for Terminal Glide Path
Acquisition for Various Headings

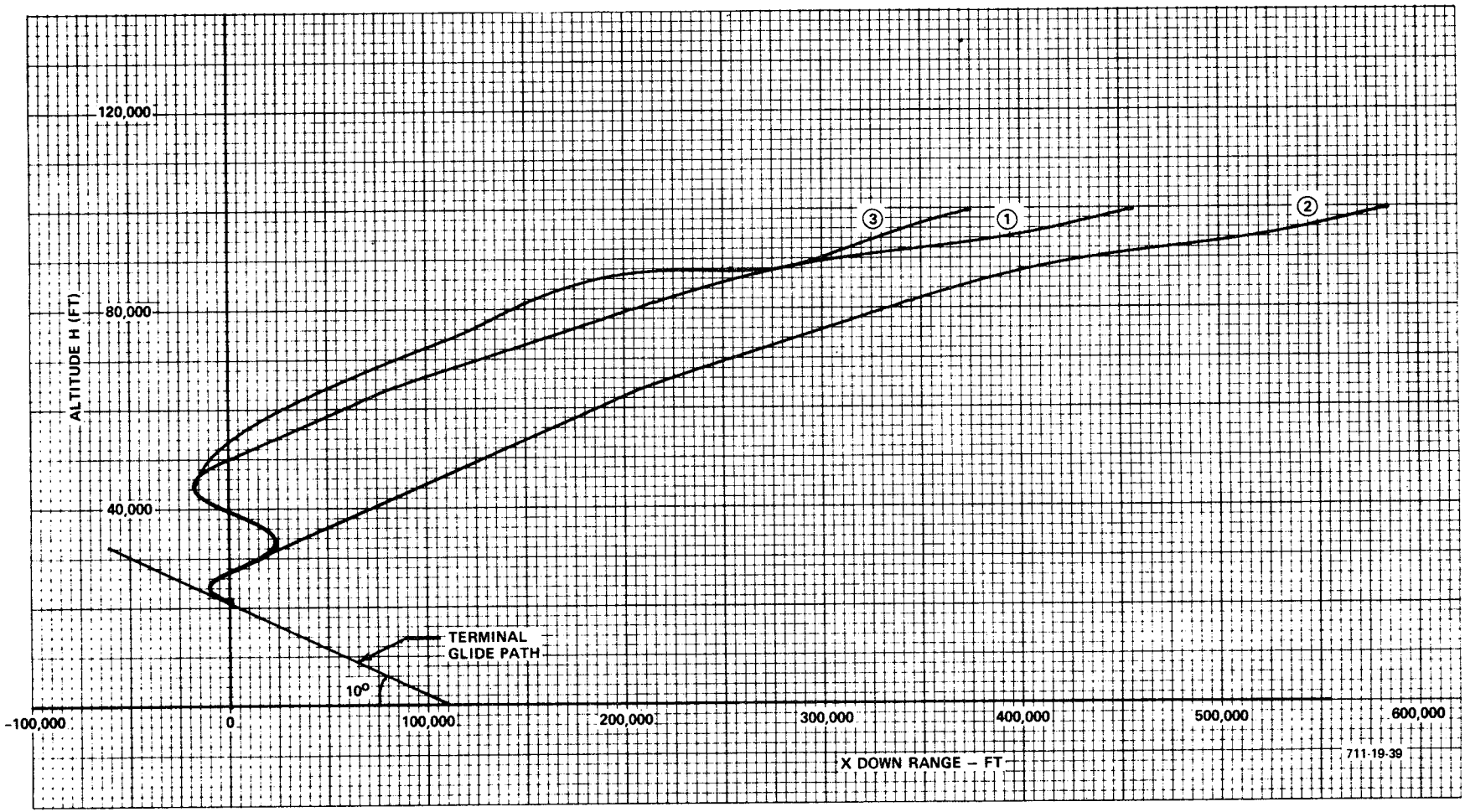

Figure 3-41
HCR Terminal Energy Management Steering (Vertical View)
for Terminal Glide Path Acquisition for Initial Range Errors

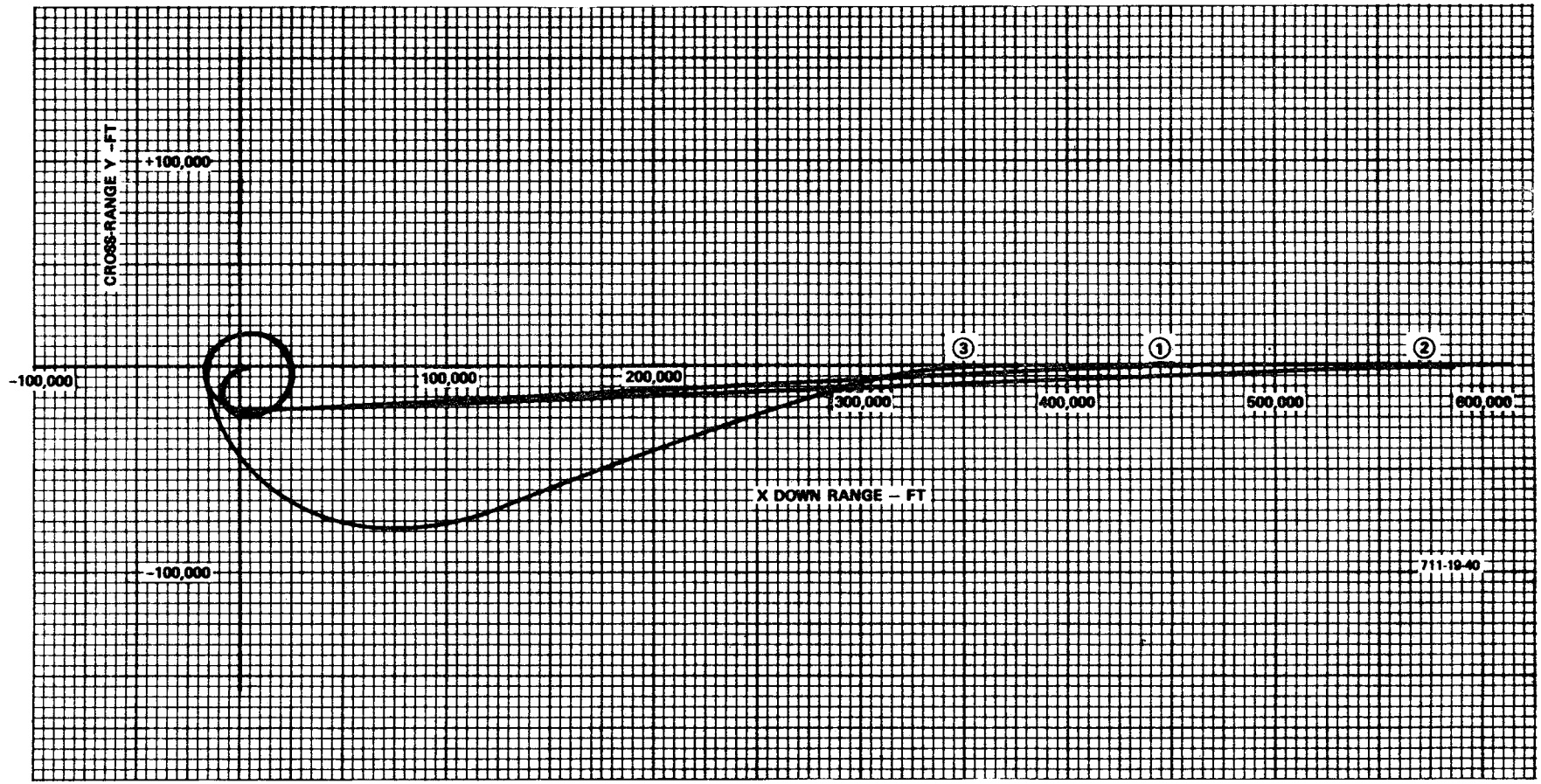

Figure 3-42
HCR Terminal Energy Management Steering (Horizontal View)
for Terminal Glide Path Acquisition for Initial Range Errors

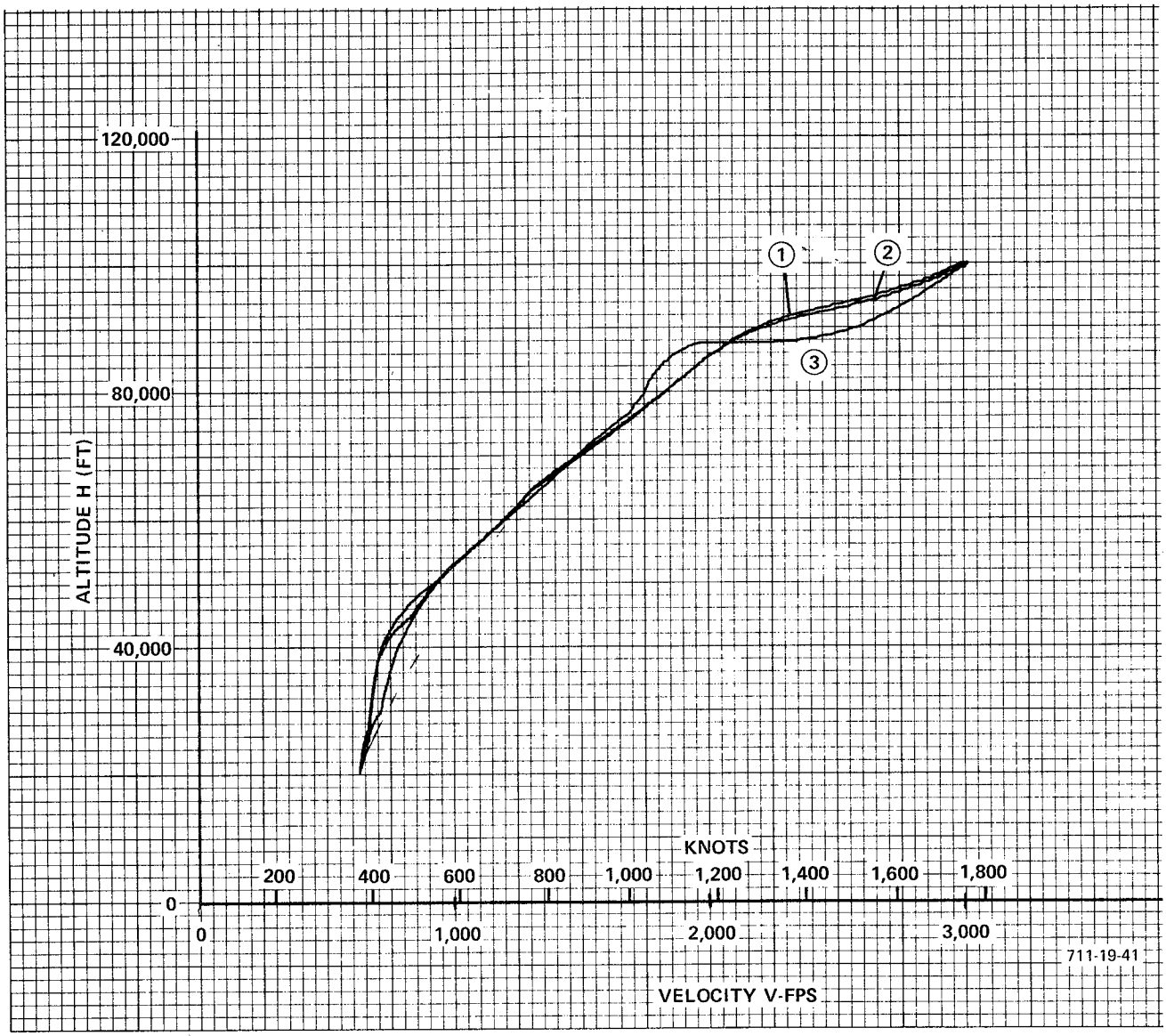

Figure 3-43
HCR Terminal Energy Management Steering
(Velocity Histories) for Terminal Glide Path
Acquisition for Initial Range Errors

r_o and spiral clockwise. Trajectory (1) reaches the first decision point ($\psi = \psi_R + \pi$) and has sufficient altitude to fly a complete turn on the r_o radius. The second time ($\psi_R + \pi$) is reached, the altitude margin for one more turn is not available. No altitude correction was required for acquisition of the terminal glide path, so a 180 degree turn on the circle of radius $r_o/2$ is commanded. Trajectory (2) did not have sufficient altitude for a complete turn when $\psi = \psi_R + \pi$ was first reached. It therefore maintained that heading until the proper altitude for the 180 degree turn on the $r_o/2$ circle was reached. As seen on Figures 3-38 and 3-39, all trajectories terminated on the terminal glide path and terminal lateral path.

Figures 3-41, 3-42, and 3-43 illustrate performance where range errors are presnet. Trajectory (1) is the same as (1) in the previous figures. Trajectory (3) is an excess energy case. To accommodate this overshoot condition, the target circle radius is initially increased to 100,000 feet [per Equations (3-97) and (3-98)]. The increased distance flown in steering to a tangetial intercept of this large circle dissipates the excess energy, and eventually the target cicle radius reduces to r_o. The vehicle eventually flies tangent to the r_o circle.

Trajectory (2) is a low energy case representing an approach from the undershoot limit. It reaches the terminal glide path without turning on the r_o circle, but makes its final turn on the $r_o/2$ circle.

9. High Altitude Energy Management Concepts for Low Cross-Range Vehicles

a. Description of Energy Management Technique

The high altitude energy management of the low cross-range, straight wing vehicle involves acquistion of the vehicle at 100,000 feet in the high angle of attack configuration, steering the vehicle to a suitable transition point, control through transition, and steering the vehicle to the 20,000-foot low key point. Pretransition maneuvering involves use of angle of attack modulation within a limited range of trimmable angles of attack and heading control to guide the vehicle to a suitable transition point, and to arrive at that point at the correct altitude velocity and heading. Suitable transition points

are those points from which the transition can be accomplished so that the 20,000-foot low key point can be achieved with the vehicle arriving at the 20,000-foot point aligned with the terminal lateral and glide paths at the proper velocity. For the purpose of setting up the windows it was assumed that transition will be accomplished at a constant heading (zero bank angle). It should be noted that turning is possible during the latter part of the transition maneuver and can result in an increased window size. Also energy management is possible during the period between completion of transition and the 20,000-foot low key point. This capability has been reserved to handle off-nominal transition maneuvers and hence is not reflected in the acquisition window size.

Vertical and horizontal views of the high altitude guidance problem for cases where the aircraft heading is the same as the runway heading are shown in Figure 3-44. Energy management is provided by adjusting angle of attack and heading to guide the vehicle to the transition area heading toward the transition aiming point. To accomplish this an energy error term is developed based on energy error from the nominal path. The vertical profile in Figure 3-44 shows the small range control available with angle of attack modulation. The guidance system stores the nominal $\alpha = 60°$ trajectory along with corresponding nominal velocities in look-up tables. Off nominal energy is calculated as follows:

$$\Delta E_p = W [h - C_1 (D_K)] \tag{3-102}$$

$$\Delta E_{KE} = \frac{WV}{g} [V - C_2(D_K)] \tag{3-103}$$

where $C_1 (D_K)$ and $C_2 (D_K)$ are stored tables of nominal altitude versus range and velocity versus range. Note that D_K is the range (distance) to the transition aiming point identified in Figure 3-44.

Longitudinal correction for off-nominal energy is accomplished through angle of attack modulation as follows:

$$\alpha_c = \alpha_o + C_E \cdot \Delta E_p + C_K \Delta E_{KE} \tag{3-104}$$

where

α_c = commanded angle of attack

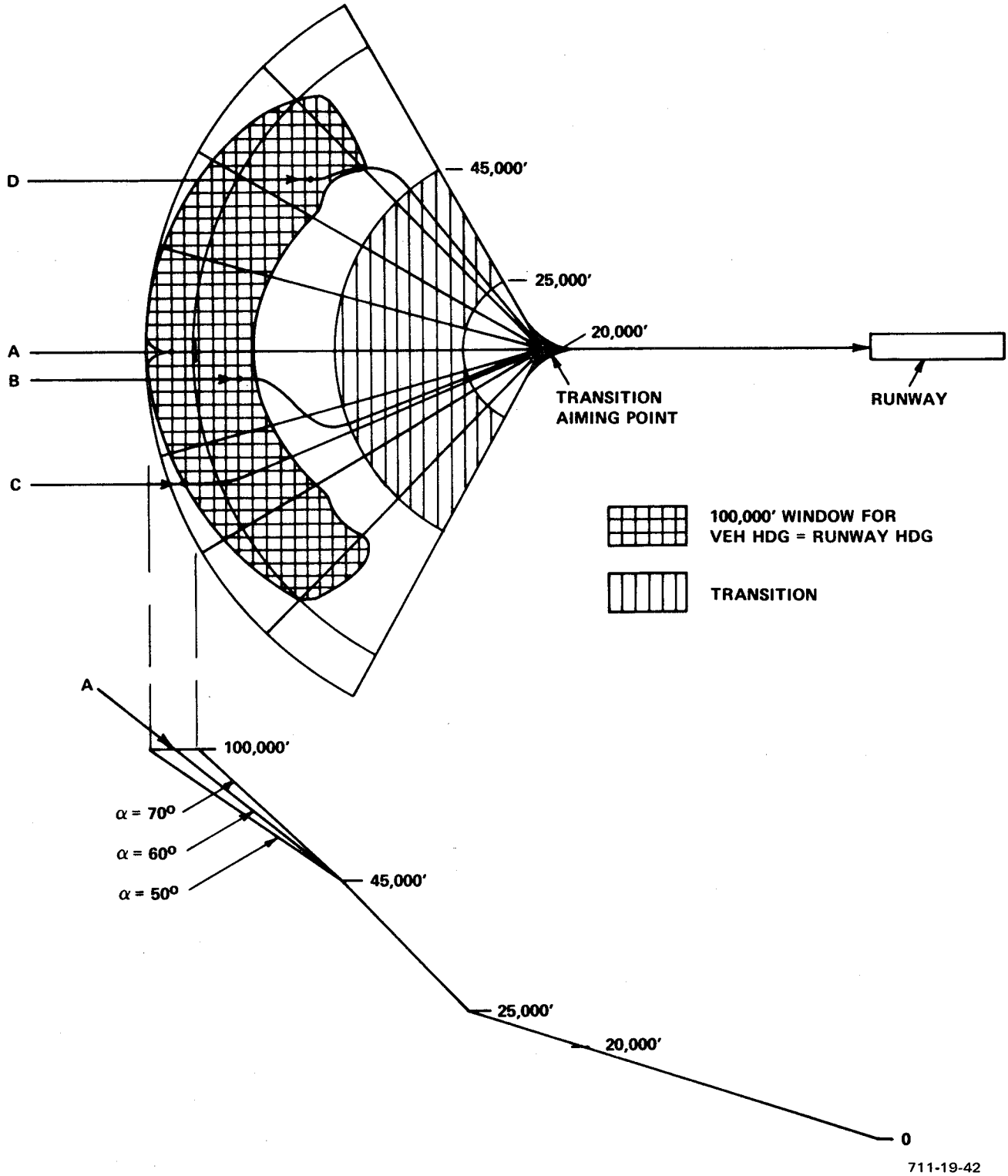

Figure 3-44
Low Cross-Range Vehicle 100,000 Foot Terminal Guidance

α_o = angle of attack for nominal trajectory

C_E and C_K are gain constants

Lateral corrections are useful for excess energy conditions only and involve steering away from the transition aiming point to lengthen the path to the transition initiation point. As the excess energy is dissipated the heading is changed to aim the vehicle to the transition aiming point. The energy correction path for trajectory B of Figure 3-44 is shown in Figure 3-45.

Referring to Figure 3-45

ψ_{RW} = runway heading

ψ_1 = bearing of the vehicle with respect to the transition aiming point

ψ_V = vehicle (velocity vector) heading

The commanded vehicle heading is the heading required to aim the vehicle to the transition aiming point plus the energy error as follows:

$$\psi_{COM} = \psi_1 + \Delta\psi_E \text{ if } \psi_V > \psi_1 \tag{3-105}$$

$$\psi_{COM} = \psi_1 - \Delta\psi_E \text{ if } \psi_V < \psi_1 \tag{3-106}$$

$\Delta\psi_E$ is always positive for excess energy and zero for low energy conditions. As the excess energy is dissipated, the $\Delta\psi_E$ term approaches zero and the vehicle heading is shifted until the vehicle is headed to the transition aiming point.

b. Energy Management Capability Using Longitudinal and Lateral Control

To establish the tables for C_1 (D_K) and C_2 (D_K), trajectories at various angles of attack were simulated. These trajectories are shown in Figures 3-46 and 3-47. Although a trajectory for $\alpha = 40°$ is included, this condition was not used because it is beyond the range of aerodynamically trimmable angles of attack for the straight wing vehicles that were studied. The angle of attack range from 50 to 70 degrees is used for longitudinal energy management.

The lateral correction capability is dependent on the turning capability of the vehicle. Using 45 degrees as the maximum bank angle, maximum bank

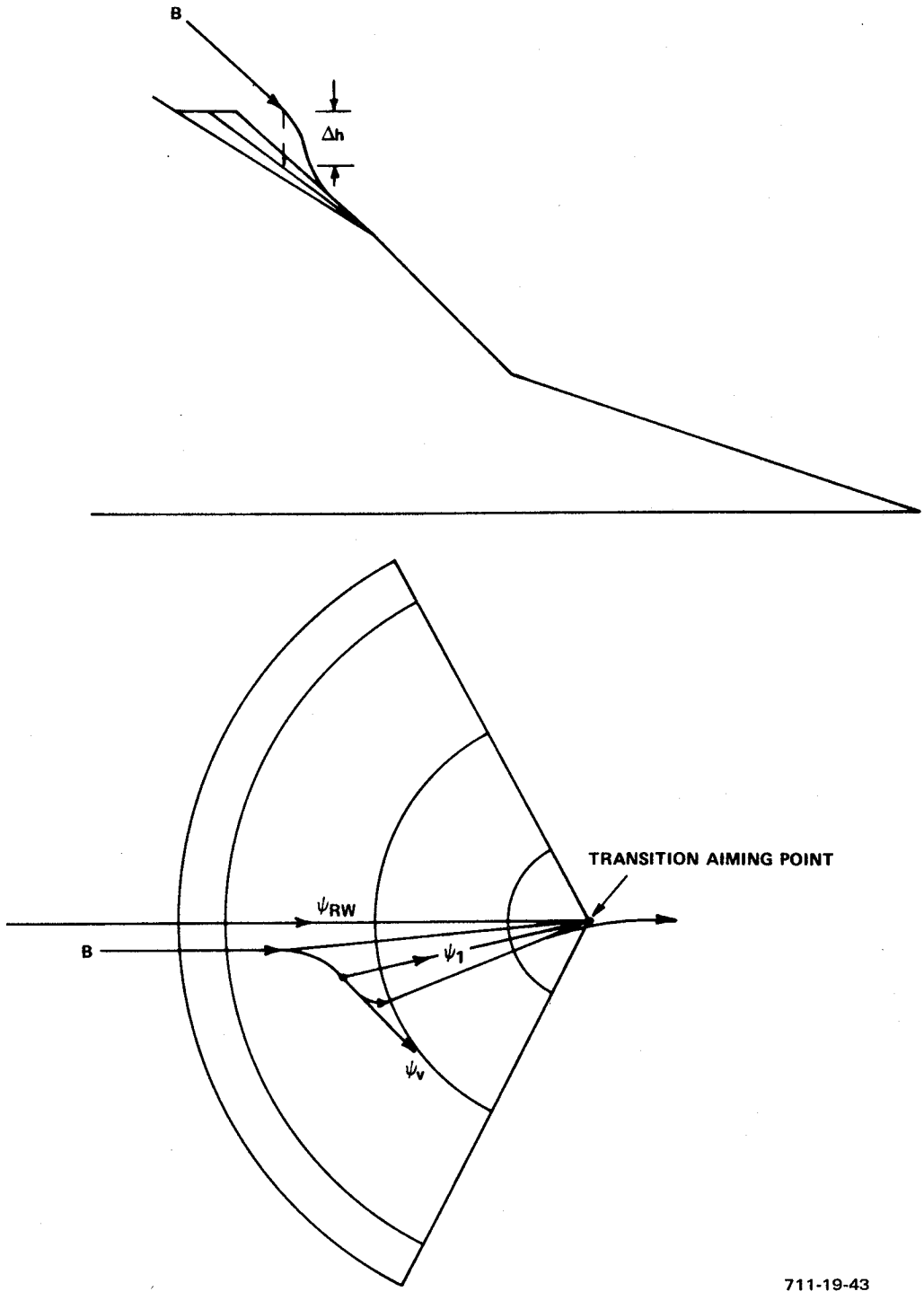

Figure 3-45
Low Cross-Range Vehicle High Altitude Energy Management Geometry

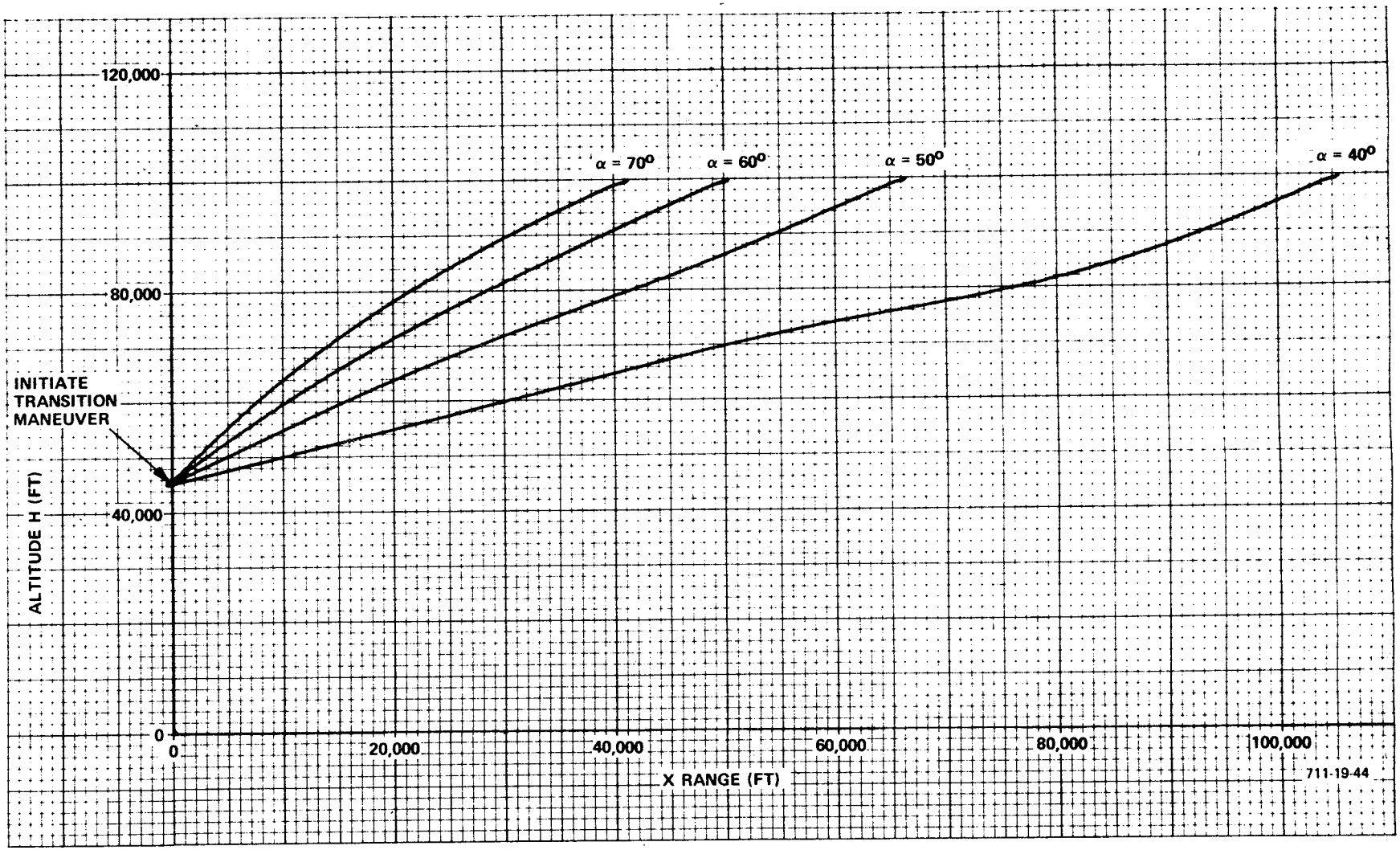

Figure 3-46
LCR Vehicle Range Adjustment
for Straight-In Approach

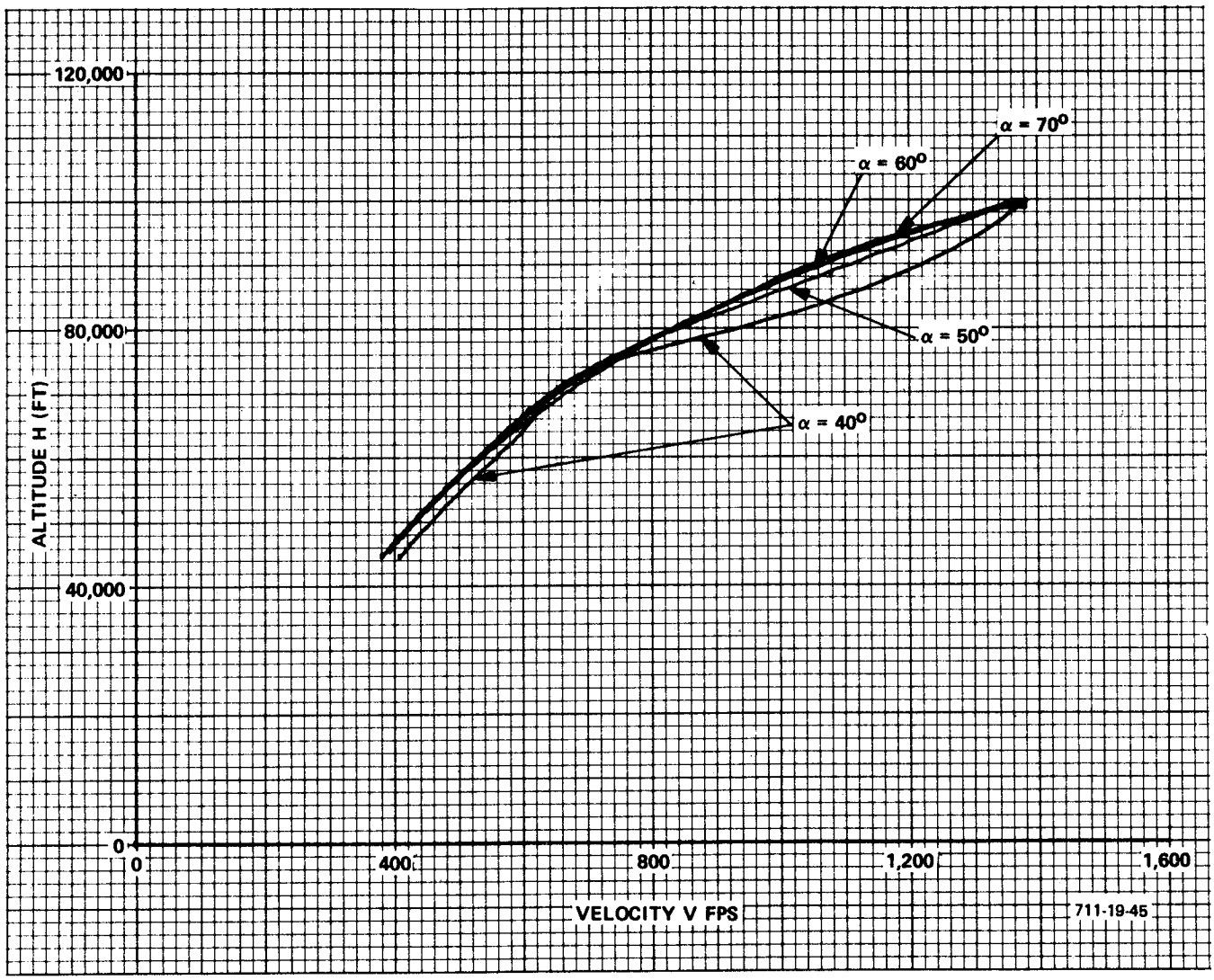

Figure 3-47
LCR Vehicle Velocity History
for Straight-In Approach

angle trajectories were run for the nominal and end limit angles of attack. These trajectories along with straight-in runs are presented in Figures 3-48, 3-49 and 3-50, horizontal, vertical, and velocity profiles, respectively. These runs show the maximum maneuvering capability of the vehicle and the correction possible with angle of attack control. Detailed data on the 100,000 feet window and the various ramifications of high altitude energy management for LCR vehicles will be covered in the later section on the specific design and performance of the McDonnell Douglas straight wing guidance and control system.

10. High Altitude Reaction Control System for LCR Vehicles

a. Pitch Control (Blended Aerodynamics and Reaction Controls)

In the pretransition flight regime where dynamic pressure (Q) varies between about 25 to 40 pounds per square foot, the primary method of flight control is the reaction rocket system. In the case of pitch control, a fixed elevator (or horizontal stabilizer) position will not provide the trim condition for a fixed angle of attack. Hence, it is necessary to modulate elevator position to maintain the reference angle of attack. (A fixed elevator would necessitate enormously increased reaction rocket fuel consumption.) The reaction control system used in this study employs a simple threshold switch with hysteresis. The firing threshold is ϵ_o and the hysteresis is h. The control law is:

$$(\alpha_E + 2q \frac{\tau S}{\tau S + 1}) (\frac{1}{0.2S + 1}) = \epsilon \qquad (3\text{-}107)$$

where

ϵ = input to threshold switch,

q = body axis pitch rate

τ = 4 seconds

and

$$\alpha_E = (\alpha - \alpha_{command}) \qquad (3\text{-}108)$$

The nominal threshold ϵ_o has been set at 0.5 degrees (or 0.125 deg/sec pitch rate) and 20 percent hysteresis (or h = 0.1 degree) has been used to improve limit cycle characteristics. The 0.2 second lag time constant acts as a

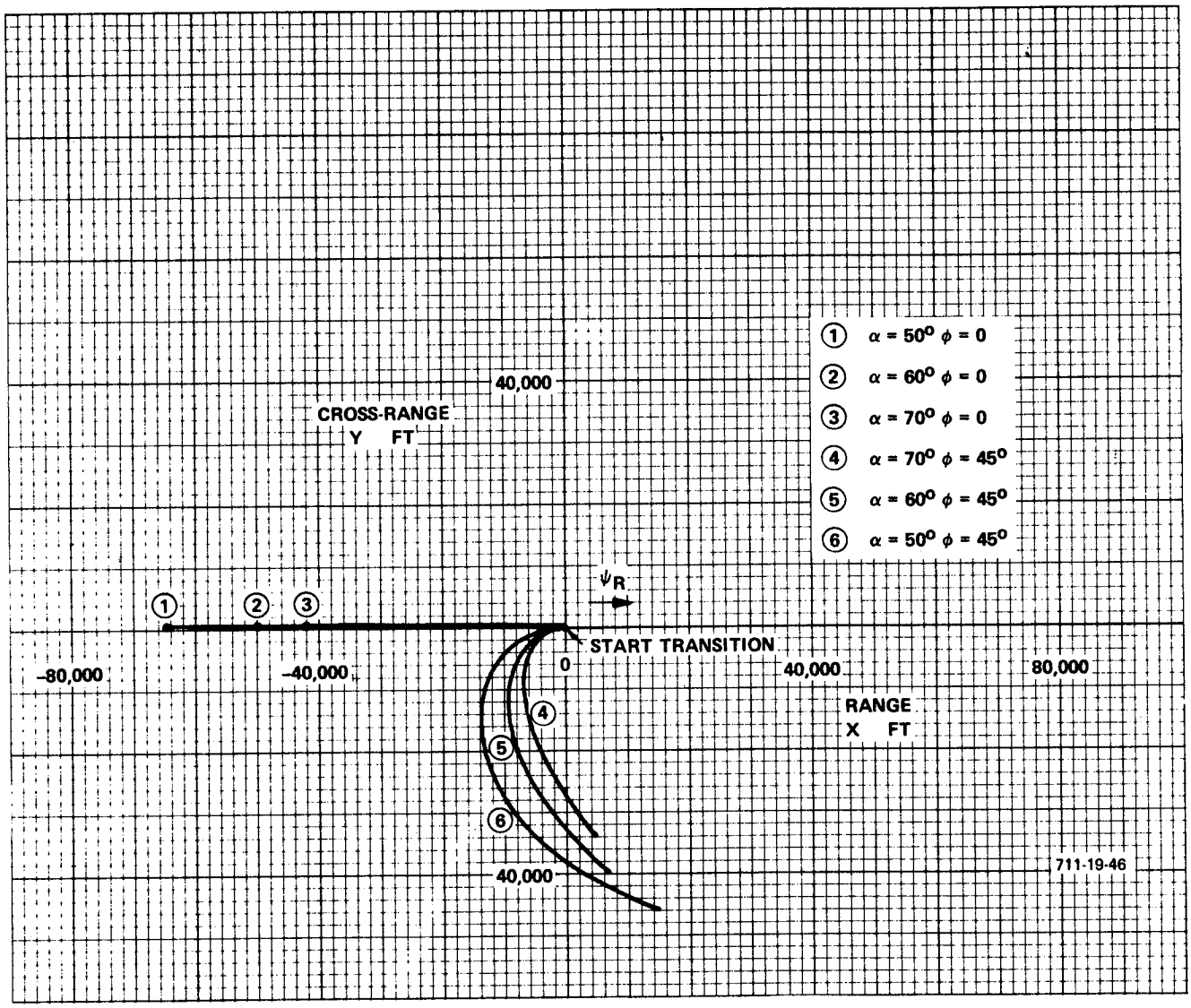

Figure 3-48
LCR Vehicle Pretransition Maneuvering
Capability (Horizontal View)

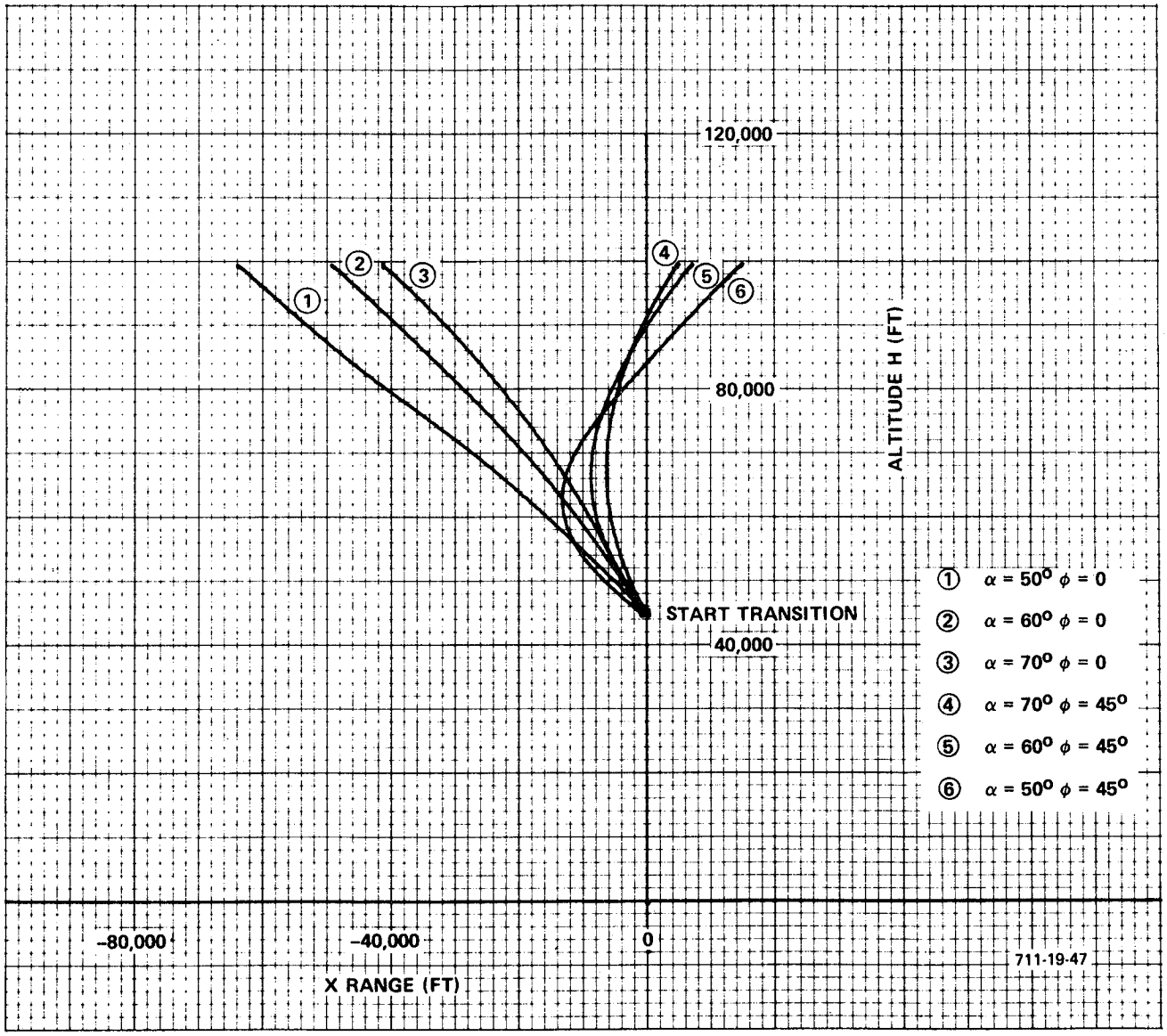

Figure 3-49
LCR Vehicle Pretransition Maneuvering
Capability (Vertical View)

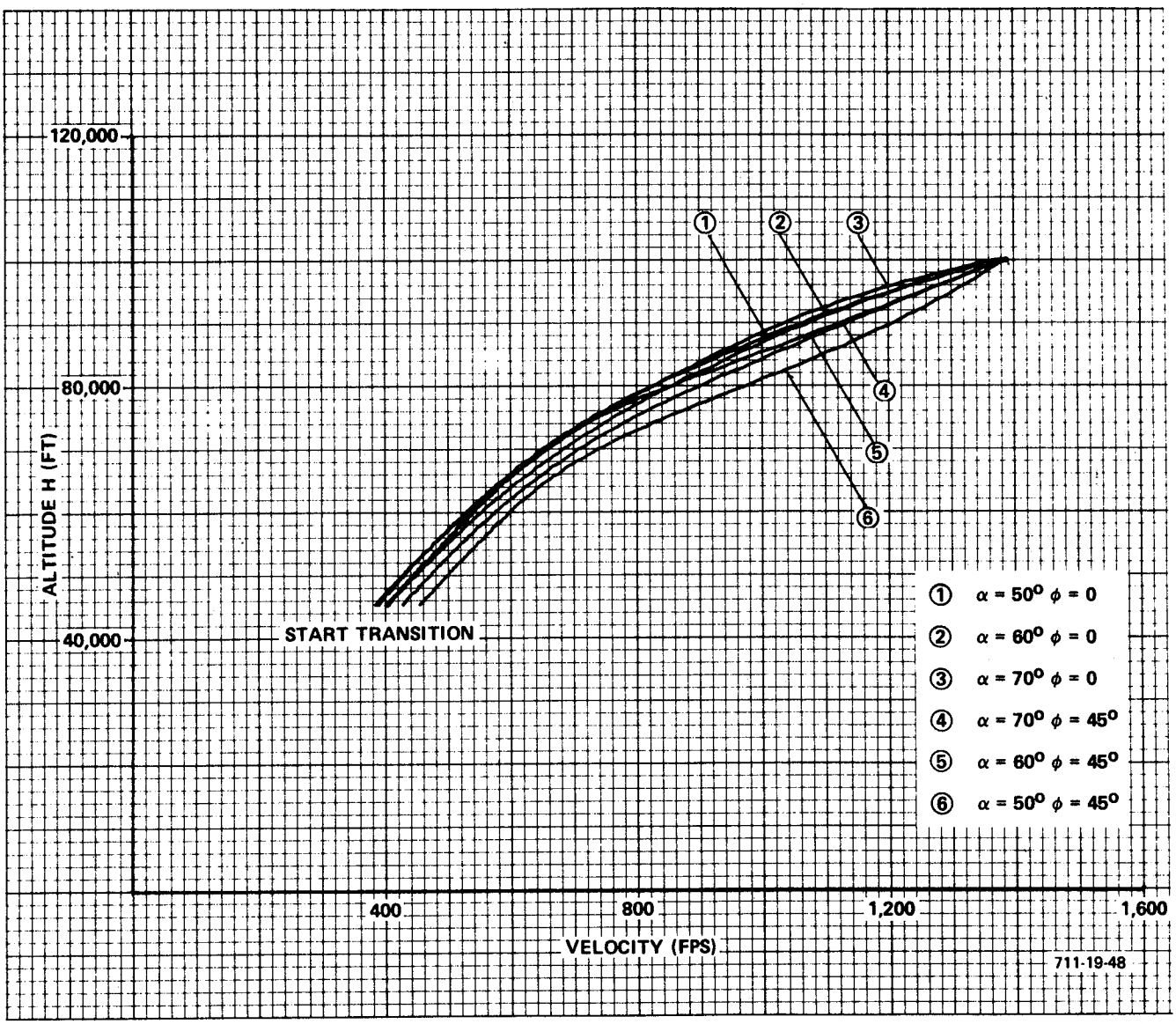

Figure 3-50
LCR Vehicle Pretransition Maneuvering
Capability (Altitude-Velocity Profile)

noise filter and also helps improve limit cycle performance by allowing the response to coast further into the deadzone. These parameters gave reasonable performance with the MDAC-2 low cross-range vehicle whose nominal pitch axis reaction rockets give a 0.86 deg/sec^2 torque-to-inertia ratio.

The simultaneous closure of an aerodynamic control loop is needed to minimize reaction control fuel consumption. The control law for the aerodynamics loop is:

$$\delta_E = \left[\alpha_E \left(1 + \frac{0.1}{S}\right) + 2q \frac{\tau S}{\tau S + 1}\right] k_\alpha + \delta_{E_\alpha} (\alpha, M) \qquad (3\text{-}109)$$

where

τ = 4 seconds

α_E is the angle of attack error as defined previously

δ_{E_α} (α, M) is the predicted trim value of the elevator for the desired α reference at the existing Mach number. (This value requires a stored table and interpolation in the autopilot computer.)

The gain k_α is varied with dynamic pressure in accordance with the following linear Q schedule:

$$k_\alpha = 5.0 \text{ for } Q < 50 \text{ pounds/ft}^2$$

$$k_\alpha = 5.0 - 0.0225\ (Q - 50) \text{ for } 250 \geq Q \geq 50$$

$$k_\alpha = 0.5 \text{ for } Q > 250$$

The gain at the low Q conditions is impractically high and in a final design this type of gain could be achieved only with considerable roll-off type filters and additional limiters on the total error signal.

b. Lateral Directional Reaction Control System

In the high angle of attack, low Q flight regime from 100,000 feet to transition (45,000 feet), the LCR vehicle's lateral directional stability problems are severe. The reaction control moments are adequate to overpower the

the aerodynamic forces. Within the Reaction Control System (RCS) deadzones, however, a hard limit cycle reflecting the vehicle instability is expected. A study optimizing RCS performance for this phase of flight was performed. The performance criteria were qualitative but can be summarized as follows:

- Roll angle limit cycle activity below about 1 degree and 1 deg/sec
- Sideslip constrained to below about 4 degrees during rolling maneuvers. (Vehicle must roll about velocity vector, and thus requires combined body axis roll and yaw moments.)
- Control deadzones selected on the basis of fuel minimization if practical.

The resulting control system was used in the simulations of the high altitude energy management system for the LCR vehicle.

The lateral-directional control equations are:

a) Roll Error = E_ϕ

$$E_\phi = \left\{ \left[p\, H_1(s) - p_{com} \right] \frac{K_p}{K_\phi} + (\phi - \phi_{com}) \cos \alpha \right\} K_\phi \qquad (3\text{-}110)$$

p = Roll Rate

$H_1(s)$ = Stabilization filter

p_{com} = Feedforward roll rate command

ϕ = Roll Euler angle, ideally about a frame aligned with the velocity vector. If α does not get much larger than 60 degrees, however, the measurement of ϕ in a local vertical frame will give acceptable results in the control equation.

$$M_\phi' = C_1\left(\frac{E_\phi}{\tau_1 S + 1}\right) = \text{Roll RCS moment command to threshold switch} \qquad (3\text{-}111)$$

$C_1 = 0$ if $Q \geq Q_o$

$C_1 = 1.0$ if $Q < Q_o$

The roll jets fire and produce a moment M_ϕ when a threshold ϵ_ϕ is exceeded. The threshold switch includes 20 percent hysteresis.

M_ϕ is positive (⊕ roll acceleration) if $M_\phi' - \epsilon_\phi > 0$

M_ϕ is negative (⊖ roll acceleration) if $M_\phi' - \epsilon_\phi < 0$

b) Yaw Error = E_ψ

$$E_\psi = \left[rH_2(s) - \frac{g}{V}\sin\phi_c\cos\theta + (\phi - \phi_c)\sin\alpha\right]K_r\,\frac{\tau_2 S}{\tau_2 S + 1} - K_\beta\,\beta \qquad (3\text{-}112)$$

where:

$H_2(s)$ = Stabilization filter

τ_2 = Washout time constant

K_r = Yaw rate gain

K_β = Sideslip gain (β = sideslip angle computed from INS measurement)

$$M_\psi' = C_2\left(\frac{E_\psi}{\tau_3 S + 1}\right) = \text{Yaw RCS moment command to threshold switch} \qquad (3\text{-}113)$$

When the threshold switch with breakout value ϵ_ψ -20 percent hysteresis is exceeded, positive and negative moments M_ψ are produced in the same manner as for the roll RCS.

The gains used were:

Q_o = 100 lb/ft^2

K_ϕ = 2.0

K_p/K_ϕ = 4.0

K_r = 4.0

K_β = 1.0

$\tau_1 = \tau_3$ = 0.2 sec

τ_2 = 10.0 sec

ϵ_ϕ = roll RCS threshold = 1.0 deg/sec or for K_p/K_ϕ = 4.0 and K_ϕ = 2.0, ϵ_ϕ at the threshold switch = 8.0 units

ϵ_ψ = Yaw RCS threshold = 1.0 deg/sec or for K_r = 4.0, ϵ_ψ at the threshold switch = 4.0 units

M_ϕ = 3.3 deg/sec^2 and M_ψ = 2.0 deg/sec^2

Performance in the presence of a step sideslip disturbance is shown in Figure 3-51. The limit cycle has a period of about 3 seconds. The roll amplitude is less than 1/2 degree peak. Varying the deadzone from the nominal 1.0 deg/sec through a range of 0.5 to 4.0 showed no consistent influence on fuel consumption.

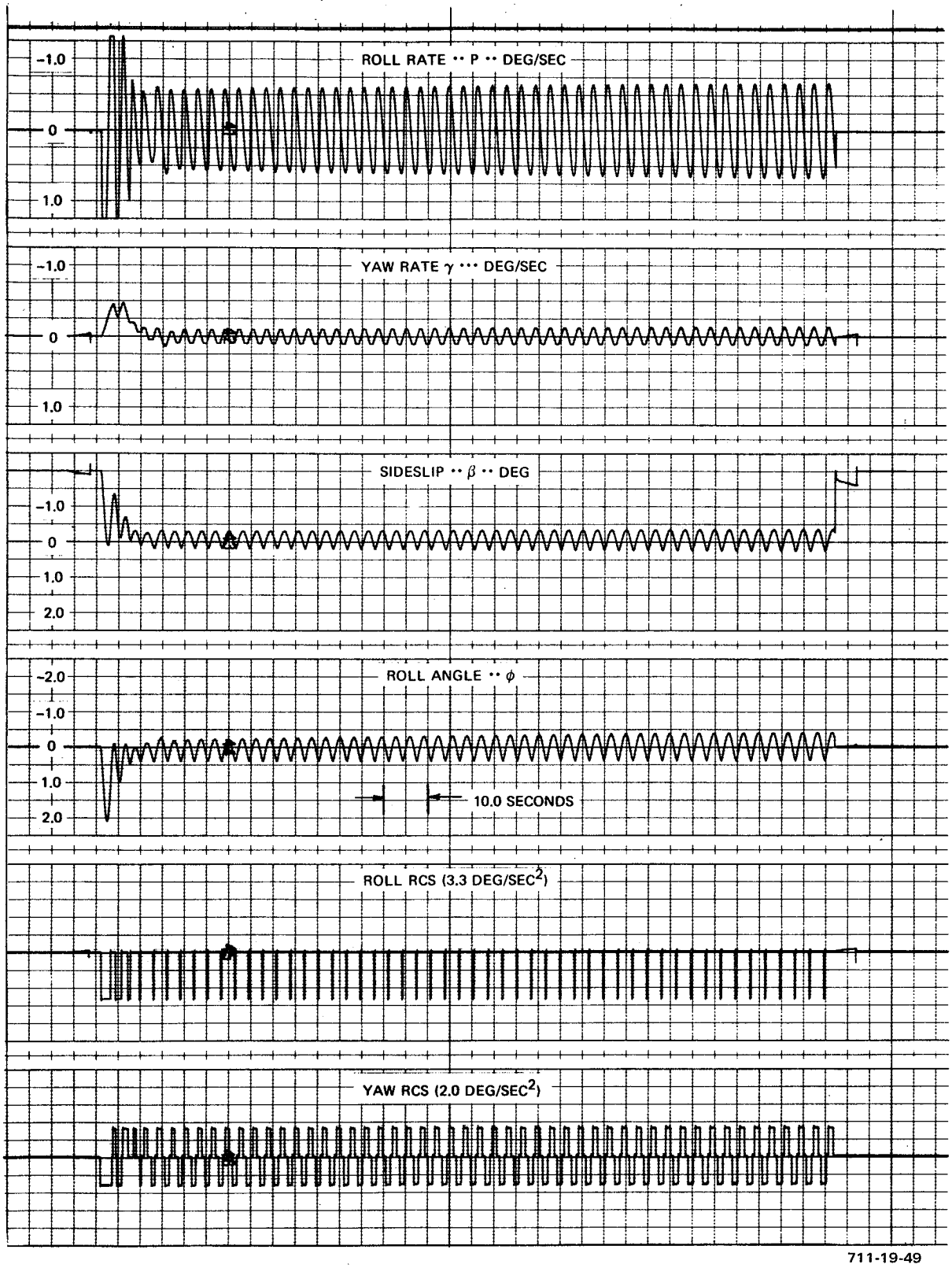

Figure 3-51
Lateral-Directional RCS Limit Cycle Performance
(h = 50,000 feet, Q = 35 pound/feet^2, and α = 60 degrees)

11. Transition Maneuver For LCR Vehicles

a. The Pitch-Over Maneuver

The transition from the high angle of attack ($\alpha \approx 60°$) reentry configuration to the low angle of attack, subsonic flight configuration involves a number of critical maneuvers. The nature of the problem may be summarized as follows:

- The reduction in α must be achieved rapidly lest the build-up in dynamic pressure Q occurs before α is sufficiently low to ensure reasonable lateral-directional aerodynamic control.

- The very high pitching rates required to achieve the desired fast transition makes surface rate limits of the elevator actuator a critical parameter in the prevention of large overshoots.

- The initial flight path angle is very steep (about -60 degrees). The nose down maneuver tends to increase the dive angle. (The steeper the dive angle, the more severe the pull-out problem.)

- Pull-out must be accomplished with angles of attack restricted to $\alpha \approx 10$ degree maximum where wing stall begins. The lateral-directional dynamics become erratic at α's greater than about 8 degrees. Hence a practical limit for the pull-out α is about 8 degrees maximum.

- Pull-out can not begin until sufficient speed (and dynamic pressure Q) increase has occurred to allow aerodynamic maneuvering. If speed builds up too rapidly Q limits can be exceeded. Also, if speed builds up too rapidly and α is not properly adjusted, normal load factor limits can be exceeded.

- Underlying all the α, Q, and load factor constraints is the desire to pull-out at the highest possible altitude so that additional altitude is available for range adjustments needed to acquire the terminal glide path.

The problem was studied first using data for the MSC 245 vehicle and then for the preliminary version of McDonnell Douglas' LCR design designated

MDAC-1. Initial simulations were done with a 3-degree of freedom, large disturbance, non-linear representation of the LCR vehicles. The 3-degree of freedom simplification is justified because the guidance scheme does not permit any bank maneuvers during transition (wing-level is commanded 3000 feet prior to reaching the transition altitude). For the 3-degree of freedom studies, a transition altitude of 40,000 feet was used. Subsequently, the guidance system was designed to start transition at 45,000 feet. Simulation results for complete trajectories starting at altitudes of 100,000 feet and including the transition maneuver (for the updated LCR configuration designated MDAC-2) are given in the section covering performance evaluation for LCR vehicles.

The initial conditions for the 3-degree of freedom parametric study of transition techniques are:

Altitude	h = 40,000 feet
Velocity	V = 310 feet per second
Dynamic Pressure	Q = 28 pounds per foot^2
Angle of Attack	α = 60 degrees
Pitch Angle	θ = 0 degree
Flight Path Angle	γ = -60 degrees
Elevator deflection	δ_E = -20.5 degrees
Weight	W = 209,000 pounds
Inertia (Longitudinal)	I_y = 10.76 x 10^6 slug-feet^2

In this study the pitch maneuver that brought α from 60 degrees to below 10 degrees was performed with elevator control only. In the final system design the initial maneuver is performed with a combination of elevator and reaction controls. The proper procedure for performing this maneuver is to set the reaction control system's α reference (Equation 3-107) to the desired new value (6.5°, for example). Simultaneously, the elevator deflection is programmed from approximately -20° to +20°. The surface rate limit may prevent the elevator from reaching the commanded value before the next programmed sequence. When α reaches within about 10 degrees of the commanded value, the elevator position command [δ_{E_α} (α, M) of Equation 3-109], and closed loop elevator control [per Equation (3-109)] is initiated. Note that the α error integral term of

Equation (3-109) is held at zero until α error approaches zero. With these control equations, α overshoot problems are eliminated and the criticality of the elevator rate limit is minimized.

With the control equations used in the 3-degree of freedom parametric study of the transition maneuver, the δ_{E_α} (α, M) predicted trim position was not used in the elevator control law. Also, the pitch reaction controls were not used and the maneuver was performed with elevator control only. Since the trim elevator position had to be generated by the closed loop control law, an α error (overshoot) was necessary and the integral part of the control equation was the only means of converging that error toward zero. The elevator program was very critical from the standpoint of timing and rate capability in order to minimize the α overshoot. That program was optimized and successful transition maneuvers were performed. The area of interest regarding the parametric study of the transition is not the initial pitch maneuver but the characteristics of the resultant dive and pull-out after the new angle of attack has been attained.

b. The Pull-Out

Figure 3-52 illustrates the critical altitude history of the initial pitch maneuver. It shows that the desired α is reached at about 39,000 feet after a loss of about 1000 feet of altitude, and the steady state α is reached after a loss of about 3000 feet. The objective of the rapid nose down maneuver was to traverse the $40° > \alpha > 10°$ region before dynamic pressures and hence the associated aerodynamic forces and moments reach values that start to overcome the capability of the lateral-directional RCS. As seen in Figure 3-53, the dynamic pressure is below 50 pounds/ft^2 when α goes below 10 degrees. Thus the erratic and unstable lateral-directional aerodynamics in the $40° > \alpha > 10°$ region are experienced for only about 2.5 seconds (Figure 3-54) and only when Q's are below 50 pounds/ft^2.

The dynamic pressure history shown in Figure 3-53 and the normal acceleration and velocity histories in Figure 3-55 demonstrate the key points of the transition problem. The vehicle must pick up speed and hence dynamic pressure in order to develop the normal acceleration needed to pull-out of the dive. The transition philosophy demonstrated here is to hold the maximum permissible value of α and hence the maximum lift coefficient and then wait for

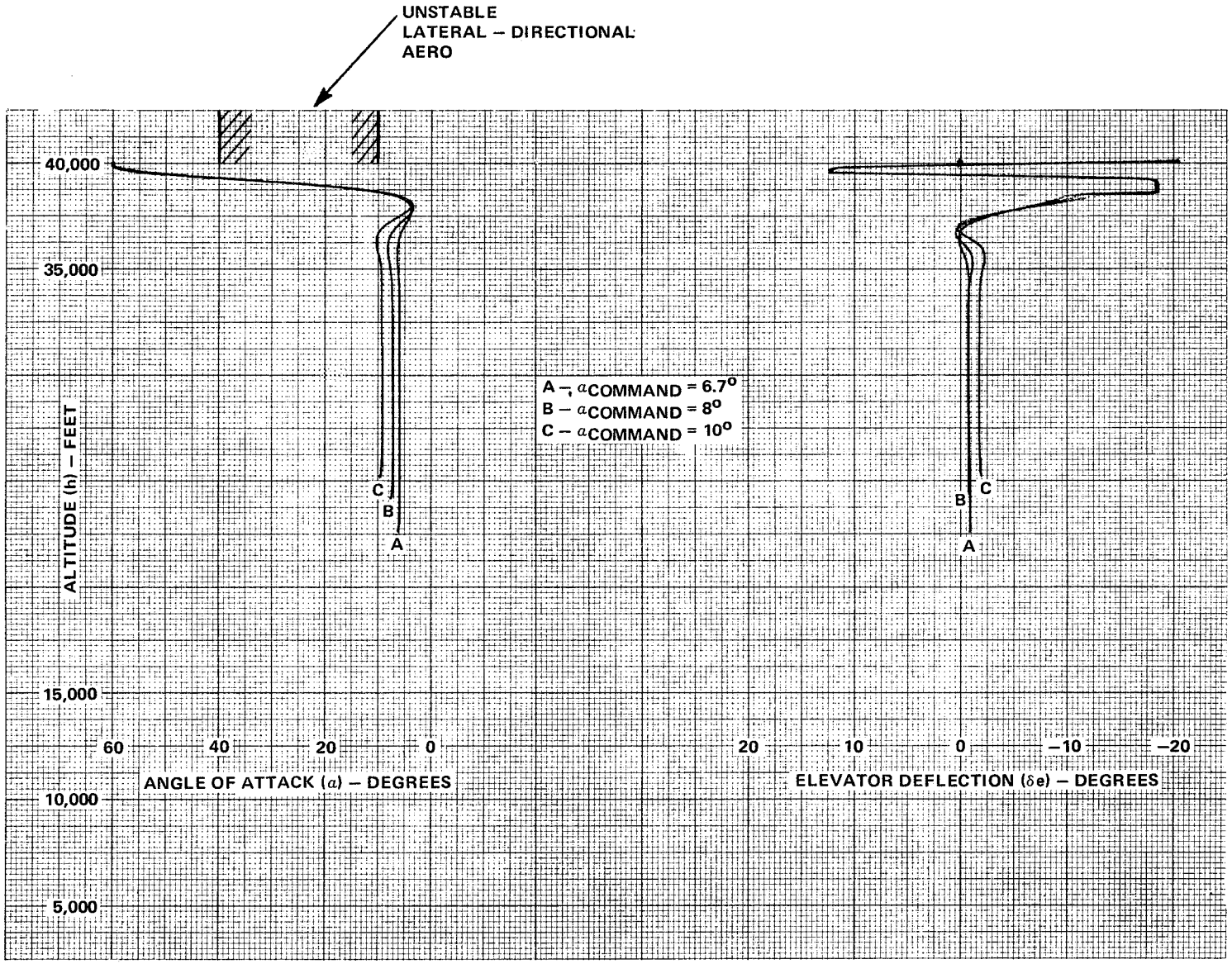

Figure 3-52
LCR Orbiter, Transition Maneuver and Pull-Out,
Angle of Attack and Elevator versus Altitude

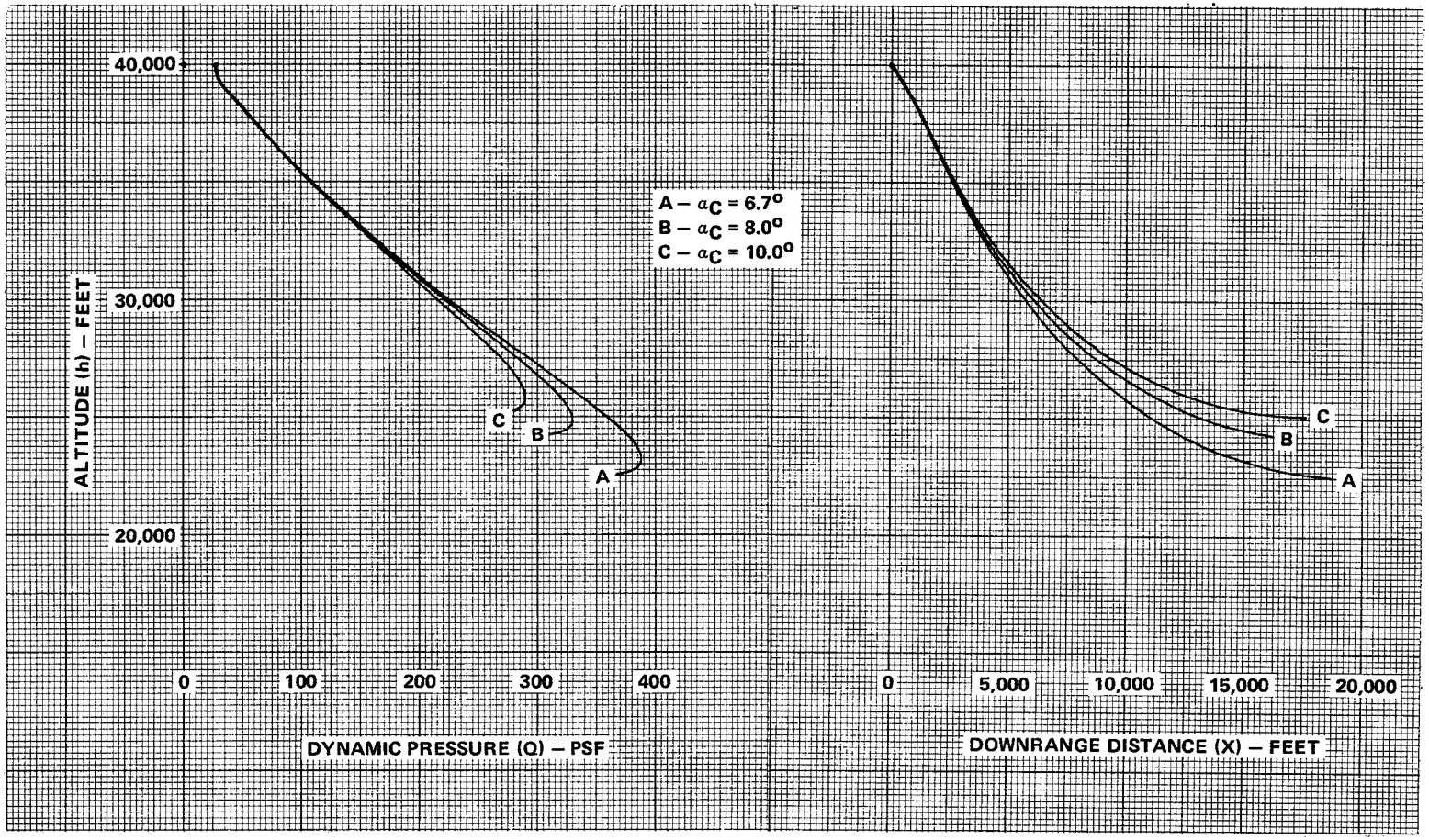

Figure 3-53
LCR Orbiter, Transition Maneuver and Pull-Out, Dynamic Pressure and Down-Range Distance versus Altitude

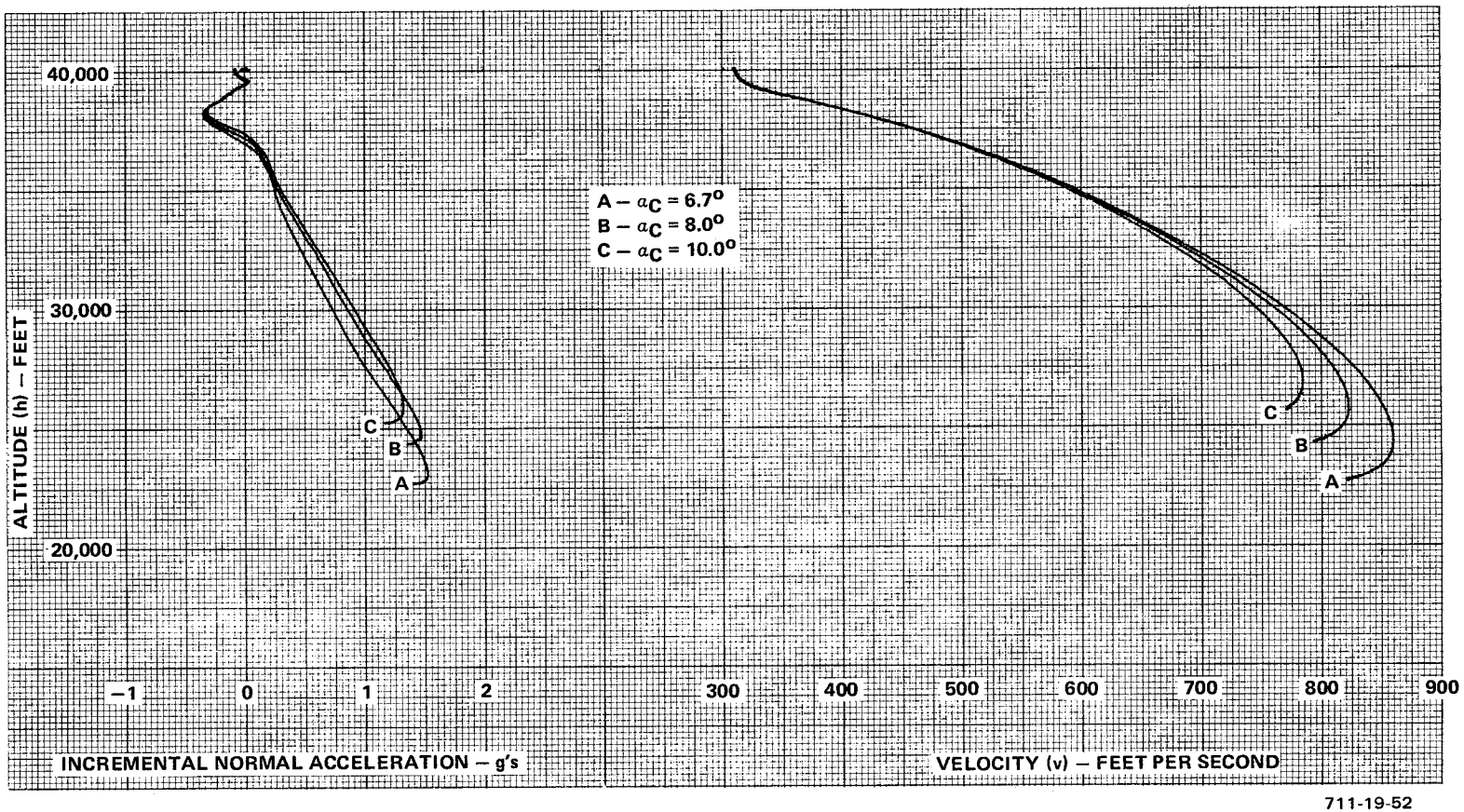

Figure 3-54
LCR Orbiter, Transition Maneuver and Pull-Out,
Normal Acceleration and Velocity versus Altitude

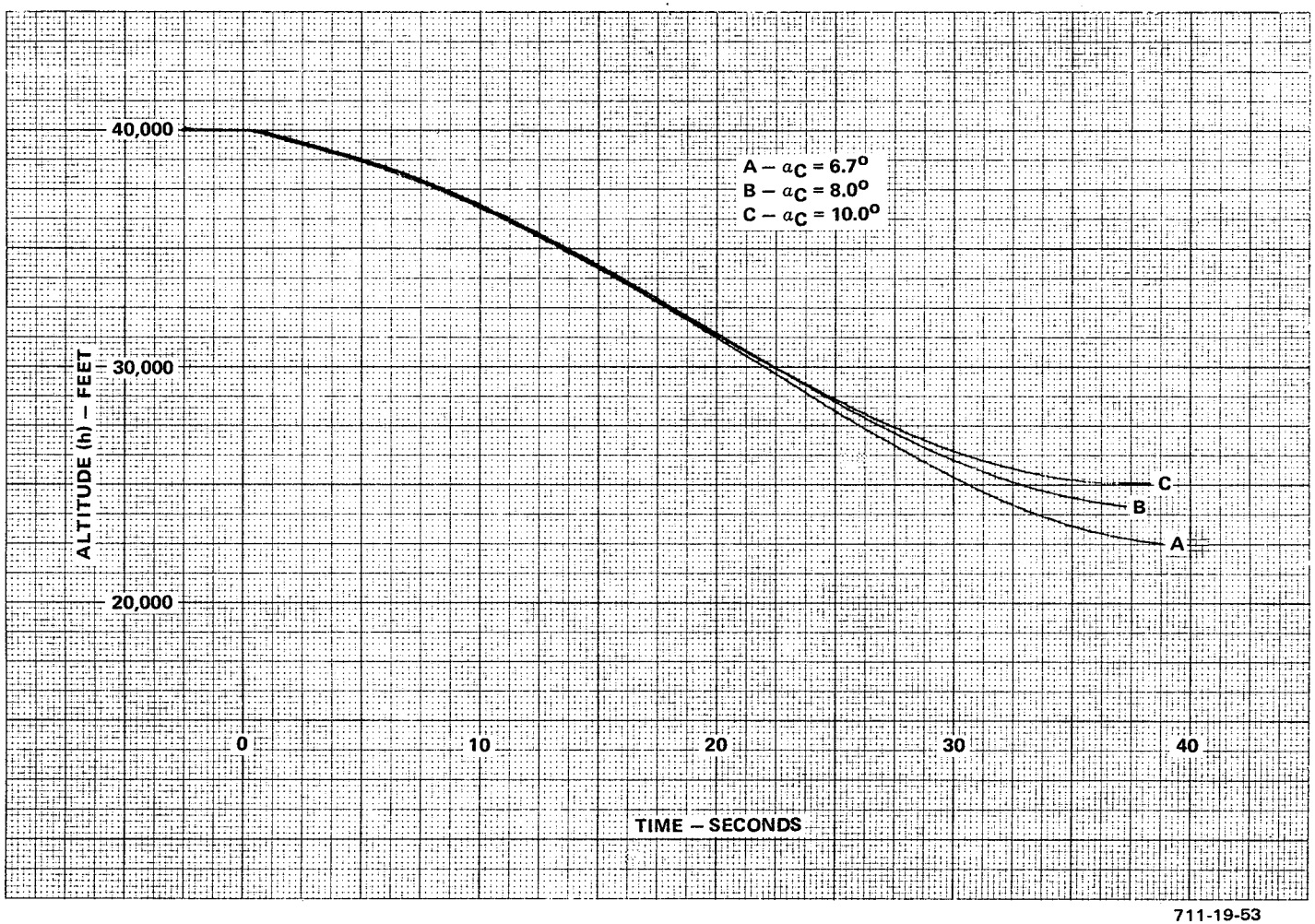

Figure 3-55
LCR Orbiter, Transition Maneuver, Altitude versus Time

the pull-out g's to develop. The maximum α is determined by the lateral-directional stability considerations. Figures 3-53 and 3-55 demonstrate that the higher α's result in higher altitude pull-outs. The effect of α increments on pull-out altitude is about 1000 feet higher altitude per degree α. Note that pull-out is defined as the point that $\alpha = -12°$, the nominal final approach angle for the vehicle. It requires about 14,000 to 17,000 feet of altitude loss and approximately 38 seconds to accomplish the transition. In every case the pull-out reached the normal acceleration limit for the vehicle (1.5g's incremental).

c. Potential Problems and α Measurement

There are some interesting implications in Figures 3-53 and 3-55. The pull-out required a speed build-up and for the three cases shown, the velocity reached between 780 and 860 feet per second. In each case, the Mach number rose above 0.7 above 30,000 feet. This speed increase was obtained with all aero models used for LCR vehicles. It would appear that the drag data in the Mach 0.7 and above region may be optimistic for a blunt nose, straight wing vehicle of the LCR class investigated thus far. A vehicle of this configuration should have encountered severe buffet before Mach 0.8 can be reached. If the drag is, in fact, higher than that used in the simulations, then transition pull-out could be delayed by a considerable amount. Pull-out above 20,000 feet is desired so that the additional altitude can be used for energy management in acquiring the terminal approach glide path. It will be shown in the subsequent discussions of the LCR vehicle's high altitude energy management window that almost all of the range adjustment below 100,000 feet must be obtained after transition. If transitions at higher altitudes are required (above 50,000 feet) then the lateral-directional α stability margin will have to be traded off against buffet problems.

Another interesting problem associated with the transition maneuver is the α measurement requirement. In this work we have assumed that α will be computed from vertical speed, forward speed, pitch and roll attitude. For the zero bank angle condition of the transition maneuver, and in zero sideslip flight,

$$\alpha = \theta - \sin^{-1} \frac{\dot{h}}{V_T} \qquad (3\text{-}114)$$

where V_T is true airspeed and $\dot{h}$ is vertical speed obtained from a blend of inertial $\ddot{h}$ and air data derived $\dot{h}$. Also the h measurement for initiating the transition would be obtained from air data computation. Two problems are apparent. First, can the vehicle in its high α flight configuration deploy an adequate probe or other device for static and total pressure sensing? Second, how elaborate a computation would be needed to establish accurate values of α in the true roll and sideslip environment? Reference 28 develops the required equations for airborne computation of angle of attack under all conditions of sideslip and roll angle. In general, it appears feasible to make the zero β (sideslip) assumption and compute α from the equation

$$\frac{\dot{h}}{V_T} = \cos \alpha \sin \theta - \sin \alpha \cos \theta \cos \phi \qquad (3\text{-}115)$$

Then, all that is required is a platform for θ and ϕ and pitot-static probe for $\dot{h}$ and V. Since the usual procedure for computing V_T involves Mach computation (from pitot and static pressure) and true air temperature, (measured with a temperature probe) there may be a problem regarding the temperature probe in the high α flight configuration. Some other scheme that uses inertial velocity with updates based on strategic measurements of air data may be needed to provide an estimate of V_T and thereby account for the wind component in V_T.

Two main conclusions can be drawn from the parametric transition study. They are:

- Accurate α measurement is essential during the pull-out
- When the transition maneuver is started at h = 40,000 feet, the g limits for the MDAC-1 vehicle (1.5g incremental) are reached for reasonable values of α. The transition maneuver should be initiated at higher altitudes and h = 40,000 feet should be viewed as the lower altitude limit for start of transition.

D. MANUAL CONTROL CONCEPTS

1. Discussion of Control and Display Concepts and Requirements

The system developed and evaluated in this study has three modes of operation. They are:

- Fully Automatic
- Augmented Manual (with Flight Director)
- Back-up Manual (with Raw Data Displays)

All three modes of operation include the following ground rules:

- Start at 100,000 feet altitude.
- Capture the terminal glide path at 20,000 feet.
- Perform a two-stage flare to touchdown from the high energy terminal glide path.
- Limit bank angle commands to 45° (on manual modes there is no restriction although flight director cues observe this limit).
- Limit operations to front side of L/D curve (except during final flare).

At this point, it should be made very clear that the present study scope is not concerned with recommending operational concepts regarding primary and back-up modes of control. Such recommendations must be totally dependent upon the avionics system philosophy and the specific design details of that avionics system. Indeed, as discussed previously in the section on Operational Considerations, if the present Fail-Op, Fail-Op, Fail-Safe guidelines for space shuttle vehicle avionics prevail, the concept of back-up systems is not tenable. The flight director mode would use the same computer for steering computations, and the same computer and actuators for control as the automatic mode. The back-up mode would use the same fly-by-wire control computers and actuators and the same computer controlled data transmission systems for displays as was used in the fully automatic mode. These modes cannot be viewed as back-up modes if they use the identical equipment as the primary modes. Consequently, the two manual modes designed and evaluated in this study are presented not as recommended

system concepts for space shuttle vehicles, but rather as techniques which are available for consideration by those who specify space shuttle avionics system requirements.

a. Automatic Mode

The automatic mode is intended as the primary mode for terminal control and landing. The manual modes are available at all times to cope with different failure or emergency situations. The main displays for all modes are an electronic attitude director indicator (EADI) and a map display which was mechanized in the simulator cab from an x-y plotter. Nominal altitude circles are overlayed on the map display to provide an assessment of available energy. Not included in the simulator, but an obvious requirement, is the presentation on the map display of the predicted trajectory (trend vector). Also needed to improve presentation of system assessment and status is a mode annunciation panel which displays information similar to that found on the Approach Progress Annunciators used in present-day aircraft automatic approach and landing systems. With the automatic mode engaged, the vehicle will automatically fly the computed turning trajectory that manages the potential and kinetic energy such that a perfect alignment with the final approach path occurs by the time an altitude of 20,000 feet has been reached. Automatic control down the high energy approach path (steep glide path) continues and the two stage flareout maneuver and decrab maneuvers are executed to complete the automatic landing. The EADI displays the computed steering commands being performed by the automatic system. It also displays a continuously varying performance window, altitude and altitude cues, speed error, flight path angle and the horizon (roll and pitch attitude). Figure 3-56 illustrates the scaling of the performance window during different parts of the landing trajectory.

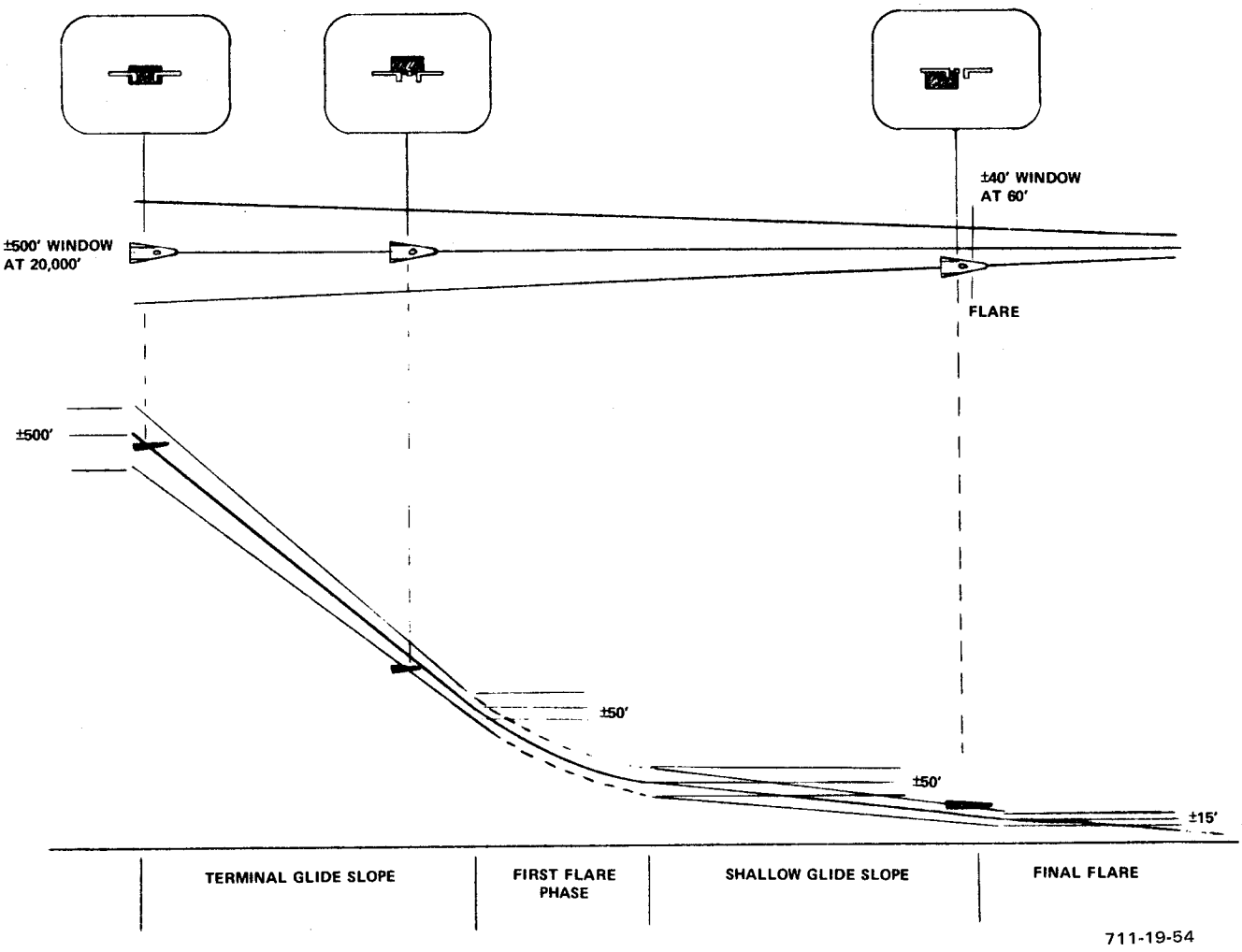

Figure 3-56
Terminal Approach EADI Display
(Performance Window Definition)

b. Augmented Manual (Flight Director) Mode

The flight director guidance laws are essentially the same as those used for the automatic mode (except for the manner in which control law integration is implemented). All control sequences are the same as for the automatic mode. The vehicle is maneuvered with the sidestick controller. The manual augmented control system is a high performance attitude rate command system with attitude hold inherent with release of the stick command. Steering cues are provided for all aspects of flight covering high altitude energy management turns through flareout and decrab. The pitch and roll steering commands are displayed on the EADI. The pilot uses the sidestick controller in the manually augmented mode to follow these commands. Figure 3-57 the EADI display symbology that was used. In addition to the roll and pitch flight director steering bars, the EADI displays roll and pitch attitude, airspeed, altitude, heading, and vertical and lateral path deviation data. Flight path angle and a vertical altitude tape display are also available on the EADI but they were not found useful for the problem being studied. Figure 3-58 shows how the flight director steering commands are generated from the guidance system commands. In the case of roll, the generation of flight director commands is straightforward. The roll commands are lagged and summed with roll attitude. The pilot inserts roll rate commands with the sidestick controller. The command bar centers when the vehicle reaches the bank angle demanded by the guidance equation. In the case of pitch, however, the forward integration in the pitch guidance laws must be removed. Forward path integration is not used in flight directors because small errors result in large commands when the pilot is not continuously and accurately following the command bars. This results in over control and stability problems. To provide the equivalent of integration, a washout of about 15 seconds is used on the sum of the pitch attitude feedback and all open-loop predictive commands.

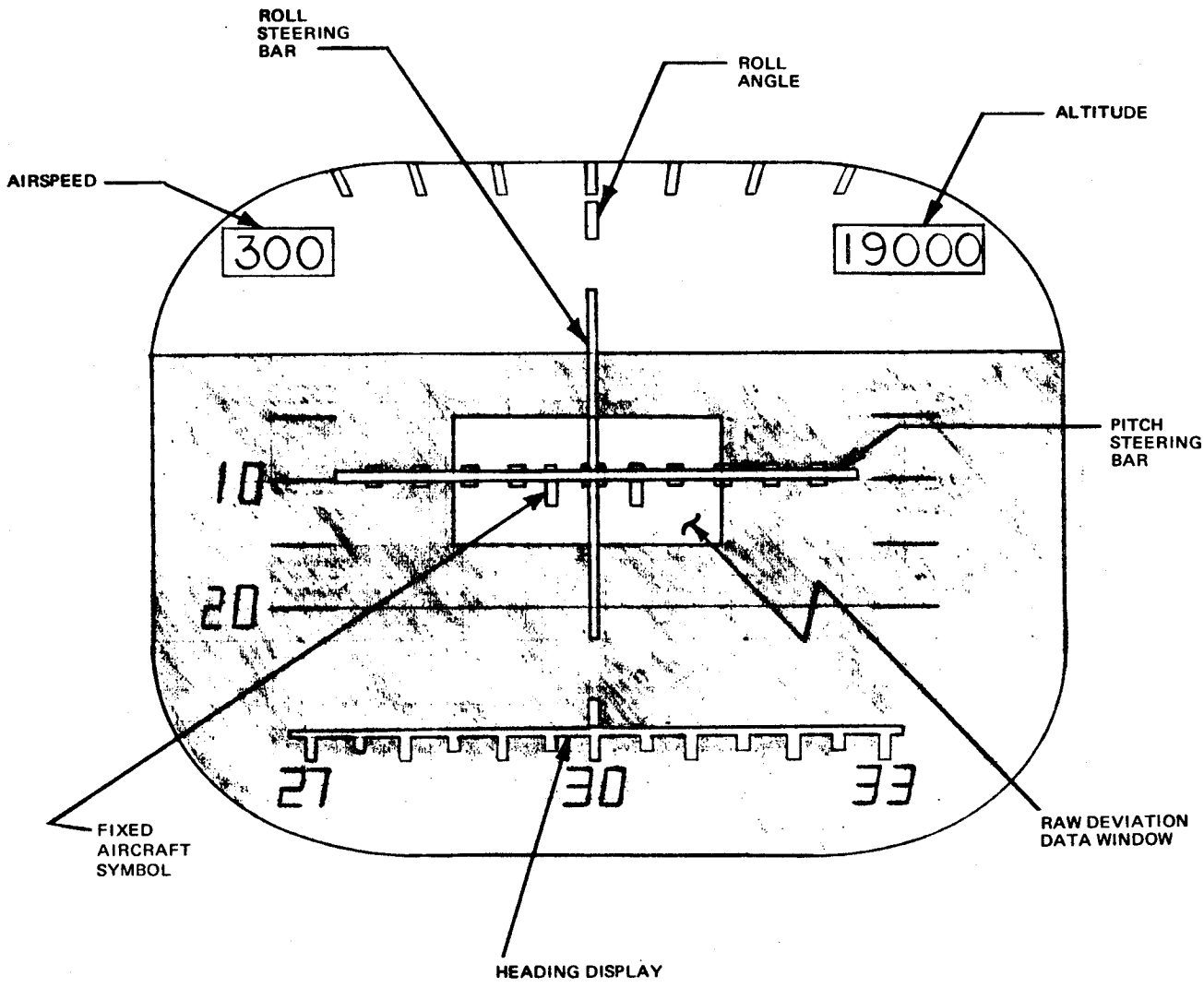

Figure 3-57
Flight Director Presentation

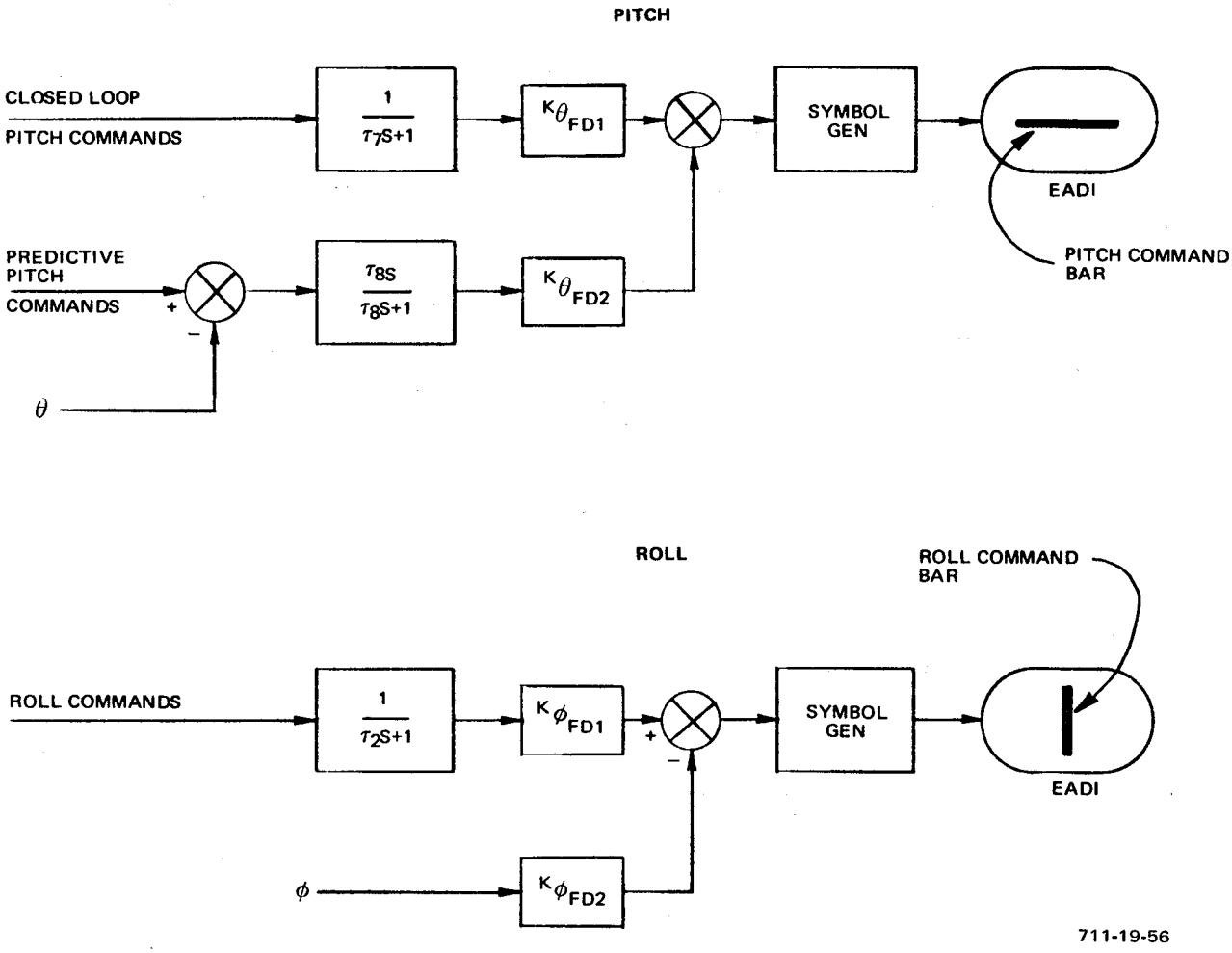

Figure 3-58
Flight Director Steering Command Block Diagram

c. Back-Up Manual Mode (Raw Data Mode)

The concept of a back-up, raw data mode implies the availability of on-board position information that is independent of the airborne computer system. Such a system could be mechanized by locating a scanning beam glide path at the intersection of the steep approach path with the ground and the location of a conventional ILS glide slope and localizer at their usual positions with respect to the runway. The ILS localizer would have to have a slant-angle capability of about 12°. (Conventional ILS localizers are usually specified for 7° angles, although they provide adequate information at elevation angles greater than 7°.) The airborne receivers will provide all of the required guidance information. A direct interface between the receivers and the attitude-director indicator permits presentation of deviation information directly with cross-pointer symbols.

Figure 3-59 illustrates the operation of such a system if the landing is to be made on the instrument runway at Edwards AFB. A GCA technique is used to vector the vehicle into the required turning trajectory that heads toward intersection with an outbound radial from the landing site at Point (B). That radial is a 10° deviation from the localizer. A scanning beam localizer would have sufficient width to provide the required reference signals. The fixed outbound radial is flown until the vehicle intersects the slant plane that is elevated 4° from the 10° glide path. This occurs at Point (C). The EADI uses the pointer on the left side of the display as a turn cue. The horizontal bar represents deviation from the 10° reference path. The turn cue represents deviation from a 14° glide path. When the turn cue is zeroed, the 14° glide path has been penetrated. This cues the start of a procedure turn (190°) that ends on the 240° in-bound localizer and tangent to the 10° glide path (Point (D)).

The pilot flies the raw data glide path and localizer cross-pointer display to either a fixed altitude Point (E) (read on a barometric altimeter) or to a specified deviation from the shallow glide path. This requires switching the raw data reference from the steep glide path receiver to the shallow glide path receiver. The first flare is performed to achieve a tangential intercept

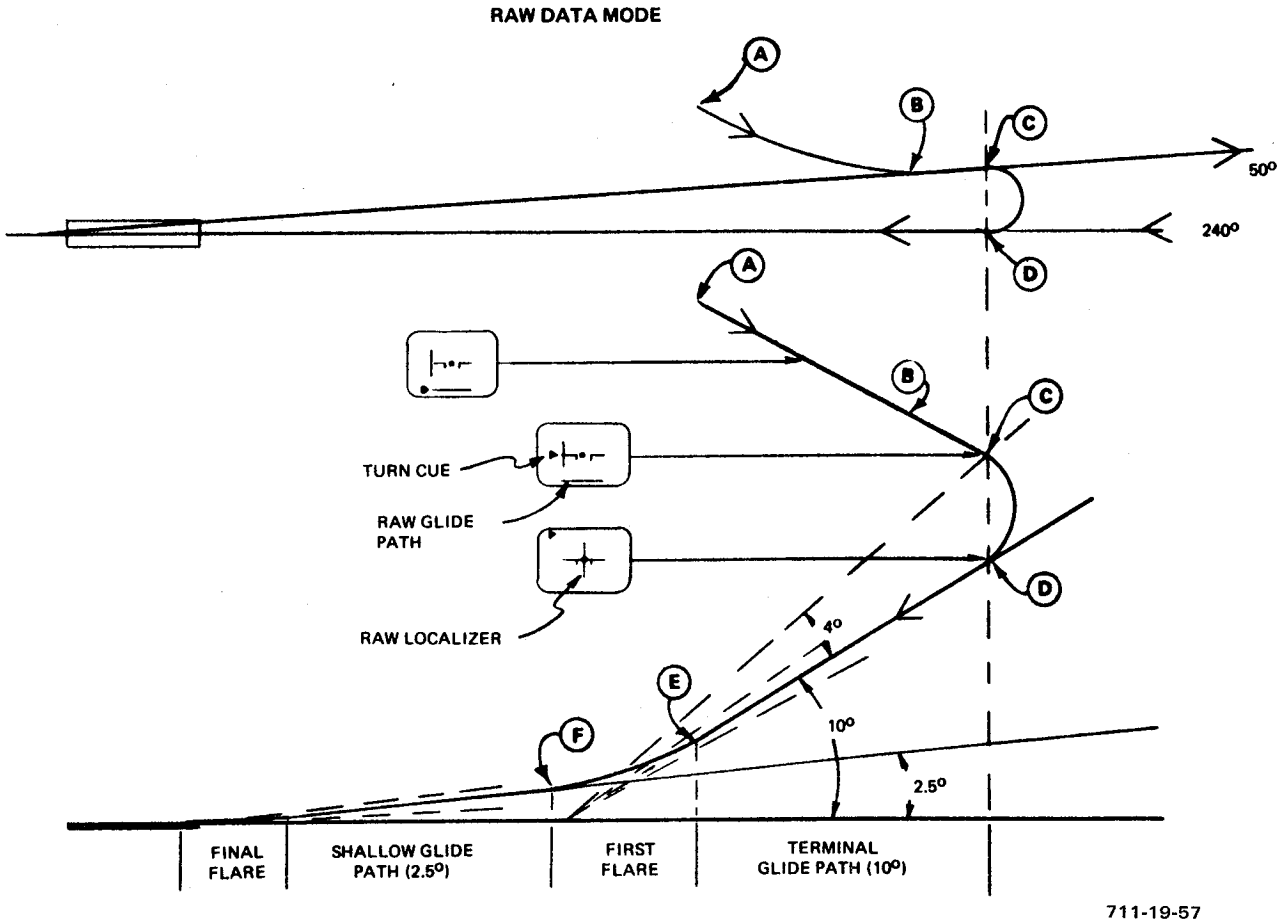

Figure 3-59
Raw Data Mode Geometry and EADI Display

of the shallow glide path at Point (F). If visual contact is made before Point (E), then the entire flareout would be performed VFR. In either case, the final flare is performed with visual reference to the runway.

2. Manual Control Laws

a. Pitch

The pitch manual control system allows the pilot to insert maneuvering commands directly into the fly-by-wire pitch stabilization system. Assume a sidestick controller with a force-stick displacement characteristic given by

$$\delta_\theta = k_s F_s = \frac{\delta_{STICK(\theta)}}{\delta_{STICK(\theta)_{MAX}}} = \text{Ratio of full scale stick deflection} \qquad (3\text{-}116)$$

where:

F_s = applied force

K_s = stick force gradient ... pounds per ratio of stick deflection

The conversion of stick commands to pitch rate commands is illustrated in Figure 3-60. Note that the threshold logic function may be used for automatic mode switching from automatic to manual modes. The stick deadzone shown on Figure 3-60 may be accomplished mechanically but in this study it was made adjustable within the computer software. In this manner it prevented the transmission of stick sensor null signals in the simulator.

The pitch rate maneuvering system control law is

$$\delta_E = k_{D\theta}\delta_\theta + k_\theta \left(1 + \frac{0.1}{S}\right)\left(\theta_E + \frac{k_q}{k_\theta} q_E\right) \qquad (3\text{-}117)$$

where $k_{D\theta}$ is a direct fly-by-wire link to the surface that bypasses the closed loop control law, k_θ is the pitch loop gain, and k_q/k_θ is the ratio of pitch rate to displacement gain. Note that k_θ is mechanized as an inverse function of dynamic pressure Q.

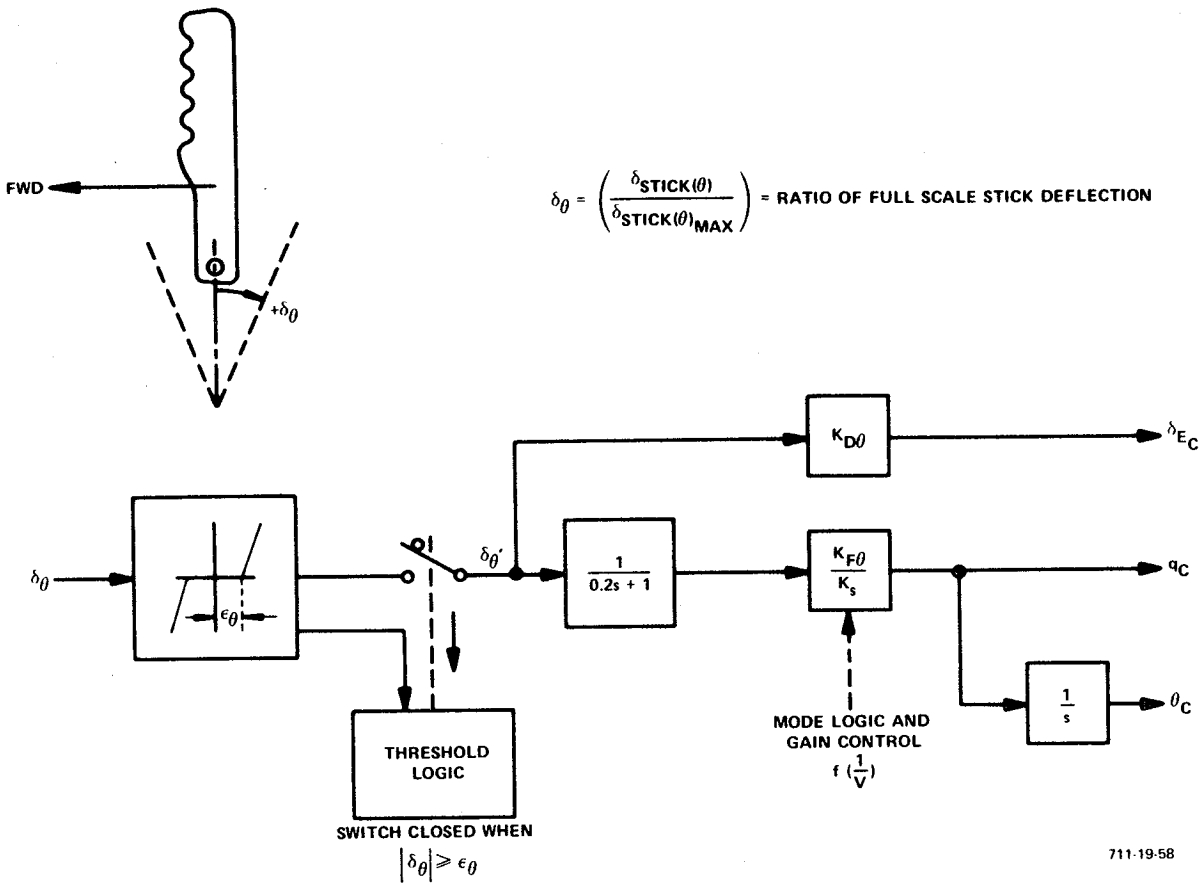

Figure 3-60
Manual Pitch Maneuvering Block Diagram

$$\theta_E = (\theta - \theta_c) \tag{3-118}$$

and

$$q_E = (q - q_c) \tag{3-119}$$

where:

$$\theta_c = \frac{F_s}{(0.25S + 1)} \quad \frac{k_F}{S} = \frac{\delta_\theta}{(0.25S + 1)} \left(\frac{k_F}{k_S}\right)\left(\frac{1}{S}\right) \tag{3-120}$$

$$q_c = \frac{F_s}{(0.25S + 1)} \quad k_F = \frac{\delta_\theta}{(0.25S + 1)} \left(\frac{k_F}{k_S}\right) \tag{3-121}$$

and k_F is the stick force maneuvering gain in degrees per second pitch rate per pound.

Since a normal accelerometer is not used in this maneuvering system, the gain k_F must be made inversely proportional to velocity to provide a relatively constant stick force per g. (That is,

$$k_F = k_{F_o}\left(\frac{V_o}{V}\right) \tag{3-122}$$

for $V > V_o$ and $k_F = k_{F_o}$ for $V < V_o$, where $V_o \approx 300$ feet per second.) For the manual mode prior to high α to low α transition, k_F/k_S should be a constant equal to about 20 deg/sec pitch rate command for full scale stick displacement.

The velocity dependent gain is used after transition. A good value of k_F/k_S is 5000/V. This gain yields 10 deg/sec full scale pitch rate at V = 500 ft/sec.

Typical responses with a low cross-range vehicle are illustrated in Figures 3-61 and 3-62. In these illustrations, k_F is normalized to be 1.0 although in a practical mechanization a realistic value of k_F would be 0.25 to 0.5 for a large transport. The open loop response (Figure 3-61c) is obtained with the direct fly-by-wire link only. This response is indicative of the free airframe pitch rate to elevator response. The closed loop responses are obviously far superior; a phenomenon easily achieved with a relatively high gain control system.

b. Roll

The roll manual maneuvering system is exactly analogous to the pitch system. Figure 3-63 is the block diagram.

Expressing the control law in terms of the stick displacement ratio, δ_ϕ, where

$$\delta_\phi = \left(\frac{\delta_{STICK(\phi)}}{\delta_{STICK(\phi)_{MAX}}} \right) = \text{Ratio of Stick Lateral Displacement to Full Scale Displacement} \tag{3-123}$$

then

$$\delta_{AC} = \text{Aileron Feedforward} = K_{D_\phi} \delta_\phi \tag{3-124}$$

$$P_c = \left(\frac{K_{\delta_\phi}}{0.2S + 1} \right) \delta_\phi = \text{Roll Rate Command} \tag{3-125}$$

$$\phi_c = \left[\frac{K_{\delta_\phi}}{S\ (0.2S + 1)} \right] \delta_\phi = \text{Roll Angle Command} \tag{3-126}$$

For a vehicle of the space shuttle orbiter size, the maximum command roll rate should be about 40 deg/sec. Hence, $K_{\delta_\phi} = 40$.

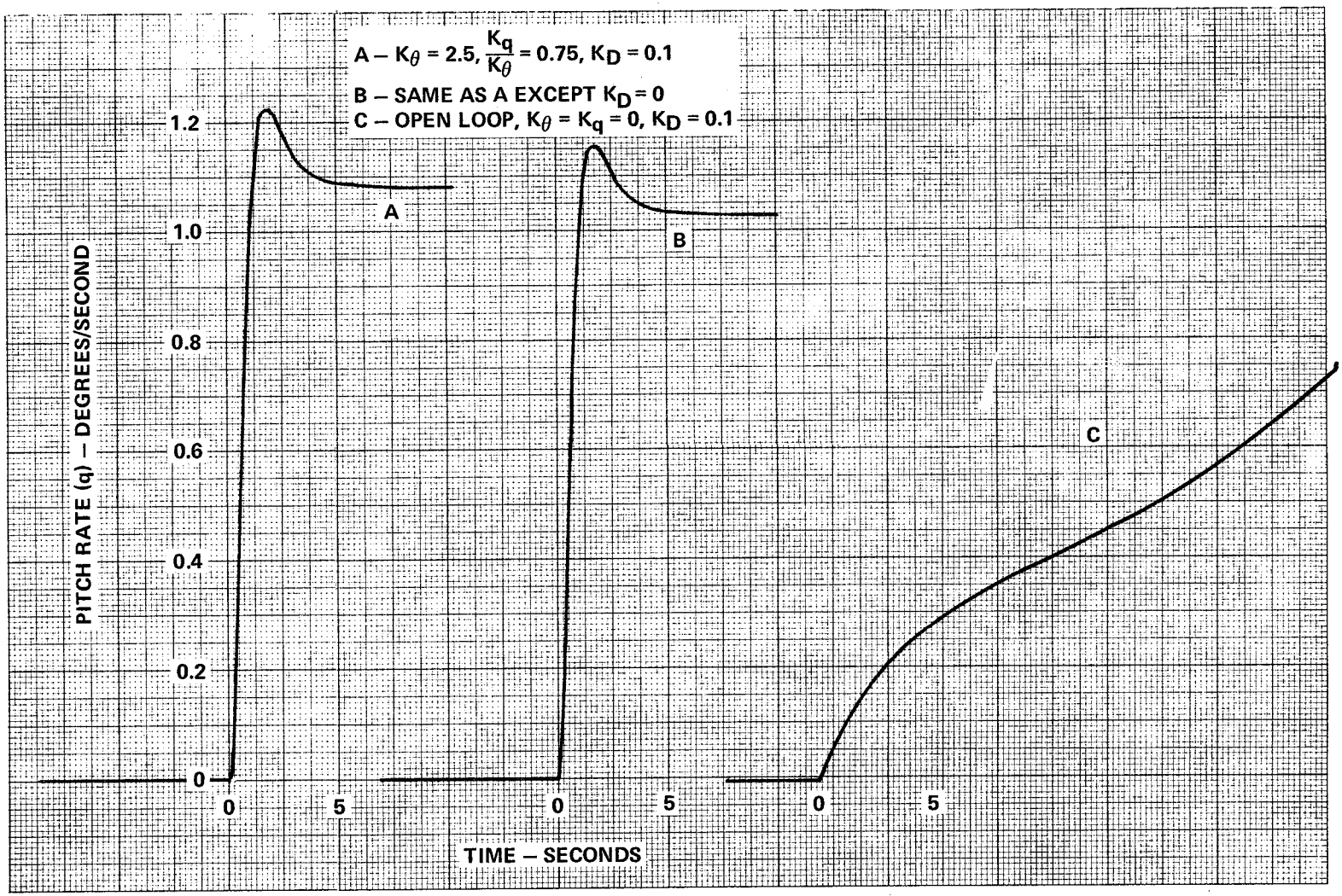

Figure 3-61
Pitch Rate Maneuver System, Low Cross-Range Orbiter,
Landing Flight Condition, Pitch Rate Step Response

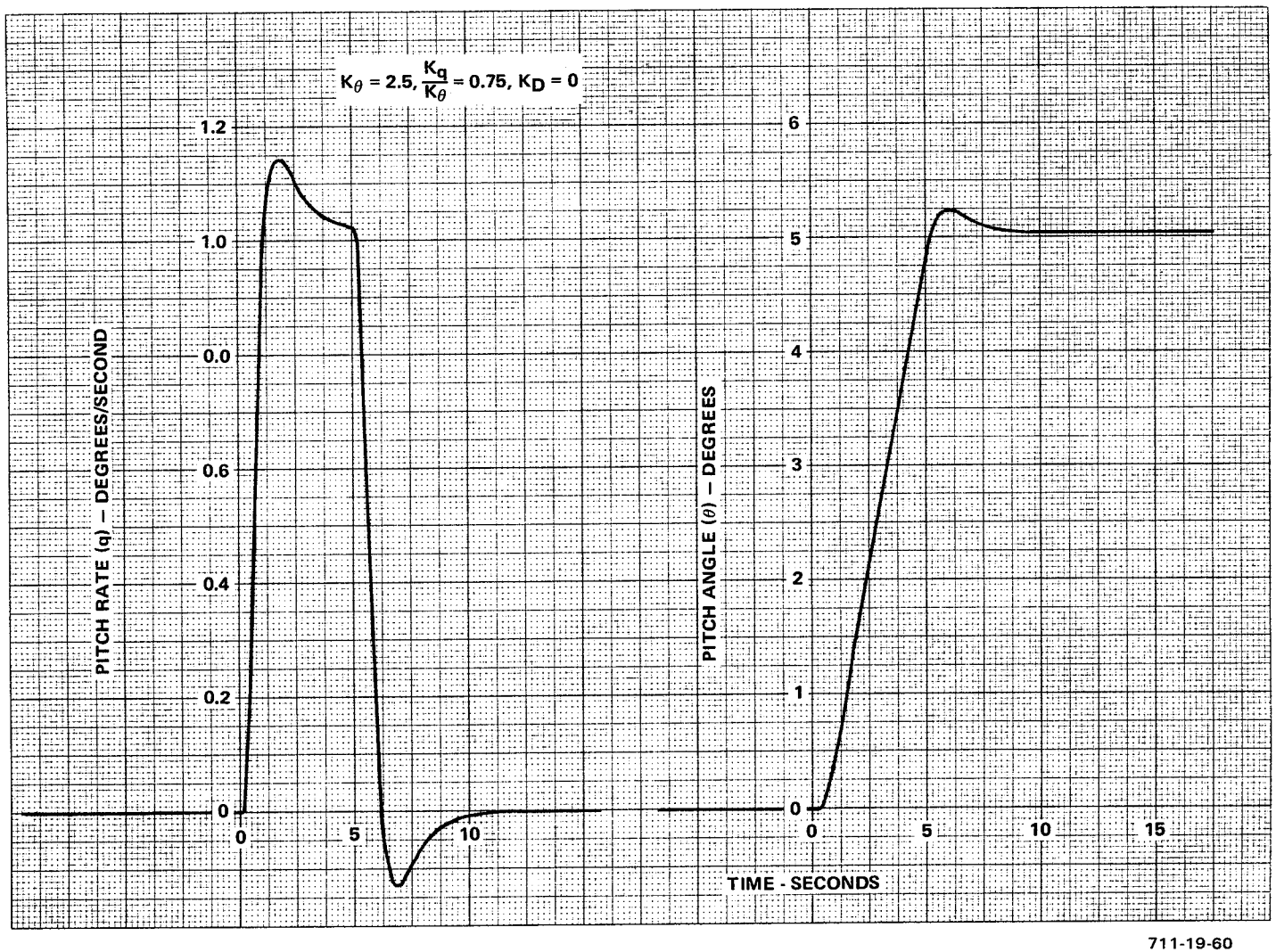

Figure 3-62
Pitch Rate Maneuver System, Low Cross-Range Orbiter,
Landing Flight Condition, Pitch Rate and Angle Response

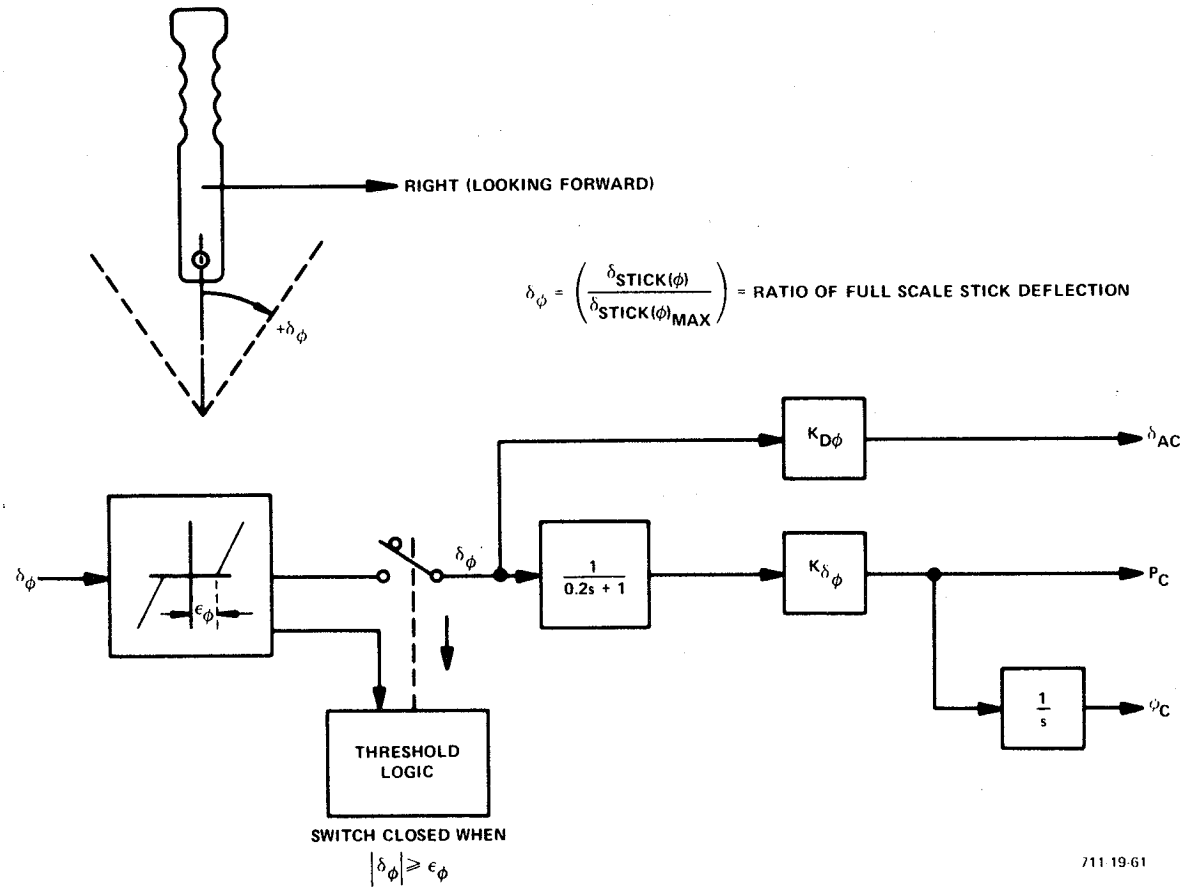

Figure 3-63
Manual Roll Maneuvering Block Diagram

c. Yaw (see Figure 3-64)

The yaw manual command is a skid command derived from rudder pedal transducers (preferably force transducers if a variable spring load or an uncertain null position exists). The command is summed into the Lateral Stabilization system as a "skid command," or direct δ_R command. This command sums against the yaw stabilization feedback quantities (r, A_y) so that the type of skid response is dependent upon how the stabilization feedbacks are handled. For example, if the rudder pedal force threshold logic on Figure 3-64 is exceeded, the A_y feedback could be disabled so that a yaw rate maneuver is commanded (although the washout on yaw rate could produce undesirable characteristics).

The control equation (for a force sensor) is

$$\delta_{R_C} = F_R \frac{K_{RP}}{0.1S + 1} \tag{3-127}$$

Typical gains for K_{RP} allow full scale rudder command for about 20 pounds of applied force. For a rudder limit of ±30°,

$$K_{RP} = 1.5 \text{ degrees } \delta_R \text{ commanded per pound of force.}$$

In general, this skid mode is not recommended for manual control, especially for vehicles with lateral-directional stability problems. In this study, all manual control steering objectives were satisfied using the sidestick controller alone.

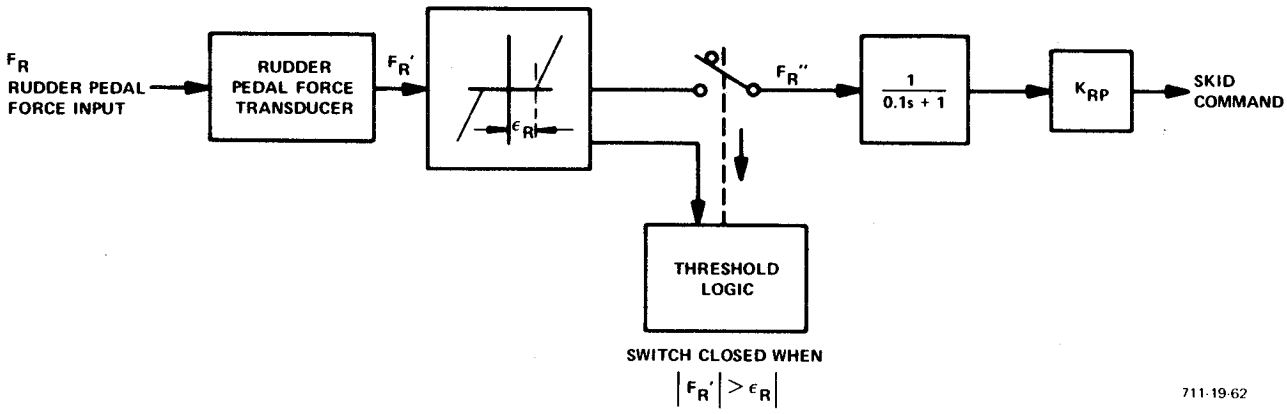

Figure 3-64
Manual Rudder Skid Command Block Diagram